Doctotral Thesis

The Role of Methane Hydrate on Thermal Evolutions of Icy Moons

Ryusuke Nishitani

Department of Earth and Space Science
Graduate School of Science
Osaka University

February 2, 2021

Abstract

Most of the moons in our solar system beyond Jupiter have surfaces covered with ice. These are called icy moons, and they have a variety of appearances. The differences in the appearance of each icy moon depend on the history of how the moon acquired and dissipated heat. The main heat source in the long-term evolution of icy moons is the decay of long-lived radioactive elements. Therefore, the larger the size of the rocky core of an icy moon, the more active the moon is expected to become. In other words, the bulk density and the size of the moon are thought to determine the appearance and activity of icy moons roughly. However, Saturn's moon Enceladus, which is small but has a subsurface ocean, and Saturn's moon Titan, which is not fully differentiated but has a thick atmosphere, cannot be reproduced computationally by heating a mixture of ice and rocks only with heat from radioactive decay. Therefore, in this study, I newly added the calculation of methane concentration to the thermal evolution of icy moons, and developed a thermal evolution model that takes methane hydrate into account. Methane hydrate is a compound of methane gas and water molecules, and it has a lower thermal conductivity and an order of magnitude higher viscosity than ice. Both of these properties have a significant impact on the thermal evolution of icy moons. I also applied the developed model to the thermal evolution of icy moons of various sizes and bulk densities. In Chapter 3, I applied the model to Saturn's moons Enceladus and Mimas. Enceladus and Mimas are small moons with radii of 252 km and 192 km, respectively. Despite the small size of both icy moons, exploration data suggests the existence of a subsurface ocean in both. In order to maintain these subsurface oceans, previous studies attempted to solve the problem by adding ammonia, but it was found that excess ammonia was necessary. As a result of my calculation of the thermal evolution considering the methane hydrate layer, it was found that both Enceladus and Mimas can maintain an ocean with a thickness similar to the current ocean with a tidal heating rate consistent with observations and the results of other studies. In Chapter 4, I applied this

model to Saturn's moon Titan. Saturn's moons have thick atmospheres ($\sim$ 0.15 MPa), which contain about 0.5% methane. It is known that the methane in the current atmosphere disappears in a few million years by photolysis. In this study, I considered the role of methane hydrate as a methane reservoir in Titan. As a result of the thermal evolution calculation considering methane hydrate, it was found that a large amount of methane can be released to the atmosphere by the dissociation of methane hydrate. The amount of methane released to atmosphere depends on the formation time of methane hydrate, and if methane hydrate starts to form more than 500 Myr after the formation of Titan, methane will not be supplied to the atmosphere. In Chapter 5, thermal evolution simulations were performed for generic icy moons of various sizes and bulk densities. Depending on the bulk density and radius, differences in the thickness of the subsurface ocean and the presence or absence of methane hydrate layers were found. The moons that are most affected by the presence of methane hydrate are those with a radius of 750 to 1500 km. The existence or nonexistence of the subsurface ocean changes depending on the presence or absence of methane hydrate in moons with a radius of about 1000 km. It was also found that moons with a radius of about 1000 km may have an atmosphere depending on the initial methane concentration. In this study, I investigated the thermal evolution from the small icy moon Mimas to the large icy moon Titan, and showed that the thermal evolution of icy moons is greatly affected by the presence of methane hydrate. Using bulk density and radius as variables, I showed that methane hydrate plays a role as an internal insulating layer and methane reservoir even in icy moons of various sizes. If considering methane hydrates, the existence of a subsurface ocean in icy moons may be more universal. Methane hydrate is one of the key compounds to consider in the thermal evolution of icy moons.

Contents

Chapter 1

General Introduction

1.1 Icy moons

Most of the moons in outer solar system are covered with H_2O ice on their surfaces. They are called icy moons. Even if they are covered with the same H_2O ice, they look very different. Figure 1.1 shows images of major icy moons and the Earth's moon [1]. In Europa and Enceladus, geysers have been observed [2, 3]. In Ganymede and Tethys, a large rift valley runs across the surface. Titan is covered by a thick atmosphere composed of nitrogen and methane. The surface of Mimas is inactive and there are few Herschel craters on the surface that have not relaxed. How these diverse looks were formed is a mystery. The internal structure of icy moons is constrained from observations by spacecraft. Figure 1.2 shows the relationship between bulk density and size of icy moons [4]. If we assume that the density of rock is 3000 $\mathrm{kg\,m^{-3}}$ and that of ice is 920 $\mathrm{kg\,m^{-3}}$, we can infer the approximate ice/rock ratio from the bulk density of icy moons. Also, if we know the Moment of Inertia (MoI) of an icy moon, we can determine how much mass is concentrated in the center of the moon. In other words, we can see how differentiated the moon is. If the MoI of a sphere is 0.4, it is a homogeneous sphere; if it is smaller than 0.4, it has a structure with differentiated mass.

In many icy moons, a liquid layer, or internal ocean, is thought to exist beneath the icy shell. In Europa and Callisto, the induced magnetic field induced by Jupiter's magnetic field has been observed [5]. This indicates that conductors such as salty ocean exist in the subsurface. Although magnetic fields have been observed in Ganymede, it is difficult to conclude the existence of an ocean simply because Ganymede has its own magnetic field [6]. Libration also predicts the

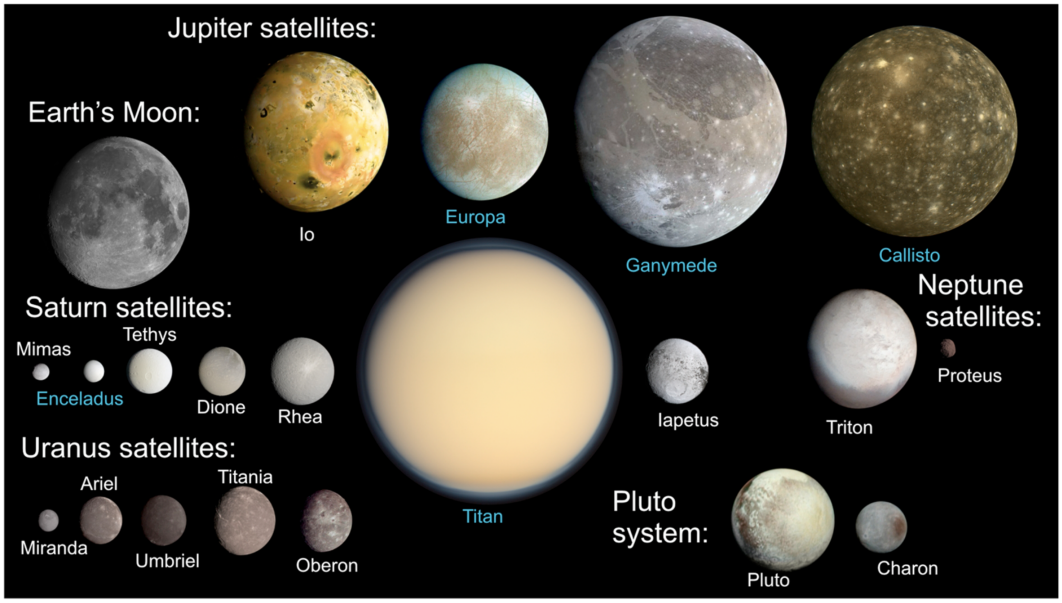

Figure 1.1: Icy moons, Earth's moon and Io are drawn on a common scale. This figure is taken from Nimmo and Pappalardo(2016)[1]. Moons written in blue indicate the existence of an internal ocean.

existence of internal oceans in icy moons. Libration is the periodic variation of rotational motion caused by the gravity from the primary. When the rocky core and icy shell of an icy moon are separated by the ocean, the response of tidal forces to the icy moon is different from that to a completely solid body. This property is used to determine the presence or absence of an internal ocean. In Enceladus, a larger libration amplitude was observed than when assuming complete solidification [7]. Therefore, it is believed that Enceladus has a global internal ocean. Similarly, large amplitudes were observed in Mimas [8].

Therefore, there is a possibility that the internal ocean exists in Mimas, but it is not known whether the internal ocean actually exists because the amplitude of the libration is large even when the rocky core is lumpy.

Thus, the present state of each icy moon has been revealed by previous explorations.

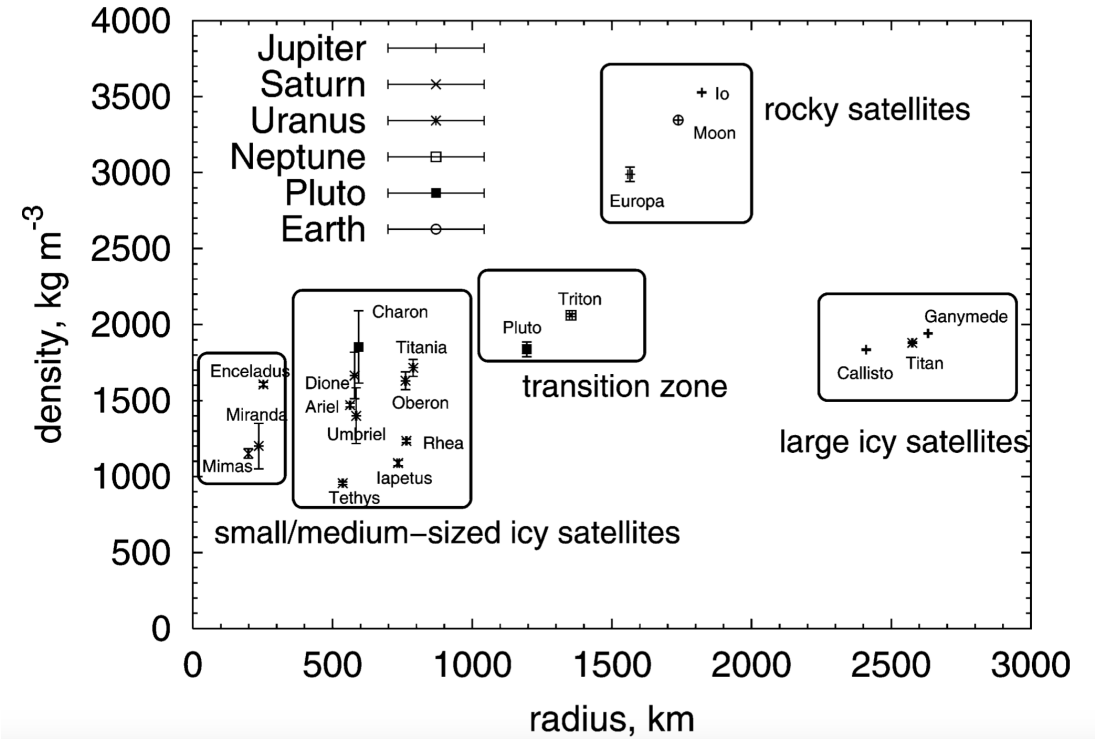

Figure 1.2: Relationship between moon radius and bulk density. This figure is taken from Hussmann et al. (2006)[4]. Different symbols indicate different planetary systems.

1.2 Thermal evolutions of icy moons

It is very important from the viewpoint of the celestial evolution of the solar system to clarify the process by which the current state of icy moons was achieved and the factors that determine their current state. In order to trace the evolution of icy moons, it is useful to calculate the thermal evolution of icy moons, which traces how they acquire and dissipate thermal energy. When studying local geological activity or convection inside the icy shell, 3D or 2D simulations are used. However, due to the high computational cost of 3D or 2D simulations, 1D simulations are often used to explore the long-term evolution of icy moons (e.g., [9]). In the 1D thermal evolution calculation, the icy moon is divided into three layers (icy shell-ocean-rocky core) and the balance of heat loss and gain within these layers is calculated. The means by which the icy moons lose heat is through radiation at the surface. There are three main ways for icy moons to acquire heat. The first is the release of gravitational energy during the accretion of icy moons. This is an important energy when considering the early evolution of icy moons. The second is the decay of radioactive elements contained in rocks. The rocky cores of icy moons contain many radioactive elements that affect the thermal evolution of icy moons. The short-lived radioactive elements such as ^{26}Al affect the early evolution of icy moons after accretion. While, long-lived radioactive elements such as ^{238}U, ^{235}U, ^{232}Th and ^{40}K affect the long-term evolution of icy moons. The third is tidal heating. A satellite in an eccentric orbit experiences deformation and stress due to tidal forces from the planet. Some of the energy applied to the satellite by these tidal forces is dissipated as thermal energy inside the satellite. The existence of oceans in small icy moons depends on the magnitude of tidal heating. Accurate calculations of the time evolution of these heat transfers will reveal the thermal evolution of icy moons. In order to clarify the thermal evolution of icy moons, there are various approaches to research. There are studies that not only calculate the thermal evolution but also consider the orbital evolution and the heat of chemical reactions in the interior [10, 11]. However, it has not yet been possible to comprehensively explain the interior structures and the current orbital properties of each icy moon. Small and medium-sized icy moons cannot sustain their subsurface oceans with only the heat from radioactive decay. Instead of considering of the additional heat

sources such as tidal heating to maintain the subsurface oceans, one way is to depress the freezing point of water by contaminating the oceans with antifreeze molecules, such as ammonia [4, 12]. If 33 wt% of ammonia is dissolved in the subsurface ocean, the melting point of ice would be down to 175 K, and the icy shell would melt easily [13]. However, comets, which are thought to be the raw materials for icy moons, do not contain this much ammonia [14]. If ammonia is dissolved in the subsurface ocean, some ammonia will be left in the icy shell as the shell grows, and the lower part of the shell will become like mush [15]. When the icy shell is like mash containing ammonia, the viscosity of the shell drops significantly [16]. When the viscosity of the icy shell is low, convection in the shell gets stronger, which shortens the lifetime of the subsurface ocean [12, 17, 9]. Therefore, it is difficult to explain the maintenance of the subsurface ocean only by the ammonia in the ocean.

1.3 Methane hydrate in icy moons

The composition of subsurface ocean is very important information for understanding the materials that make up icy moons. The Cassini spacecraft collected geyser components near the south pole of Enceladus that appear to be derived from the subsurface ocean [2]. Part of the geyser composition is shown in Table 1.1. The geyser composition shows that the inner ocean of icy moons is not pure water, but contains many gaseous components.

Table 1.1: Some of the components found in the plume of Enceladus.[18]

Species	Mixing ratio
H_2O	0.87
H_2	0.11
CO_2	5.2×10^{-3}
CH_4	1.9×10^{-3}
NH_3	6.1×10^{-3}
CO	$\leq 6.4 \times 10^{-3}$
N_2	$\leq 6.1 \times 10^{-3}$
HCN	$\leq 1.2 \times 10^{-3}$
H_2S	2.1×10^{-3}

According to the thermodynamic statistical model, gas hydrates can be formed by assuming ocean with a geyser component under the Enceladus subsurface ocean pressure (3.6 - 5.3 MPa) and temperature (∼273 K) [18]. Gas hydrates are compounds in which volatiles are trapped in a cage formed by a network of hydrogen bonds between water molecules [19]. Figure 1.3 shows a cartoon of gas hydrates. There are several types of cages. Main types of cages are three: S-cage (pentagonal dodecahedron, 5^{12}), M-cage (tetrahedron, $5^{12}6^2$), and the L-cage (hexahedron, $5^{12}6^4$). The combination of these cages forms the unit cell. The major unit cells are Structure I, which consists of 2 S-cages and 6 M-cages, and Structure II, which consists of 16 S-cages and 8 L-cages. Depending on the size of the volatiles, the cage in which the volatiles are enclosed changes, and the stable structure also changes. For example, methane hydrate and carbon dioxide hydrate are Structure I, while propane hydrate is Structure II. It is not necessary that volatiles are enclosed in all the cages that consist of gas hydrates. If all the cages in Structure I are occupied by methane, the compositional formula would be $CH_4 \cdot 5.75\,H_2O$. Gas hydrates look similar to ice, but their physical properties are different from ice. First, the thermal conductivity of gas hydrates is about four times lower than that of ice [20]. This is because the gas molecules entrapped in the gas hydrate behave like a free gas. If gas hydrates are contained in the icy shells of icy moons, heat is more easily retained inside the icy moons. Second, the viscosity of gas hydrates is about one order of magnitude larger than that of ice [21]. The greater the viscosity, the less likely it is that solid-state convection of the icy shell will occur. Convection is an efficient means of transferring heat from the interior of a icy moon to the surface. These two features are thought to have a significant impact on the thermal evolution of icy moons. Methane hydrate seems to be the most common gas hydrate in icy moons. Hydrogen, carbon dioxide, and methane are the most common materials that can form gas hydrates in icy moons. Hydrogen hydrate is unlikely to exist in satellites of small size due to the high pressure required to produce it. Carbon dioxide hydrate has a density of ∼1100 $\mathrm{kg\,m^{-3}}$ and is generally thought to sink in the interior ocean, depending on the density of the interior ocean. Sunk hydrate will eventually decompose due to heat from the rocky core. Methane hydrate, with a density of ∼920 $\mathrm{kg\,m^{-3}}$, can float in the interior ocean and can exist as a layer under the icy shell. Figure 1.4 shows the phase diagram of methane hydrate. It can be seen

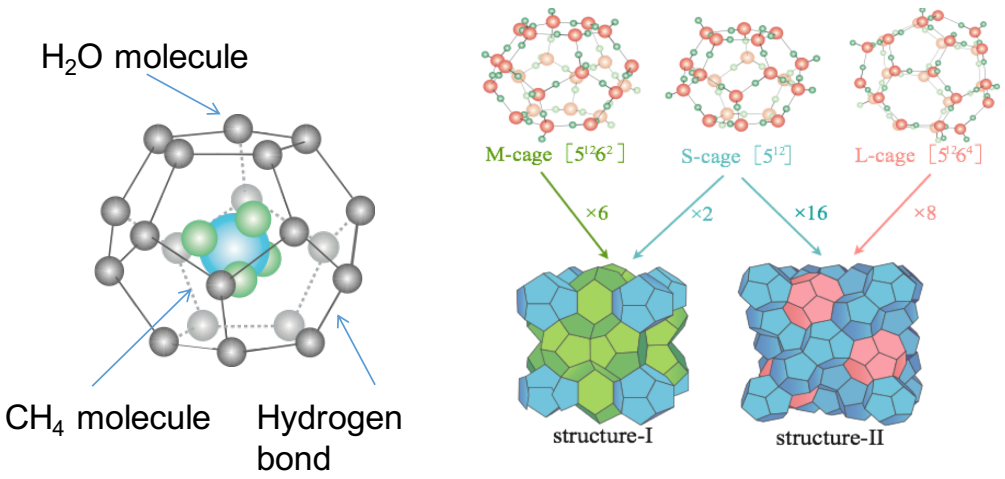

Figure 1.3: Cartoon showing methane hydrate. The left figure shows the methane gas contained in the S-cage. The right figure shows the structure of the gas hydrate formed from each cage.

that methane hydrate is stable under low temperatures and high pressures, such as in icy moons. Kamata et al., (2019) calculated the 1D thermal evolution of Pluto considering the existence of methane hydrate layers [17]. The results show that the existence of thin methane hydrate layer can maintain a thick subsurface ocean for 4.6 Gyr. In addition, Kalousova and Sotin (2020) performed 2D thermal evolution calculations on Titan [22]. This also shows that the methane hydrate layer prevents the heat from the inside from escaping to the surface. However, these studies assume that there is enough methane in the subsurface ocean for simplicity. Also, Tobie et al. (2006) shows that the presence of methane hydrate in the Titan may have supplied large amounts of methane to the atmosphere through the dissociation of methane hydrate within the past 1 Gyr [23]. Thus, methane hydrate may be an important material in the evolution of icy moons.

1.4 Aim of the thesis

As mentioned above, icy moons are low-temperature and high-pressure environments where methane hydrates can exist. The existence of methane hydrates is likely to have a significant impact on the thermal evolution of icy moons. How-

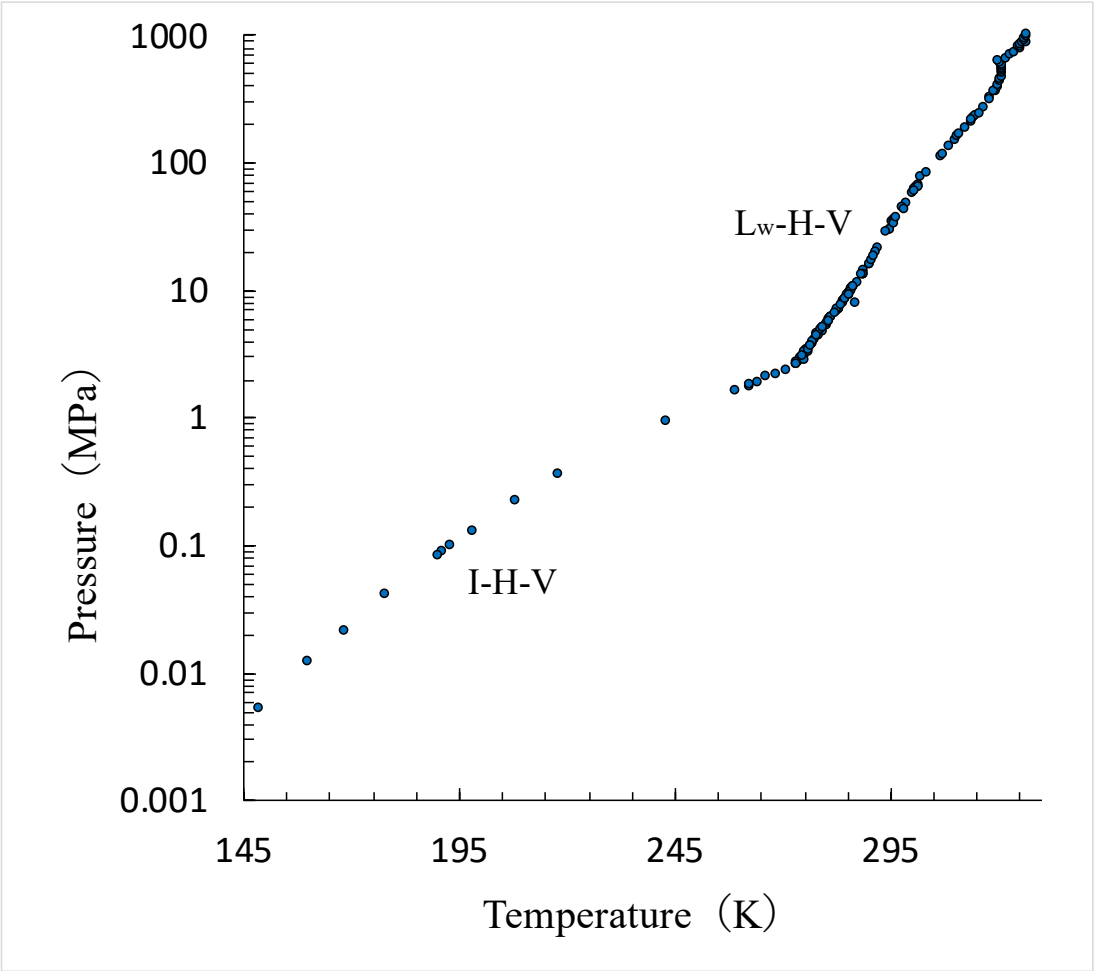

Figure 1.4: Phase diagram of methane hydrate[19].

ever, the production of methane hydrate decreases the amount of methane in the subsurface ocean, so it is not possible to produce methane hydrate indefinitely. Previous computational models have assumed that methane is infinite in the ocean. In this study, I develop a new model for calculating thermal evolution that takes into account the methane concentration in the ocean. Furthermore, I apply the developed model to real and generic icy moons to clarify how the thermal evolution of icy moons in the presence of methane hydrate is different from that in the absence of methane hydrate. Since methane hydrate requires a low-temperature and high-pressure environment to exist, I also investigate what size and bulk density of icy moons in Figure 1.2 have a significant effect on the existence of methane hydrate. Thus, the purpose of this thesis is to clarify the influence of methane hydrate on the thermal evolution of icy moons by investigating the above, and to investigate how universal the existence of the subsurface ocean is. I think that not only the bulk density and radius but also the methane concentration in the subsurface ocean can be a new evaluation axis to clarify the existence of the subsurface ocean of icy moons.

In Chapter 2, I present the numerical method used in this study. The details of the newly added parts and the benchmarks are described. Chapter 3 describes the thermal evolution of Mimas and Enceladus in the presence of methane hydrate layers. Through calculations, I explore the conditions under which the internal ocean exists in both Mimas and Enceladus and Mimas is more inactive than Enceladus. In Chapter 4, the calculation code developed in this study is applied to Titan. I investigate the existence of methane hydrate layer inside Titan and how the methane hydrate affects the amount of methane in Titan's atmosphere. In Chapter 5, the developed code is applied to generic icy moons. I explore how methane hydrate affects thermal evolution for icy moons of various sizes and densities. Finally, a summary of this study is given in Chapter 6.

Chapter 2

Development of a Methane Hydrate Growth Model for Icy moons

In this section, I describe in detail the numerical model of icy shell evolution developed in this study, which takes into account the methane concentration in subsurface oceans of icy moons.

In previous studies, 1D thermal evolution calculations of icy moons have considered icy moons divided into 3 or 4 layers, such as H_2O ice-ocean-rocky core (-metal core). In this study, I develop the conventional numerical model into a model which includes the 6 layers of ice-methane hydrate-mix-ocean-high pressure ice-rocky core. Here, the mix layer is defined as a mixed layer of methane hydrate and ice. Figure 2.1 is a cartoon showing the internal structure. In the thermal evolution calculation, each layer is divided into thinner layers and the time evolution of heat exchange in each layer is tracked. The following subsections summarize what formulas are used to perform the calculations.

2.1 Governing equations

In this section, I summarize the thermal evolution calculation model using the modified mixing length theory, which was the basis of my thermal evolution calculation model.

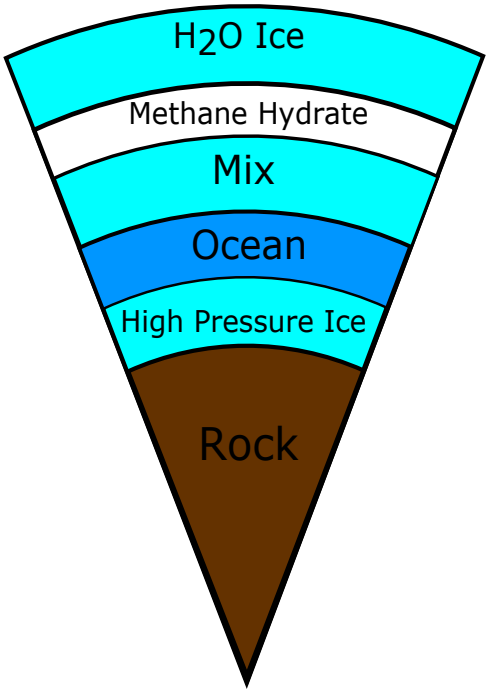

Figure 2.1: Illustration of the internal structure considered in this study

2.1.1 Heat transfer

The governing equation in 1D thermal evolution calculations is generally the energy equation under the Boussinesq approximation. In order to consider the thermal evolution of celestial bodies in this study, it is necessary to solve the energy equation of heat in a spherical coordinate The governing equation is given by

$$\rho C_p \frac{\mathrm{d}T}{\mathrm{d}t} = -\frac{1}{r^2}\frac{\mathrm{d}}{\mathrm{d}r}\left(r^2 F_{\mathrm{cond}} + r^2 F_{\mathrm{conv}}\right) + Q \tag{2.1}$$

where ρ is the density, C_p is the specific heat, T is the temperature, r is the radius, F_{cond} is the conductive heat flux, F_{conv} is the convective heat flux, and Q is the volumetric heating rate. In this study, the above equation is mainly used when considering heat transport in the solid parts of an icy moon. Since the heat transport in the liquid part (subsurface ocean) is sufficiently fast compared to the heat transport in the solid parts, the heat transport in the liquid part is assumed to be instantaneous. In other words, no thermal calculations are performed in the subsurface ocean and a constant temperature is assumed. Since the adiabatic temperature gradient in the ocean is a small value, it is ignored in this study. Heat sources in icy moons include the release of gravitational energy during accretion, energy from the decay of short-lived radioactive elements in rocks (e.g., ^{26}Al), and energy from the decay of long-lived radioactive elements in rocks (e.g., ^{238}U, ^{235}U, ^{232}Th, ^{40}K). Among these, the decay of long-lived radioactive elements has the greatest impact on long-term evolution. In this study, rocky cores are assumed to have CI chondrite compositions unless otherwise noted [24]. The amounts of long-lived radioactive elements in CI chondrites are listed in Table 2.1. The heat due to decay of long-lived radioactive elements is as follows:

$$Q = \sum_i c_i H_i \exp\left(-\lambda_i t\right) \tag{2.2}$$

where subscript i represents each radioactive element, c_i is the initial concentration in a rock, H_i is the decay energy, and λ_i is the decay constant.

Table 2.1: The concentration and properties of radioactive elements [24]

	Concentration (ppb)	Decay energy (W/kg)	Half life time (Myr)
^{238}U	19.9	94.65×10^{-6}	4468
^{235}U	5.4	568.7×10^{-6}	703.81
^{232}Th	38.7	26.38×10^{-6}	14030
^{40}K	738	29.17×10^{-6}	1277

Heat transport by conduction is expressed by the following equation:

$$F_{\text{cond}} = -k\frac{\mathrm{d}T}{\mathrm{d}r} \tag{2.3}$$

where k is the thermal conductivity. Heat transport in the solid phase considering convection is often evaluated using the Nusselt number Nu, which is the ratio of all heat transport to heat transport by conduction. Nu is obtained from the relationship with the Rayleigh number, which is estimated from 2D or 3D simulations and laboratory experiments. the Rayleigh number is defined as follows:

$$\mathrm{Ra} = \frac{\alpha g \rho \Delta T d^3}{\kappa \eta} \tag{2.4}$$

where α is thermal expansivity, g is the gravitational acceleration, ρ is density, ΔT is the difference between temperature at the top of the layer and temperature at the bottom, d is the layer thickness, κ is the thermal diffusivity, and η is viscosity. Gravitational acceleration is determined from hydrostatic equilibrium. The relationship between the Rayleigh number and the Nusselt number can be written as follows:

$$Nu = aRa^{\beta} \tag{2.5}$$

where a is taken between 1 and 10, and β is is taken between 0.2 and 1/3 [25]. Parameterized convection using Nu can describe surface heat flux well, but it cannot describe internal temperature accurately. Therefore, in this study, I use the mixing length theory to evaluate the solid-state convection.

2.1.2 Mixing length theory

The mixing length theory is a theory that discusses the motion of a fluid in a turbulent flow using the mixing length that represents how far a fluid parcel can travel. In the context of thermal evolution calculations, the theory evaluates the convection terms in the governing equation 2.1. It was first applied to the thermal evolution of a celestial body by Sasaki and Nakazawa (1986)[26], and formulated by Kimura et al. (2009)[27]. The summary of the theory is given below.

Consider that a heat parcel in a fluid is moving due to buoyancy while undergoing viscous resistance. The velocity of a parcel U is described by the terminal velocity obtained from Stokes' equation.

$$U = \frac{2\left(\rho - \rho_0\right) g \left(\frac{l}{2}\right)^2}{9\eta} = \frac{\left(\rho - \rho_0\right) g l^2}{18\eta} \tag{2.6}$$

where ρ is the parcel density, ρ_0 is the surrounding density, and l is the mixing length. The density difference between the fluid and the parcel can be described as follows:

$$\rho - \rho_0 = \rho \alpha \Delta T \tag{2.7}$$

where ΔT is the difference between the parcel temperature and the surrounding temperature. The temperature difference from the surroundings, or temperature perturbation, can be written as

$$\left[\left(\frac{dT}{dr}\right) - \left(\frac{dT}{dr}\right)_{\mathrm{ad}}\right] l = \Delta T \tag{2.8}$$

where $(\mathrm{d}T/\mathrm{d}r)_s$ is the adiabatic temperature gradient, that is $-\alpha g T / C_p$, and C_p is specific heat. Then,

$$U = \frac{\rho \alpha \Delta T g l^2}{18\eta} = \frac{\rho \alpha g l^3}{18\eta}\left[\left(\frac{dT}{dr}\right) - \left(\frac{dT}{dr}\right)_{\mathrm{ad}}\right]. \tag{2.9}$$

The distance required for the temperature difference of the temperature perturbation to disappear can be interpreted as the mixing length. Finally, the convection

term can be described as follows:

$$\begin{aligned} F_{\mathrm{conv}} = \rho c_p \Delta T U &= \frac{\rho^2 c_p \alpha g l^4}{18\eta} \left[\left(\frac{dT}{dr} \right) - \left(\frac{dT}{dr} \right)_{\mathrm{ad}} \right]^2 \\ &= -k_v \left[\left(\frac{dT}{dr} \right) - \left(\frac{dT}{dr} \right)_{\mathrm{ad}} \right]. \end{aligned} \tag{2.10}$$

Considering that convection cannot occur without sufficient temperature perturbation, F_{conv} and k_v is 0 when $(\frac{dT}{dr}) > (\frac{dT}{dr})_{\mathrm{ad}}$.

If the mixing length is defined as the distance to the nearest boundary, the relationship between Nu and Ra determined by experiment and 2D convection can be reproduced [27]. The mixing length theory is superior to parameterized heat transport calculations in that it can accurately describe the internal temperature structure.

2.1.3 Modified mixing length theory

The reproducibility of the mixing length theory was valid for 2D cartesians. However, the evolution of celestial bodies should be considered in spherical coordinates, and the usefulness of the mixing length theory in spherical coordinates was not known. Therefore, Kamata (2018) redefined the mixing length and constructed a scaling law using the results of 3D simulations. The scaling law is described below.

First, the mixing distance is defined as follows:

$$l = \begin{cases} \frac{b}{a} \left(R_{\mathrm{top}} - r \right) & \text{for } R_{\mathrm{top}} - r \leq aD \\ \frac{b}{1-a} \left(D - (R_{\mathrm{top}} - r) \right) & \text{for } R_{\mathrm{top}} - r > aD \end{cases} \tag{2.11}$$

where R_{top} is the radius of the layer top, r is radius, D is the layer thickness. aD and bD represent the peak depth and peak value of the mixing length, respectively. Figure 2.2 shows the conceptual diagram of the mixing length. Let f be the ratio of the radius of the bottom of the layer to the radius of the top of the layer. γ is a coefficient that represents the contrast in viscosity between the top

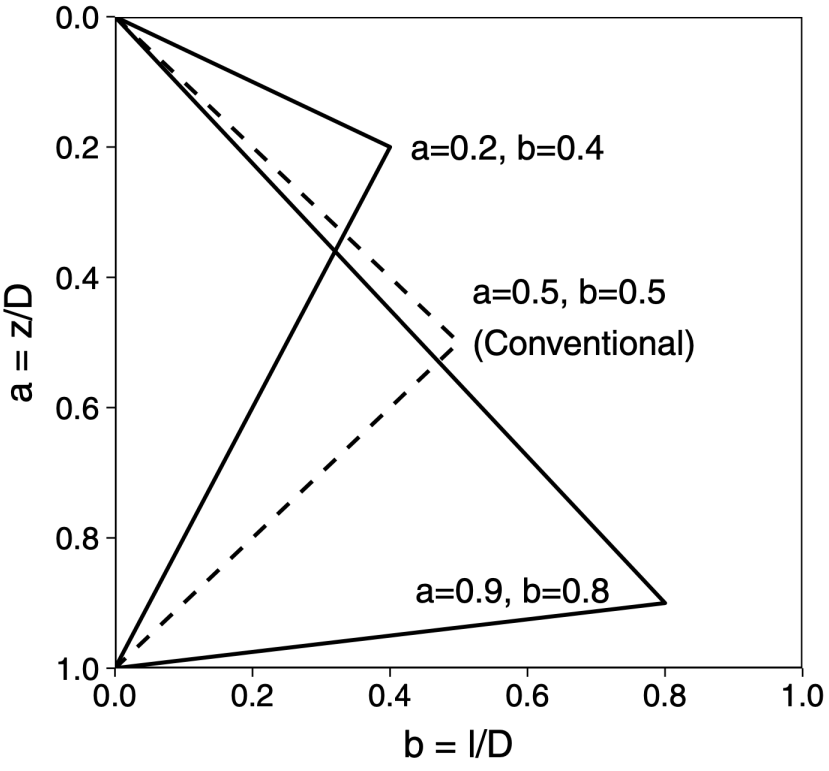

Figure 2.2: Conceptual diagram of the definition of mixing length. This figure is taken from Kamata (2018) [12]

and bottom of the layer. γ can be expressed as follows:

$$\frac{\eta\left(T_0\right)}{\eta\left(T_0+\Delta T\right)}=\exp(\gamma) \tag{2.12}$$

where T_0 is the temperature at surface. Consider both a and b to be functions of f and γ, and use the results of the 3D calculation to scale a and b using f and γ. Both a and b are considered to be functions of f and γ. It is assumed that a and b are given by

$$\begin{aligned} a(f,\gamma) &= a_2(\gamma)f^2+a_1(\gamma)f+a_0(\gamma) \\ b(f,\gamma) &= b_2(\gamma)f^2+b_1(\gamma)f+b_0(\gamma) \end{aligned} \tag{2.13}$$

As the icy shell approaches Isoviscous, a and b can be written as functions of f only, so the coefficients in the above equation can be written as exponential functions. Fitting the above equation to the results of the 3D calculation, the following scaling law is obtained.

$$\begin{aligned} a_2(\gamma) &= -41.2\exp(-0.297\gamma)-0.456 \\ a_1(\gamma) &= 58.6\exp(-0.292\gamma)+0.704 \\ a_0(\gamma) &= -21.0\exp(-0.290\gamma)+0.624 \\ b_2(\gamma) &= 3.96\exp(-0.167\gamma) \\ b_1(\gamma) &= -6.93\exp(-0.178\gamma) \\ b_0(\gamma) &= 2.90\exp(-0.127\gamma) \end{aligned} \tag{2.14}$$

These can successfully reproduce the results of 3D simulations, but there are conditions of use. These can successfully reproduce the simulation results in 3D. However, the scaling low is not recommended for low γ ($\leq$10) and low f ($<$0.5) because no 3D simulations have been done. Note that this means that the modified mixing length theory cannot be used for the rocky core.

2.1.4 Growth of ice layer

The thermal evolution calculation considers not only heat transport but also the phase change of H_2O. In the thermal evolution of icy moons, ice growth in the interior ocean and ice melting at the bottom of the ice layer is described as

follows:

$$\rho_{\mathrm{ice}} L_{\mathrm{eff}} \frac{\mathrm{d}D}{\mathrm{d}t} = F_{\mathrm{out}} - F_{\mathrm{in}} \tag{2.15}$$

where D is the icy shell thickness, L_{eff} is the effective latent heat, F_{out} is the heat flux outgoing from the shell bottom, and F_{in} is the heat flux incoming into the shell bottom [12]. L_{eff} represents the combined heat required to change the H_2O phase at the base of the ice layer and the heat required to change the temperature of the ocean, and is expressed by the following equation:

$$L_{\mathrm{eff}} = L - \frac{\rho_{\mathrm{oce}} g_{bot} C_{p,\mathrm{oce}} V_{\mathrm{oce}}}{4\pi R_{\mathrm{bot}}^2} \frac{\mathrm{d}T_{\mathrm{m}}}{\mathrm{d}P_{\mathrm{bot}}} \tag{2.16}$$

where L is the latent heat, V_{oce} is the volume of the ocean, and R_{bot} is the radius at the bottom of the layer. This means that ocean temperature is constant at the melting point of the bottom of ice layer. The specific heat of the ocean is temperature dependent [13] and is described as follows:

$$C_{p,\ \mathrm{oce}} = 4190 + 9 \exp\left(-0.11\left(T_{\mathrm{oce}} - 281.6\right)\right) \tag{2.17}$$

where T_{oce} is the ocean temperature.

2.1.5 Physical parameters for the simulation

The parameters used in the thermal evolution calculation are shown in the Table 2.2. Unless otherwise stated, the values in Table are used for physical properties. The melting point of ice $T_{\mathrm{m,ice}}$ depends on pressure, and is given by

$$T_{\mathrm{m,ice}}(P) = 273.1 - c_1 P - c_2 P^2 \tag{2.18}$$

where P is the pressure, $c_1 = 7.95 \times 10^{-8}\,\mathrm{K\,Pa^{-1}}$, and $c_2 = 9.6 \times 10^{-17}\,\mathrm{K\,Pa^{-2}}$ ([28]). Temperature dependence of the viscosity of ice and methane hydrate is taken into account. It is known that the viscosity of ice can be expressed by the

following equation[29]

$$\eta(T) = \eta_{\mathrm{ref}} \exp\left(\frac{E_a}{R_g T_{\mathrm{ref}}}\left(\frac{T_{\mathrm{ref}}}{T} - 1\right)\right) \tag{2.19}$$

where η_{ref} is the reference viscosity and corresponds to the viscosity at T_{ref}, T_{ref} is the melting point, E_a is the activation energy, and R_g is the gas constant. Assume that the same equation can be used for methane hydrate. I assume that the reference viscosity of ice is 10^{14} Pa s and that of methane hydrate is 2.0×10^{15} Pa s [17, 21]. In icy moons, the strain rate of ice derived from convection is considered to be smaller than that of glacier on the earth [30]. Therefore, if the deformation mechanism of ice is controlled by diffusion creep, the viscosity depends on the grain size of ice [29]. The viscosity of ice is about 10^{14}; Pa s when the grain size is about 0.3 mm [31]. The viscosity of methane hydrate is about one order of magnitude larger than that of ice [21]. However, these values are uncertain and it is difficult to determine the exact value. The predominant deformation mechanism of ice differs depending on the magnitude of strain rate [29]. It has also been suggested that the dominant deformation mechanism in the ice shell varies with temperature [32]. The grain size of ice in icy moons is not yet known, but numerical calculations suggest that the grain size is about the same or an order of magnitude larger than that of glaciers on the earth [30]. Temperature dependent viscosity is also taken into account for serpentine. An experimental equation for the viscosity of serpentine is presented by Hilaire et al. (2007) and can be written as follows [33]: equation[29]

$$\eta(T) = \eta_{\mathrm{ref}} \exp\left(\frac{E_a - PV^*}{R_g T_{\mathrm{ref}}}\left(\frac{T_{\mathrm{ref}}}{T} - 1\right)\right) \tag{2.20}$$

where P is pressure and V^* is activation volume. T_{ref} is the reference temperature and I choose 773 K. The reference viscosity is chosen4×10^{19} Pa s

2.1.6 Setting of simulations

I solved the above equations using the following method. The finite volume method was used for spatial integration. The number of grids is 100 divisions

Table 2.2: Parameters used in numerical simulation. $\rho_{\rm core}$ is chosen the similar value to carbonaceous chondrite.

Parameter	Symbol	Units	Value	reference
Density of ice	$\rho_{\rm ice}$	kg m^{-3}	920	[17]
Density of methane hydrate	$\rho_{\rm hyd}$	kg m^{-3}	920	[17]
Density of ocean	$\rho_{\rm oce}$	kg m^{-3}	1000	[17]
Density of rocky ice III	$\rho_{\rm iceIII}$	kg m^{-3}	1150	[22, 34]
Density of rocky ice V	$\rho_{\rm iceV}$	kg m^{-3}	1240	[22, 34]
Density of rocky ice VI	$\rho_{\rm iceVI}$	kg m^{-3}	1330	[22, 34]
Density of rocky core	$\rho_{\rm core}$	kg m^{-3}	2500	[35]
Specific heat of ice	$C_{\rm p,ice}$	J kg^{-1} K^{-1}	2100	[17]
Specific heat of methane hydrate	$C_{\rm p,hyd}$	J kg^{-1} K^{-1}	2100	[17]
Specific heat of HP ice	$C_{\rm p,HPice}$	J kg^{-1} K^{-1}	2650	[36]
Specific heat of rocky core	$C_{\rm p,core}$	J kg^{-1} K^{-1}	1000	[12]
Thermal conductivity of ice	$k_{\rm ice}$	W m^{-1} K^{-1}	2.6	[37]
Thermal conductivity of methane hydrate	$k_{\rm hyd}$	W m^{-1} K^{-1}	0.6	[20]
Thermal conductivity of HP ice	$k_{\rm HPice}$	W m^{-1} K^{-1}	1.6	[38]
Thermal conductivity of rocky core	$k_{\rm core}$	W m^{-1} K^{-1}	3.0	[12]
Reference viscosity of ice	$\eta_{\rm ice}$	Pa s	1.0×10^{14}	[29]
Reference viscosity of methane hydrate	$\eta_{\rm hyd}$	Pa s	2.0×10^{15}	[21]
Reference viscosity of rocky core	$\eta_{\rm core}$	Pa s	4.0×10^{19}	[33]
Reference temperature of rocky core	$T_{\rm ref,core}$	K	773	[33]
Activation energy of ice	$E_{\rm a,ice}$	J mol^{-1}	60000	[29]
Activation energy of methane hydrate	$E_{\rm a,hyd}$	J mol^{-1}	90000	[21]
Activation energy of HP ice	$E_{\rm a,HPice}$	J mol^{-1}	30000	[39]
Activation energy of rocky core	$E_{\rm a,core}$	J mol^{-1}	8900	[33]
Activation volume of rocky core	$V^*_{\rm core}$	m^3 mol^{-1}	3.2×10^{-6}	[33]
Thermal expansivity of ice	$\alpha_{\rm ice}$	K^{-1}	10^{-4}	[12]
Thermal expansivity of methane hydrate	$\alpha_{\rm hyd}$	K^{-1}	10^{-4}	[40]
Thermal expansivity of HPice	$\alpha_{\rm HPice}$	K^{-1}	1.5×10^{-4}	[34]
Latent heat of ice	$L_{\rm ice}$	J kg^{-1}	333000	[12]
Latent heat of methane hydrate	$L_{\rm hyd}$	J kg^{-1}	437000	[41]
Latent heat of iceIII	$L_{\rm iceIII}$	J kg^{-1}	256000	[37]
Latent heat of iceV	$L_{\rm iceV}$	J kg^{-1}	275000	[37]
Latent heat of iceVI	$L_{\rm iceVI}$	J kg^{-1}	306000	[37]

for the entire icy shell and 100 divisions for the rocky core. However, if the grid size becomes too large ($\gg\sim$1 km), I adjust the number of grids accordingly. The fourth order Runge-Kutta method was used for time integration. The time step

always satisfies the CFL condition. That is, Δt satisfies the following equation:

$$\Delta t < 0.5 \rho C_p \Delta r^2 \left(\frac{1}{k} + \frac{1}{k_v} \right). \tag{2.21}$$

where Δr is the size of computational cell and Δt is the time step. The surface boundary condition assumes the temperature is fixed at the surface temperature. The boundary condition at the center is that the spatial derivative of the heat flow is zero. That is, the center is adiabatic. For the boundary with the ocean, the boundary surface temperature is fixed at ocean temperature. Boundary conditions between different materials (e.g. rock-ice interface) determine the temperature so that the heat flow is matched at the boundary.

2.2 Growth of methane hydrate layer

In Kamata et al. (2019), which considered the growth of methane hydrate layer in the thermal evolution of Pluto, it was assumed that seawater is always saturated with methane. However, the amount of methane in the subsurface ocean is an important factor for the growth of methane hydrate layer because a large amount of methane is taken into the methane hydrate when it is formed. Therefore, I incorporate the rule that methane hydrate can only be formed if the ocean is saturated with methane into the model.

2.2.1 Calculation of methane saturated concentration

Methane saturation concentrations in ocean is determined from experiments and theories [42]. The methane saturation concentrations in ocean at the temperature and pressure conditions that methane hydrate is formed is also investigated. I fitted this methane saturation concentration with a cubic function as follows:

$$m_{\mathrm{CH_4,satu,bou}} = \exp(A(\frac{1}{T_{\mathrm{oce}}})^3 + B(\frac{1}{T_{\mathrm{oce}}})^2 + C(\frac{1}{T_{\mathrm{oce}}}) + D) \tag{2.22}$$

where T_{oce} is the ocean temperature, $m_{\mathrm{CH_4,satu,bou}}$ is the methane solubility at the ocean/shell boundary and its unit is $\mathrm{mol\,m^{-3}}$, $A = 9.1589 \times 10^9$ $\mathrm{K^3}$, $B =$

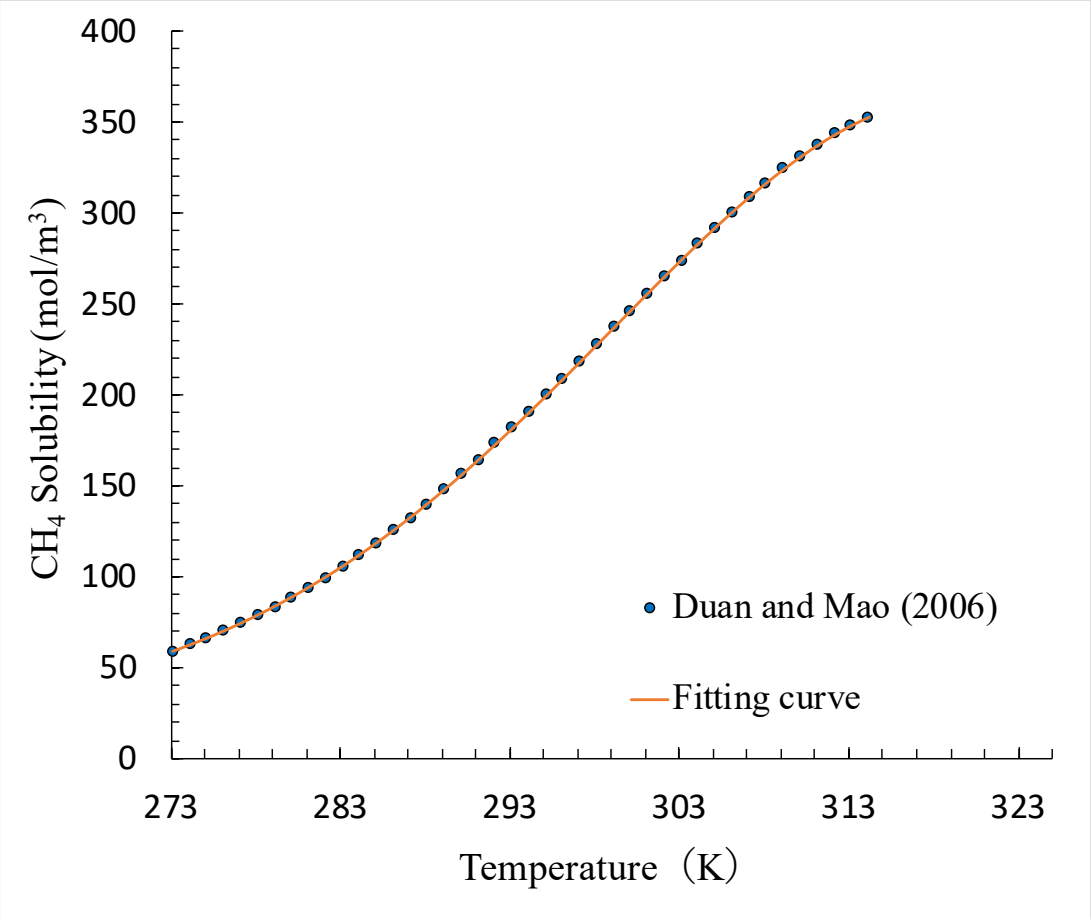

Figure 2.3: Solubility of methane against temperature is shown.The points in the figure are taken from Duan and Mao(2006)[42]. The curve represents the fitting curve used in this study. The fitting equation is 2.22

-9.7261×10^7 K^2, $C = 3.3963 \times 10^5$ K, and $D = -3.8513 \times 10^2$.

Figure 2.3 shows the obtained fitting curves and the values of Duan and Mao (2006). The horizontal axis is the dissociation point of methane hydrate. The coefficient of determination is 0.99.

2.2.2 Rules for the growth of methane hydrate layers

I set the following three rules for methane hydrate growth. (i) The ocean is supersaturated with methane in order for methane hydrate to be formed. The

phase diagram of methane hydrate shown in Figure 1.4 assumes that the methane is saturated. It is known that the dissociation point of methane in ocean drops dramatically when it becomes unsaturated [43]. The treatment of the case where ocean is methane unsaturated is discussed in a later subsection. (ii) The temperature at the bottom of the icy shell is below the dissociation point of methane hydrate. This is a natural rule. (iii) At the bottom of the icy shell, the dissociation point of methane hydrate is above the melting point of ice. In general, the larger the undercooling, which is the temperature difference from the melting point, the faster the crystal growth rate. Methane hydrate layer is assumed to grow when methane hydrate has a faster growth rate than ice.

When the above rules are satisfied, the methane hydrate layer grows. The dissociation point of methane hydrate when methane is supersaturated in ocean is given as follows:

$$T_{\mathrm{m,hyd}} = \frac{b}{\ln(\frac{P}{1000}) - a}$$

where $a = 38.980$ and $b = -8533.80$ K ([19]). The method of calculating the growth of methane hydrate layer is slightly different from that of ice layer[17]. At the bottom of methane hydrate layer, methane hydrate layer grows when the outgoing heat flux is larger than the incoming heat flux. Here, there is no change in ocean temperature. When the incoming heat flux is greater than the outgoing heat flux, the ocean temperature increases. When the ocean temperature exceeds the dissociation point of methane hydrate, the methane hydrate layers melt. Here, the ocean temperature drops to the dissociation point of methane hydrate. When calculating the heat transport in methane hydrate layer, the methane hydrate layer and the overlying ice layer are considered as separate layers. In other words, it assumes a two-layer convection-like situation in an icy shell. This assumption is based on the fact that methane hydrate is about an order of magnitude more viscous than ice and thus has a different convection style. Note that, in this study, methane hydrate layer is thinner and more viscous than ice layer, which causes little convection of the methane hydrate layer.

When methane hydrate grows or dissociates, the methane concentration in ocean changes. In this study, the compositional formula of methane hydrate

is assumed to be $CH_4 \cdot 6\,H_2O$. The hydration number of the Earth's natural methane hydrate is also comparable [44]. As shown in Table 2.2, the density of methane hydrate is assumed to be 920 $\mathrm{kg\,m^{-3}}$. In this case, the amount of methane contained in 1 $\mathrm{m^3}$ of methane hydrate $C_{\mathrm{CH_4,MH}}$ is 7419 $\mathrm{mol\,m^{-3}}$ Therefore, the change in methane concentration in ocean due to the growth of methane hydrate layer is described as follows:

$$\Delta C_{\mathrm{CH_4,oce}} = \frac{C_{\mathrm{CH_4,oce}} V_{\mathrm{oce}} - C_{\mathrm{CH_4,MH}} \Delta V_{\mathrm{MH}}}{V_{\mathrm{oce}} - \Delta V_{\mathrm{oce}}} - C_{\mathrm{CH_4,oce}} \tag{2.23}$$

where V_{oce} is the ocean volume, ΔV_{oce} is the change in the ocean volume, and ΔV_{MH} is the change in the methane hydrate layer volume.

2.2.3 Introducing the Mix Layer

As the methane hydrate layer grows, the ocean eventually becomes methane unsaturated. In this case, the icy shell is expected to grow by the following process. (i) Methane hydrate layer grows. Under the condition of methane unsaturation, the dissociation point of methane hydrate is known to drop significantly [43]. The dissociation point drops by about 40 K when the methane concentration in ocean is less than 1%. However, even if the dissociation point of methane hydrate decreases, if it is above the melting point of ice, methane hydrate grows. (ii) A mixture of methane hydrate and ice is formed. As the dissociation point of methane hydrate decreases, it eventually matches the melting point of ice. Then, a mixture of methane hydrate and ice begins to grow, and I call this layer the Mix layer. In this study, I omit the process (i) for simplicity. Since the thickness of the methane hydrate layer formed by the process (i) is considered to be thin, this assumption is not expected to have a significant impact on my results. For example, consider the case where the ocean reached a methane saturation concentration due to the growth of methane hydrate layer at a depth of 30 km ($\sim$ 3 MPa) in Enceladus. The radius of Enceladus is 252.0 km. At this time, the methane concentration in the ocean C_{oce} is 65 $\mathrm{mol\,m^{-3}}$ following the equation (2.22). Assuming that 100 m of methane hydrate will be formed from here, the

methane concentration in the ocean will decrease as follows:

$$C'_{\mathrm{oce}} = \frac{C_{\mathrm{oce}}\ \frac{4}{3}\pi R_{\mathrm{old}}^3\ - C_{\mathrm{CH_4,MH}}\frac{4}{3}\pi\left(R_{\mathrm{old}}^3\ - R_{\mathrm{new}}^3\right)}{\frac{4}{3}\pi R_{\mathrm{new}}^3} \tag{2.24}$$

where C_{oce} is the methane concentration updated by methane hydrate formation, R_{old} is the radius at the ice/ocean interface before methane hydrate formation and is 222.0 km, and R_{new} is the radius at the ice/ocean interface after methane hydrate formation and is 221.9 km. Putting all the values into the above equation, $C_{\mathrm{oce}} = 55\ \mathrm{mol\,m^{-3}}$ is obtained. The concentration is less than 0.1% . Then, the dissociation point of methane hydrate is about the same as the melting point of ice at the pressure inside Enceladus (∼a few MPa). Even if it is a large moon under high pressure, methane hydrate formation from methane saturation concentration is expected to use up methane in the ocean quickly. Therefore, in my calculations, I ignored the process (i) and introduced the layer formed by the process (ii) as a mix layer. I assume that the ocean is kept at a saturated concentration of methane as the mix layer grows.

The amount of methane hydrate contained in the mix layer is not very large. For example, as shown in the example above, if a mix layer is formed from a saturated concentration of 65 $\mathrm{mol\,m^{-3}}$, the volume fraction of methane hydrate is 65/7419 = 0.0088, which is less than 1% . So, the mix layer consists almost entirely of ice.

The physical properties of the mix layer are described by linear combination except for melting point and viscosity. The viscosity of the mix layer is described as follows:

$$\eta_{\mathrm{mix}} = \eta_{\mathrm{hyd}}^{\phi_{\mathrm{hyd}}}\eta_{\mathrm{ice}}^{\left(1-\phi_{\mathrm{hyd}}\right)} \tag{2.25}$$

where ϕ_{hyd} is the volume fraction of methane. The melting point is assumed to be the same as that of ice Ih. When the mix layer is formed beneath the methane hydrate layer for the first time, the ocean temperature must be considered. When the methane hydrate layer exists, ocean temperature may be high because the dissociation point of methane hydrate is higher than the melting point of ice. In this case, the ocean temperature has to drop to the melting point of the mix layer in order for the mix layer to start to grow. Ocean temperature changes until the mix layer starts to grow. The thermal evolution of the mix layer and the growth

of the mix layer are carried out in the same way as in the case of the ice layer.

2.2.4 Benchmark of the growth of methane hydrate layer

In order to confirm whether the introduction of methane hydrate layer into the conventional model described above is done correctly, I compared the calculation results obtained from my developed code with the results of Kamata et al. (2019). The calculations are performed for Pluto with a radius of 1188.0 km and a rocky core size of 910.0 km. The density of the rock is 3000 $\mathrm{kg\,m^{-3}}$, the density of the ocean is 1000 $\mathrm{kg\,m^{-3}}$, and the density of ice and methane hydrate is 920 $\mathrm{kg\,m^{-3}}$. The initial internal structure is 100.0 km thick of icy shell, 178.0 km thick of ocean, and 0.0 km thick of methane hydrate layer. The initial temperature conditions are as follows: the surface temperature is 40.0 K; the temperature of the bottom of the icy shell is the melting point at the depth; the interior temperature of the icy shell is a linear function connecting the surface temperature and the melting point at the bottom of the icy shell; and the rocky core and ocean temperatures are the same as the melting point at the bottom of the icy shell. The initial methane concentration was set to $1.0 \times 10^6\,\mathrm{mol\,m^{-3}}$ in order to assume a situation with sufficient methane as in Kamata et al. (2019). This concentration is well above the saturated methane concentration. Figure 2.4 shows the result of Kamata et al. (2019). Figure 2.5 shows the changes in the internal structure of Pluto over 4.6 Gyrs. Since the two figures show similar results, the implement of methane hydrate layer into the conventional model is considered to be successful.

2.3 Introduction of high pressure ice

High pressure ice (HP ice) appears in large icy moons such as Titan due to high pressure inside. Even on Pluto, HP ice appears depending on the size of the rocky core [9]. However, since the system where methane hydrate layer and HP ice layer coexist has not been considered so far, I newly introduce HP ice layer into my model.

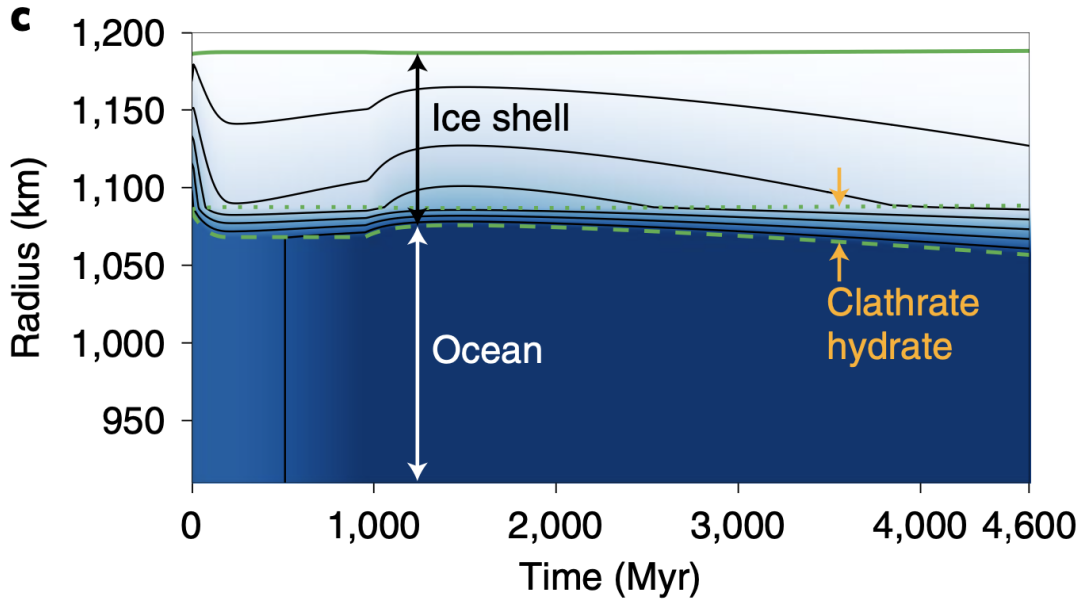

Figure 2.4: The results of the thermal evolution of Pluto in Kamata et al. (2019)[17]

2.3.1 Growth of the HP ice layer

In this study, I describe the growth of the HP ice layer using a different method from that proposed by Kimura and Kamata (2020). This is because Kimura and Kamata (2020) calculate heat transport in the ocean, while my model calculates the ocean as a heat reservoir of constant temperature. The HP ice layer starts to grow when the temperature at the top of the rocky core (equal to the ocean temperature) becomes lower than the melting point of the HP ice. The melting point of HP ice is given by [45]

$$T_{\mathrm{m,HPice}}(P) = a + bP + c\ln(P) + d/P + e\sqrt{P}. \tag{2.26}$$

Here, the coefficients differ depending on the phase of the HP ice. In this study, ice III, ice V, and ice VI are assumed to be HP ice. Each coefficient is summarized in Table 2.3.

To consider the growth of HP ice layer, I consider the conservation of thermal energy during the growth of HP ice layer and icy shell. The conservation equation

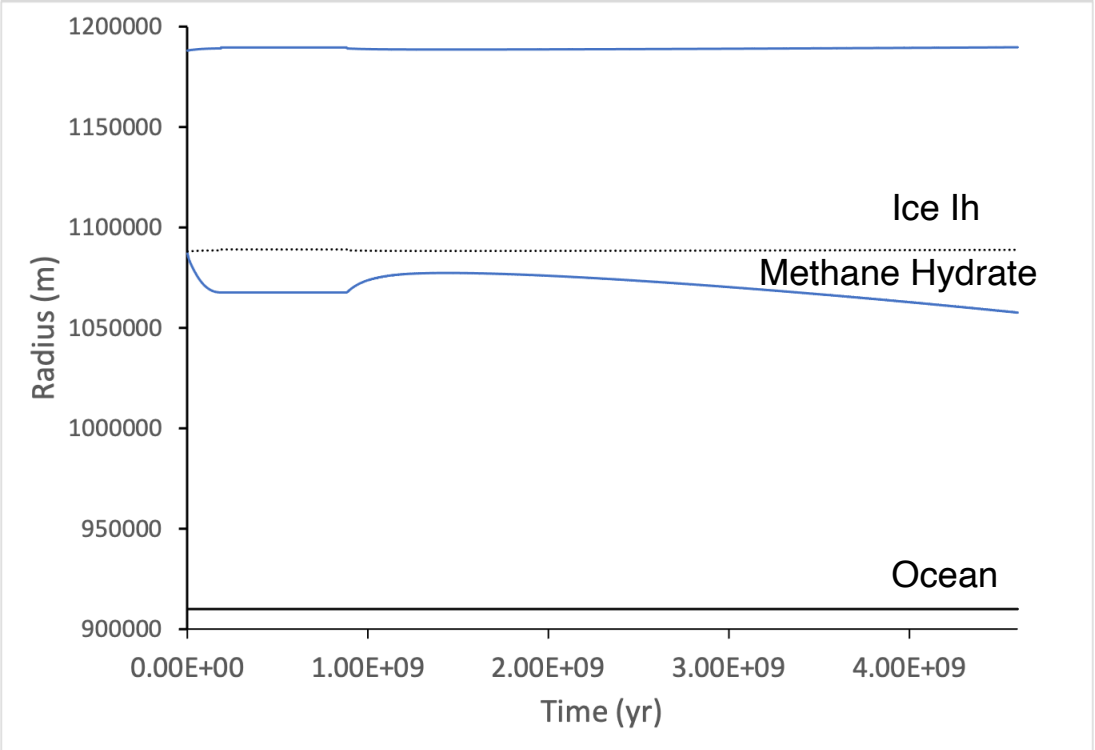

Figure 2.5: The results calculated with my computational model under the same conditions as Kamata et al.(2019). By setting the initial methane concentration to $1.0 \times 10^6\,\mathrm{mol\,m^{-3}}$, the subsurface ocean is always supersaturated, i.e., the same conditions as in Kamata et al. (2019)

Table 2.3: HP ice parameters used in numerical simulation [45].

Phase	a	b	c	d	e
Ice III	10.277	0.0265	50.1624	0.5868	-4.3288
Ice V	5.0321	-0.0004	30.9482	1.0018	0.0
Ice VI	4.2804	-0.0013	21.8756	1.0018	1.0785

for thermal energy is as follows:

$$F_{\text{in}}\, S_{\text{in}}\ - F_{\text{out}}\, S_{\text{out}} = \rho_{\text{HPice}}\, L_{\text{HPice}}\, S_{\text{in}}\, \frac{\Delta D_{\text{HPice}}}{\delta t} + \rho_{\text{shell}}\, L_{\text{shell}}\, S_{\text{out}}\, \frac{\Delta D_{\text{shell}}}{\Delta t} + \rho_{\text{oce}}\, C_{p,\ \text{oce}}\, V_{\text{oce}}\, \frac{\Delta T_{\text{m}}}{\Delta t} \tag{2.27}$$

where F_{in} is the incoming heat, F_{out} is the outgoing heat, S_{in} is the surface area at ocean bottom, S_{out} is the surface area at ocean top, ΔD_{HPice} is the change of HP ice layer thickness, ΔD_{shell} is the change of icy shell thickness, and ΔV_{oce}. Since the temperature at the ocean bottom, ocean temperature, and the temperature at the icy shell bottom are equal, I obtain the following equation:

$$\frac{\Delta T_{m,\ \text{shell}}}{\Delta D_{\text{shell}}} = \frac{\Delta T_{m,\ \text{HPice}}}{\Delta D_{\text{HPice}}} \tag{2.28}$$

where $\Delta T_{m,\ \text{shell}}$ is the change of melting point of the shell bottom material at the shell bottom pressure and $\Delta T_{m,\ \text{HPice}}$ is the change of HP ice melting point at the top of the HP layer. Using the above, I obtain the following equations for the thickness change of the icy shell and the thickness change of the HP ice layer:

$$\Delta D_{\text{shell}}\ = \frac{(F_{\text{in}}\, S_{\text{in}}\ - F_{\text{out}}\, S_{\text{out}}\,)\,\Delta t}{\left(\rho_{\text{shell}}\, L_{\text{shell}}\, S_{\text{out}}\ - \rho_{\text{HPice}}\, L_{\text{HPice}}\, A S_{\text{in}}\ + \rho_{\text{oce}}\, C_{\text{p,oce}}\, V_{\text{oce}}\ \left(\rho_{\text{shell}}\, g_{\text{shellbot}}\, \frac{dT_{\text{m,shell}}}{dP}\right)\right)} \tag{2.29}$$

$$A = \frac{\rho_{\text{shell}}\, g_{\text{shellbot}}\, \frac{dT_{m,\ \text{shell}}}{dP}}{-\rho_{\text{HPice}}\, g_{\text{HPtop}}\, \frac{dT_{m,\ \text{HPice}}}{dP}} \tag{2.30}$$

$$\Delta D_{\mathrm{HPice}} = A \Delta D_{\mathrm{shell}} \tag{2.31}$$

where g_{shellbot} is the gravitational acceleration at the shell bottom, and g_{HPtop} is the gravitational acceleration at the top of the HP ice layer. If the bottom of the icy shell is the methane hydrate layer, the rules of growth of methane hydrate discussed in Section 2.4.2 are applied. Here, F_{in} does not exceed the melting point temperature gradient of the HP ice. F_{in} exceeds the melting point temperature gradient of the HP ice, which means that the top of the HP ice melts. Since the bottom of the HP ice layer is in contact with the rocky core, it may melt due to heat from the rocky core. When the bottom of the HP ice layer melts, the melt or its heat is quickly transported to the top of the HP ice layer [46]. In my model, I assume that when the bottom of the HP ice layer exceeds the melting point, the heat flux from the rocky core is instantaneously transported to the top of the HP ice layer. In other words, it is described as follows:

$$F_{\mathrm{in}} = F_{\mathrm{in,top}} + F_{\mathrm{in,bot}} \frac{S_{\mathrm{in,bot}}}{S_{\mathrm{in}}} \tag{2.32}$$

where $F_{\mathrm{in,top}}$ is the heat flux at the top of HP ice layer, $F_{\mathrm{in,bot}}$ is the heat flux at the bottom of HP ice layer, and $S_{\mathrm{in,bot}}$ is the surface area at the bottom of HP ice layer. $F_{\mathrm{in,bot}}$ is 0 if the temperature at the boundary between the core and the HP ice layer is below the melting point of HP ice. In the calculation of thermal evolution in this model, the HP ice layer is treated as a single layer and there are no phase differences except for the melting point, latent heat and the density. This treatment is considered to generate errors when more than one phase appears in the HP ice layer. For the evaluation of convection in the HP ice layer, I use the conventional mixing length theory because it is outside the scope of the modified mixing length theory.

2.3.2 Benchmark of the growth of high pressure ice layer

In order to confirm that the introduction of the HP ice layer into my model is correct, I compare the results of my calculations with the result of Kimura and Kamata (2020). Calculations are performed for Pluto, which has a radius

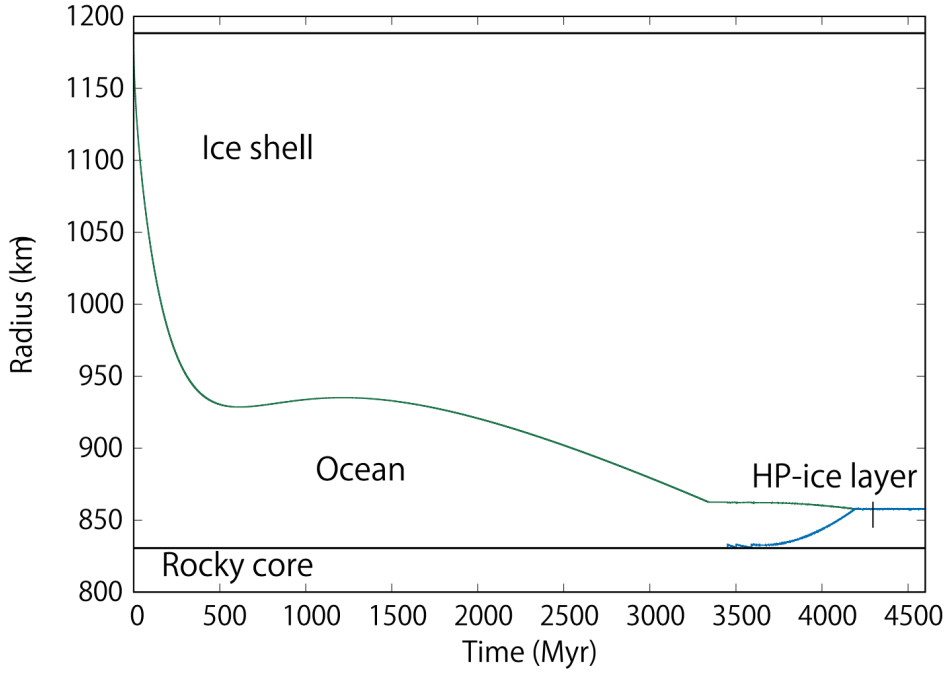

Figure 2.6: The result of the thermal evolution of Pluto considering the high-pressure ice layer in Kimura and Kamata (2020).

of 1188.0 km and a rocky core size of 830.5 km. The pressure in the interior of Pluto results in the appearance of ice III. Ice II is not taken into account. The density of rock is 3500 $\mathrm{kg\,m^{-3}}$, the density of the ocean is 1000 $\mathrm{kg\,m^{-3}}$, the density of ice Ih is 930 $\mathrm{kg\,m^{-3}}$, and the density of HP ice (ice III) is 1165 $\mathrm{kg\,m^{-3}}$. The initial internal structure is 100.0 km thick icy shell, 257.5 km thick ocean, 0.0 km thick methane hydrate layer, and 0.0 km thick HP ice layer. The initial temperature conditions are as follows: the surface temperature is 44.0 K; the temperature of the bottom of the icy shell is the melting point at the depth; the interior temperature of the icy shell is a linear function connecting the surface temperature and the melting point at the bottom of the icy shell; and the rocky core and ocean temperatures are the same as the melting point at the bottom of the icy shell. Since methane hydrate layer is not considered, the initial methane concentration is 0.0 $\mathrm{mol\,m^{-3}}$.

Figure 2.6 is the result of Kimura and Kamata (2020). Figure 2.7 shows the changes in the internal structure of Pluto over 4.6 Gyrs under the same conditions

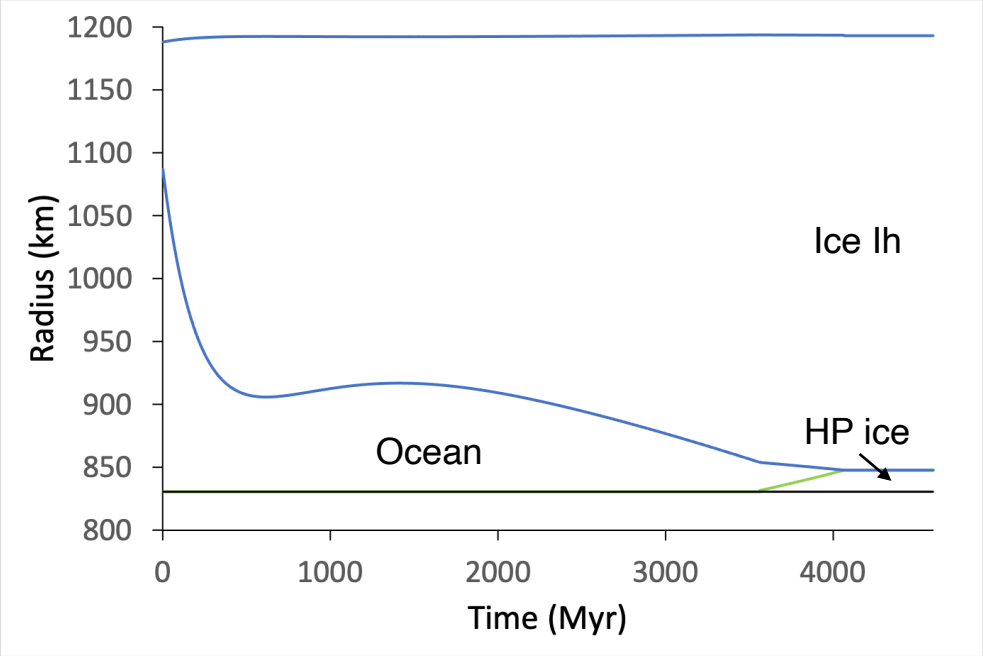

Figure 2.7: The result of the thermal evolution of Pluto obtained by my computational model under the same conditions as Kimura and Kamata.

with Kimura and Kamata (2020). The two graphs show similar results. The thicknesses are slightly different, but I attribute this to the different physical properties used in my model. Therefore, I think that the introduction of HP ice layer is also successful.

2.4 Summary of the thermal evolution model

As described above, methane hydrate layer, mix layer, and HP ice layer are introduced into the conventional thermal evolution model. The following is a summary of the thermal evolution calculations in this study. First, I consider icy moons divided into ice layer - methane hydrate layer - mix layer - ocean - HP ice layer - rocky core. Each layer except for the ocean is divided into thin sublayers, and the heat transport between each sublayer is calculated. The heat transports between the sublayers of the rocky core and the HP ice layer are calculated using the conventional mixing length theory. For the ocean, heat

transport calculation is not performed and it is assumed that heat is transferred instantaneously from the bottom to the top. In the icy shells (including ice layer, methane hydrate layer, and mix layers), heat transport calculations are performed using the modified mixing length theory. In the ocean, the methane concentration is calculated, and methane hydrate is formed in the case of methane saturation. In the case of unsaturation, the mix layer starts to grow. When the temperature of the ocean falls below the melting point of HP ice, HP ice layer grows. Using the above model, I will calculate the thermal evolution of actual icy moons in the next section and beyond.

Chapter 3

Methane Hydrate Keeps Enceladus and Mimas Oceans Thick

3.1 Introduction: active Enceladus and inactive Mimas

Saturn's moons, Enceladus and Mimas, are very different in appearance. Enceladus is very active, while Mimas is inactive. Figure 3.1 and 3.2 show their images. Table 3.1 shows the physical and orbital properties of Enceladus and Mimas. Enceladus has a radius of 252.0 km and a bulk density of 1611 $\mathrm{kg\,m^{-3}}$, while Mimas has a radius of 198.2 km and a bulk density of 1149 $\mathrm{kg\,m^{-3}}$. This difference is thought to have determined the fate of Enceladus and Mimas, but the truth is not clear.

Table 3.1: The thermal and physical properties of Mimas and Enceladus [47].

Parameter	Symbol	Units	Mimas	Enceladus
Mean surface radius	R	km	198.2	252.0
Bulk density	ρ	kg $\mathrm{m^{-3}}$	1149	1611
Surface temperature	T_{surf}	K	76	59
Semimajor axis	a	km	185,539	237,948
Orbital eccentricity	e		0.0196	0.0047

Enceladus is covered with bright ice on its surface, suggesting that it experienced some kind of surface renewal. Near the south pole, plume containing ice particles and volatiles erupts [2]. The plume contains molecular hydrogen, suggesting that there is ongoing hydrothermal activity in Enceladus [48]. Simi-

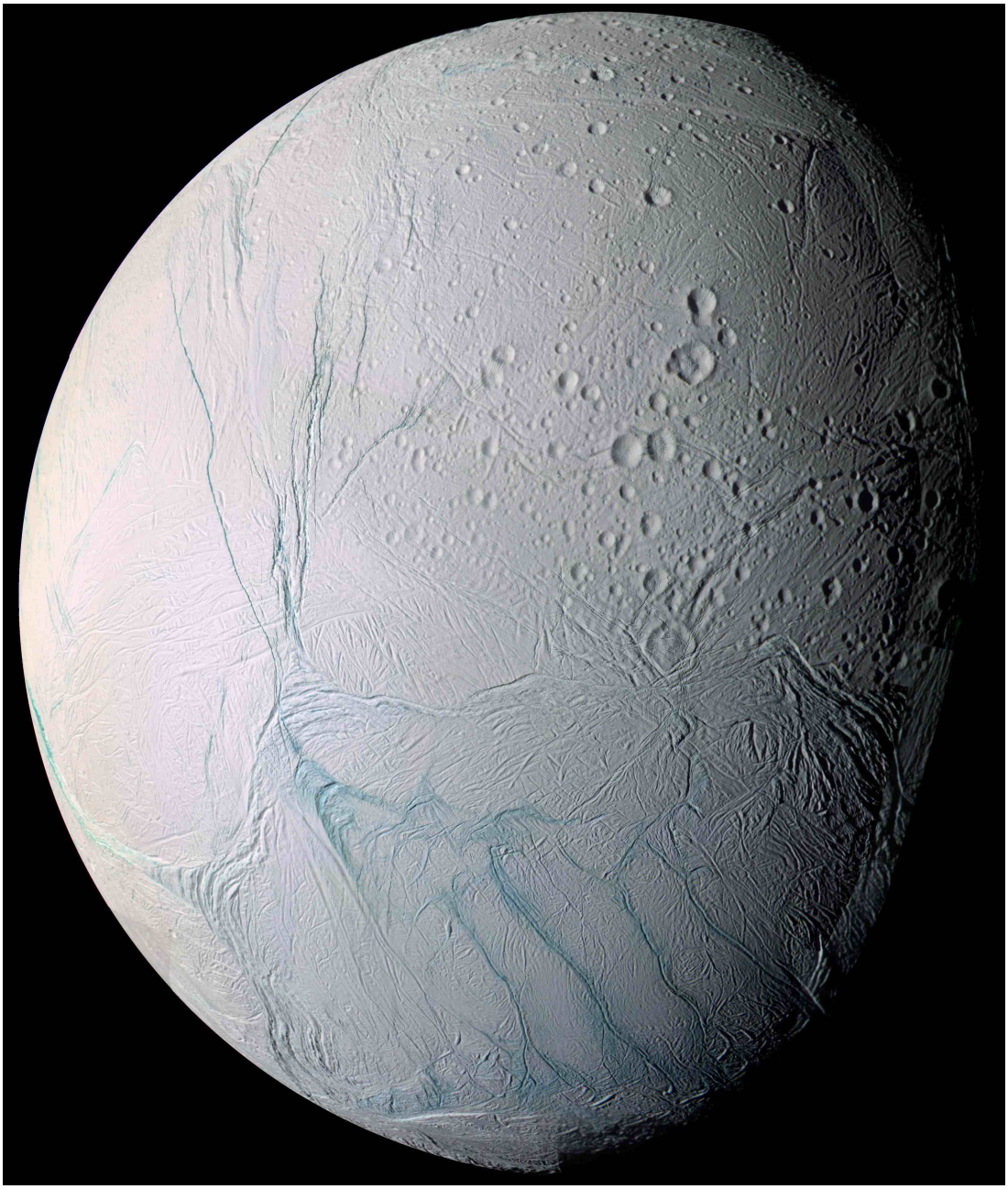

Figure 3.1: Enceladus' image. Credit:NASA/JPL/Space Science Institute

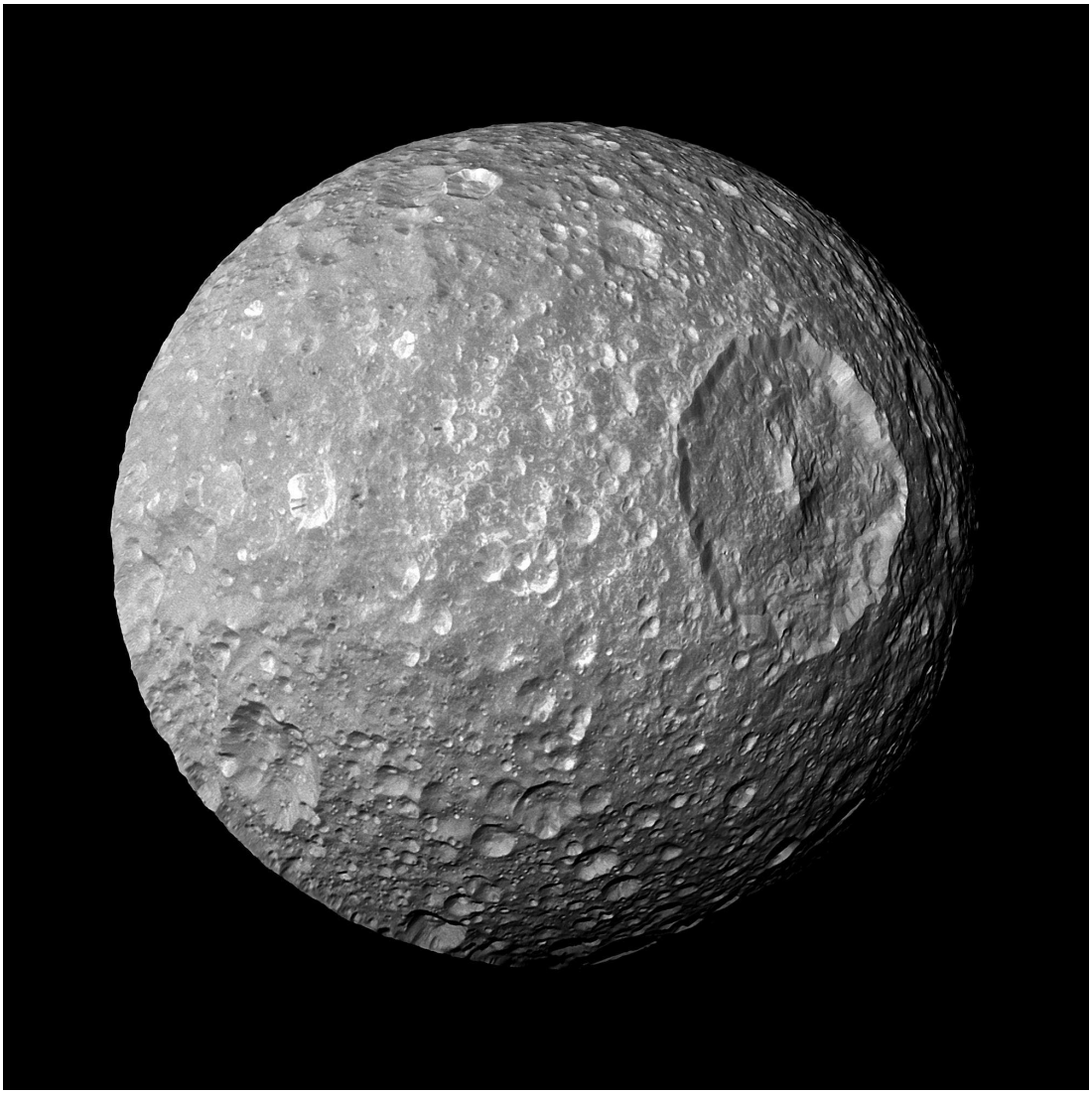

Figure 3.2: Mimas' image. Credit:NASA/JPL/Space Science Institute

larly, the E-ring particles, which originated from the Enceladus plume, contain nano-sized silica, suggesting hydrothermal activity in Enceladus [49]. In addition, the Cassini spacecraft discovered a strong heat flow (∼15 GW) from a fractured region near the south pole called the Tiger Stripe [50]. These observational facts indicate that Enceladus is very active.

In contrast to Enceladus, Mimas has a very dark surface. The surface of Mimas is covered with numerous craters, many of which have not been thermally relaxed. Even the largest crater, Herschel Crater, has very little relaxation. Since the cratering rate of Saturnian system is uncertain, the absolute age is not known. But the crater density suggests that most of the Mimas surface is older than the Enceladus surface [51]. In addition, the surface of Mimas has few fractures caused by geological activity. These facts indicate that Mimas is inactive.

The curious thing is that both moons may have a subsurface ocean. For Enceladus, it is not strange because it is active as described above. Gravity, libration, and topography also suggest the existence of an ocean [52, 53, 7, 54, 55], although the thickness of the ocean varies among the studies. For Mimas, the existence of an ocean has been considered difficult because it is difficult to reconcile an inactive surface with the presence of an ocean [47]. Rhoden et al. (2017), which assessed the tidal stress on Mimas, also concluded that the presence of ocean is not reconcilable with the lack of tectonic activity [56]. However, Tajeddine et al. (2014) reported the observation of strong libration in Mimas [8]. This strong libration suggests the existence of a subsruface ocean or a lumpy core. Noyelles (2017) states that the phase lag of the libration supports the presence of an ocean [57]. Thus, the existence of an ocean has been suggested, although uncertainly, in Mimas.

In small icy moons such as Enceladus and Mimas, heating due to decay of long-lived radioactive elements is small. In Enceladus and Mimas, the main heat source to maintain the subsurface ocean is tidal heating. In general, if the satellite is in synchronous state with the primary, the total amount of tidal heating generated by the satellite is as follows:

$$\dot{E} = -\frac{21}{2}\,\mathrm{Im}\,(k_2)\,\frac{(nR_\mathrm{s})^5}{G}e^2 \tag{3.1}$$

where $\mathrm{Im}\,(k_2)$ is the imaginary part of the Love number, G is the gravitational constant, n is the mean motion, R_s is the radius of the moon, and e is the orbital eccentricity ([58]). Since the amount of tidal heating is proportional to the square of the eccentricity, even Mimas, which has a larger eccentricity than Enceladus, may receive a sufficiently large amount of tidal heating. However, the tidal heating is proportional to the tidal Love number, which describes how much the interior of a body is deformed by tidal forces, and evaluating the tidal heating is difficult because of the complexity of evaluating the tidal Love number. On the other hand, if two moons are in mean motion resonance, the equilibrium tidal heating can be calculated [59]. The equilibrium tidal heating can be obtained by considering the conservation of angular momentum and mass, as follows:

$$\begin{aligned}\dot{E}_\mathrm{eq} = &\frac{n_0 T_0}{\sqrt{1-e_0^2}} + \frac{n_1 T_1}{\sqrt{1-e_1^2}} \\ &- \frac{T_0 + T_1}{L_0 + L_1}\left(\frac{GMm_0}{a_0} + \frac{GMm_1}{a_1}\right)\end{aligned} \tag{3.2}$$

$$T = \frac{3}{2}\frac{Gm^2 R_p^5 k_{2p}}{a^6 Q_p} \tag{3.3}$$

where T is the torque caused by the primary, L is the angular momentum, M is the mass of the primary, m is the mass of the moon, and a is the semimajor axis. Subscripts 0 and 1 represent the inner moon and outer moon, respectively. In this case, the tidal heating does not depend on the internal structure of the satellite, but can be obtained from the planet's Love number and Q_p. The current Q_p of Saturn is estimated from astrometry, which is $\sim$2000. Since Enceladus is currently in a 2:1 resonance with Dione, the equilibrium tidal heating is found to be $\sim$10 GW [60]. On the other hand, Mimas is not currently in any eccentricity-type resonance. However, orbital evolution calculations suggest that it may have experienced a 3:2 resonance with Enceladus 0.34 Gyr ago. The Q_p at this time is estimated to be 4800. In this case, Mimas is experiencing tidal heating of 3.6 GW [61].

In this study, I thought that the assumption of methane hydrate layer might be effective to reconcile the inactive surface and the existence of the subsurface

ocean in Mimas. As described in Section 1, methane hydrate has lower thermal conductivity than ice and higher viscosity than ice. These properties have the effect of preventing the heat from the rocky core from escaping to the outside, and thus thicker oceans can be realized. Kalousova and Sotin (2020) showed that the presence of methane hydrate layer on Titan's surface keeps heat from escaping from the interior and raises the temperature of the ice layer beneath the methane hydrate layer [62]. Kamata et al. (2019) showed that the existence of methane hydrate layer may explain both the maintenance of the topography of the ocean/ice interface beneath Sputonik Planitia and the existence of the subsurface ocean on Pluto [17]. There is a sufficient possibility that methane hydrate also exists in the interior of Enceladus and Mimas. It is known that gas hydrates are formed when the components in the Enceladus plume are subjected to the temperature and pressure of the Enceladus subsurface ocean [18]. Based on the above, in this study, I investigate the thermal evolution considering the existence of methane hydrate layer in the interior of Enceladus and Mimas using a one-dimensional thermal evolution model. I also look for conditions where a subsurface ocean exists in both Enceladus and Mimas and Mimas becomes less active than Enceladus, i.e., the lithosphere becomes thicker.

3.2 Methods

In this study, I use the thermal evolution model developed in section 2. The differences from section 2 and the initial setup are described below.

3.2.1 Interior structures

It is known from observations that Enceladus and Mimas are differentiated. In this study, I assume that this differentiation occurred in the early stages of the formation of both moons due to accretion heating and the heat derived from decay of short-lived radioactive elements. Schubert (2007) showed that when Enceladus accretes 1.6 Myr after CAI formation, the differentiation is completed in a few Myr [63]. It is also said that the ways for Mimas to have a differentiated structure is that Mimas accretes early and be differentiated by short-lived

radioactive elements or that ice accumulate on the initial rocky core [47]. The size of the rocky core of both moons can be determined from the moon's size, ice layer thickness, bulk density, ice density, ocean density, and rock density as follows:

$$R_{\mathrm{core}} = \sqrt[3]{\frac{R^3\left(\rho_{\mathrm{bulk}} - \rho_{\mathrm{ice}}\right) - R_{\mathrm{oce}}^3\left(\rho_{\mathrm{oce}} - \rho_{\mathrm{ice}}\right)}{\left(\rho_{\mathrm{core}} - \rho_{\mathrm{oce}}\right)}} \tag{3.4}$$

where R_{core} is the core top radius, R_{oce} is the ocean top radius, R is the moon radius, and ρ_{bulk} is the moon bulk density. If the thickness of the Enceladus icy shell is 20 km and the thickness of the Mimas icy shell is 30 km, the size of the Enceladus rocky core is 190.7 km and the size of the Mimas rocky core is 98.9 km. These values are consistent with observations [52, 8].

3.2.2 Tidal heating

As described in Section 3.1, tidal heating is the main heat source in Enceladus and Mimas. In this study, tidal heating is incorporated into my model in a similar way to Kamata (2018). The summary is given below. Tidal dissipation associated with changes in eccentricity occurs mainly in the solid parts of icy moons. If the subsurface ocean is quite thin, tidal dissipation also occurs in the ocean[64], but I ignore the effect in this study. The amount of tidal heating that occurs in the rocky core depends on the nature of the rocky core. When the rocky core is rigid, the rocky core does not dissipate much due to its high viscosity [65]. On the other hand, if the rocky core is porous like gravel, the tidal dissipation is high [66]. A study of differences in tidal deformation due to regional differences in Enceladus icy shell thickness found that the tidal heating occurring within the icy shell is less than 1 GW in most regions, thus most of the tidal heating occurs in the rocky core [67]. In addition, when the radial distribution of tidal heating is calculated taking into account the different viscosities in the icy shell, it is found that the most tidal dissipation occurs near the viscosity at the melting point [68]. From the above, I assumed that the sum of the tidal heating would be injected into the bottom of the icy shell, although I did not consider where the tidal heating was occurring. Kamata (2018) and this study assume that the sum of these tidal heating is used to melt the bottom of the icy shell and increase the ocean temperature. In other words, F_{out} in equation (2.15) is given as follows:

$$4\pi R_{\rm bot}^2 F_{\rm out} = 4\pi R_c^2 F_c + Q_t \tag{3.5}$$

where $R_{\rm bot}$ is the radius at the shell bottom, R_c is the radius at the core top, $F_{\rm c}$ is the heat flux at the top of the rocky core and Q_t is the tidal heating rate. In this study, I consider this tidal heating as a free parameter. Note that this treatment underestimates the effect of convection and overestimates the melting of the lower part of the icy shell, since tidal heating actually warms the lower part of the icy shell and promotes convection. This effect is significant for icy shell that is convecting well.

3.2.3 Initial conditions

The initial icy shell thickness is assumed to be 10 km for both Enceladus and Mimas, and 0 km for the methane hydrate layer. As described in the results section, both Enceladus and Mimas quickly reach a state of near thermal equilibrium due to their small sizes. Therefore, the initial internal structure does not have a significant impact on the final internal structure. In Pluto, it is known that the initial structure does not affect the final internal structure [9]. The initial temperature of the top of the icy shell is fixed at the surface temperatures listed in Table 3.1. The temperature at the bottom of the icy shell and in the subsurface ocean is set to the melting point at the bottom of the icy shell. The temperature inside the icy shell is a linear function of the temperature at the bottom of the icy shell and the surface temperature. The temperature of the rocky core is assumed to be a free parameter between 273 K and 1273 K because it is not known how much the rocky core was warmed by the decay heat of short-lived radioactive elements during the initial differentiation. I also assume that Enceladus and Mimas have completed their differentiation, so I begin the calculations 100 Myr after the CAI.

Only methane is assumed to be dissolved in the initial subsurface ocean. Ammonia may also dissolve in the ocean, but the amount estimated from the Enceladus plume ($\sim$1%) is not enough to affect the melting point [69, 28] and is ignored in this study. Comets that are considered as precursor materials for Enceladus and Mimas contain 1% methane [14]. This is roughly equivalent to

600 mol m^{-3}. Methane is also produced by serpentinization reactions and carbon dioxide reduction if the rocks are warmed above 300°C during differentiation [70]. Based on the above, the initial methane is assumed to be a free parameter between 0 and 1000 mol m^{-3}. The methane saturation concentration at ocean temperature of 273.15 K and pressure of 2.6 MPa is about 60 mol m^{-3} (Duan and Mao 2006) Methane production by methanogen[71] and ongoing hydrothermal reactions are considered in Enceladus, but methane generation during thermal evolution is not considered in this study.

3.3 Results

3.3.1 Time evolution of internal structure

Figure 3.3 shows an example of the thermal evolution of Enceladus and Mimas. As shown in the figure, equilibrium is reached at about 100 Myr. The time evolution of heat due to the decay of long-lived radioactive elements has little effect on the internal structure, and tidal heating controls the internal structure. In the case where methane hydrate layer exists, the ocean is thicker than in the case where methane hydrate layer does not exist. The color contour in the figure shows the area where convection is occurring in the icy shell. The presence of methane hydrate suppresses the convection in the ice layer. Figure 3.4 shows the final H_2O layer's temperature profile. The temperature is dropping drastically in the methane hydrate layer. In 3.4(a), the melting point of ice and the dissociation point of methane hydrate are reversed at the boundary between methane hydrate layer and ice layer.

Therefore, it is found that the methane hydrate layer plays the role of an insulating layer that prevents heat from escaping from the interior in the icy shell. In this study, tidal heating is assumed to be constant, but this is actually incorrect because the eccentricity and internal structure actually change due to orbital and thermal evolution, as described in Section 3.1. However, as shown in the results, Enceladus and Mimas will soon be near equilibrium due to their small size, so the final internal structure is likely to be in equilibrium for the last few hundred Myr.

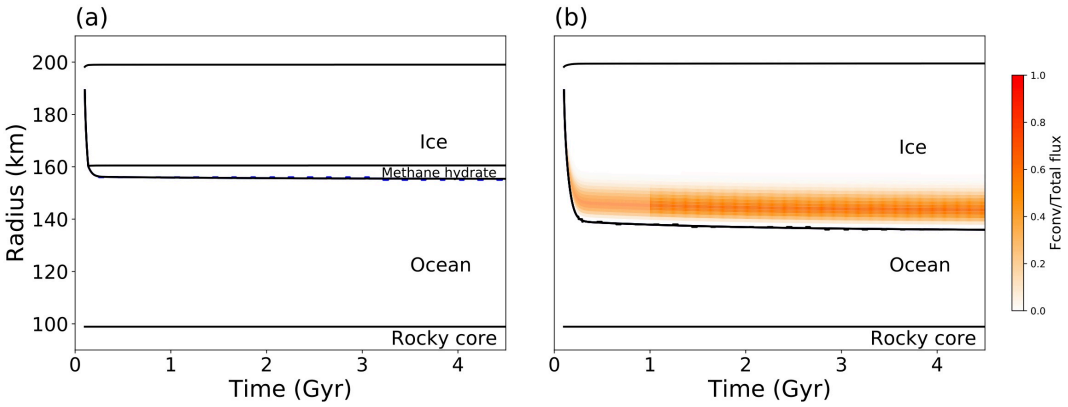

Figure 3.3: Time evolution of the internal structure of Mimas.(a) is the case where the initial methane concentration is 1000 mol m^{-3} and (b) is the case where the initial methane concentration is 0 mol m^{-3}, i.e., only ice is formed. In both cases (a) and (b), the tidal heating rate is 3 GW and the initial core temperature is 573 K. The colour contour represents the heat flux carried by convection relative to the total heat flux.

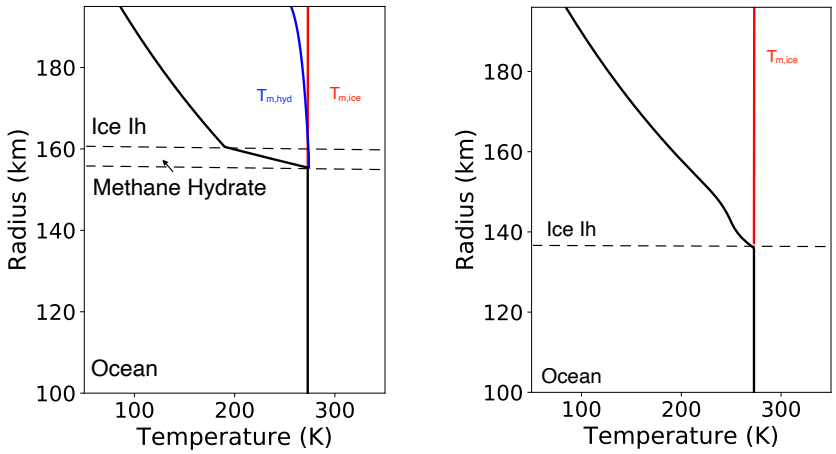

Figure 3.4: The final H_2O layer's temperature profiles are shown. (a) is the case where the initial methane concentration is 1000 mol m^{-3} and (b) is the case where the initial methane concentration is 0 mol m^{-3}. Black line represents the temperature profile. Red line represents the melting point of ice. Blue line represents the dissociation point of methane hydrate.

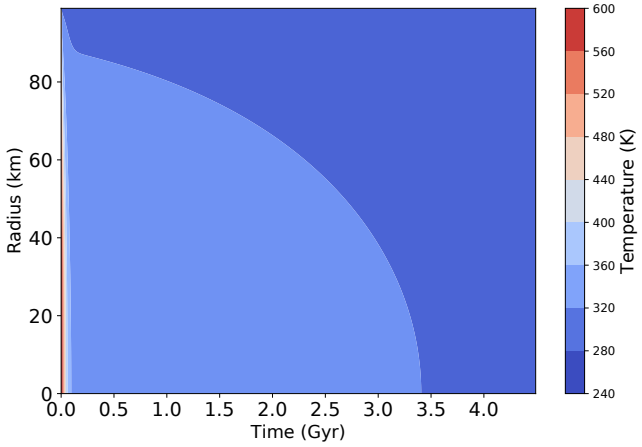

Figure 3.5: Time evolution of rock core temperature in Mimas. Initial core temperature is 573 K and Initial methane concentration is 1000 mol m^{-3}. Applied tidal heating rate is 3 GW. The colour contour represents temperature.

3.3.2 Effect of rocky core temperature on thermal evolution

Figure 3.5 shows an example of the evolution of the core temperature with time in Mimas. The initial core temperature is 573 K. As shown in the figure 3.5, the initial core temperature drops quickly and the core cannot be sufficiently heated by the heat from the decay of long-lived radioactive elements in Mimas' rocky core.

Figure 3.6 shows the difference in the evolution of the rocky core with respect to the initial temperature. It is found that the difference disappears after about 100 Myr. Similar results are obtained for Enceladus. From these results, the typical rocky core temperatures in this study are chosen 1273 K for Enceladus and 573 K for Mimas.

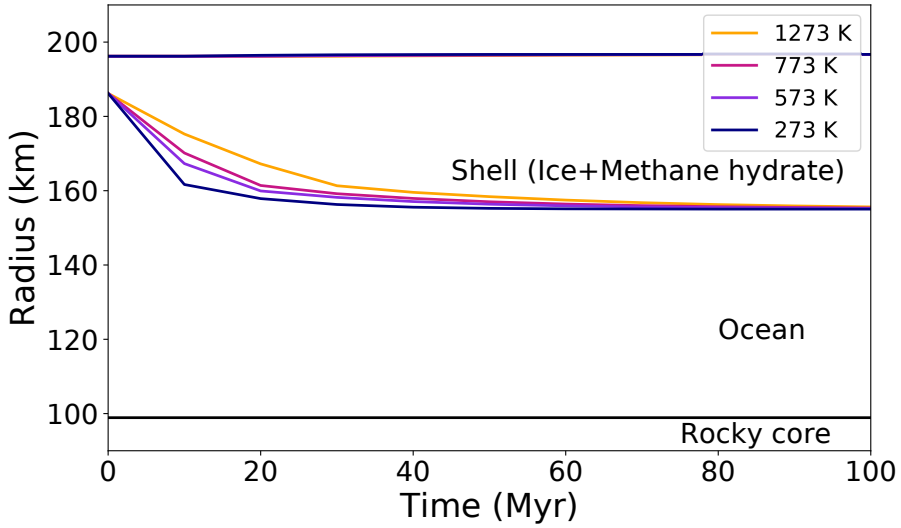

Figure 3.6: Time evolution of the internal structure of Mimas when starting from different initial temperatures.In all cases, the tidal heating rate is 4 GW and the initial methane concentration is 1000 mol m^{-3}. Only the results for the first million years are shown.

3.3.3 Effect of initial methane concentration on final internal structure

Figure 3.7 shows the difference in the final internal structure when the initial methane concentration is changed. As the initial methane concentration decreases, a mix layer appears. As the initial methane concentration is over 500 mol m^{-3}, the mix layer does not appear and the final icy shell thickness becomes the same. This implies that the ocean is oversaturated throughout the thermal evolution. In this study, the typical initial methane concentration in the presence of methane hydrate layer is assumed to be 1000 mol m^{-3}.

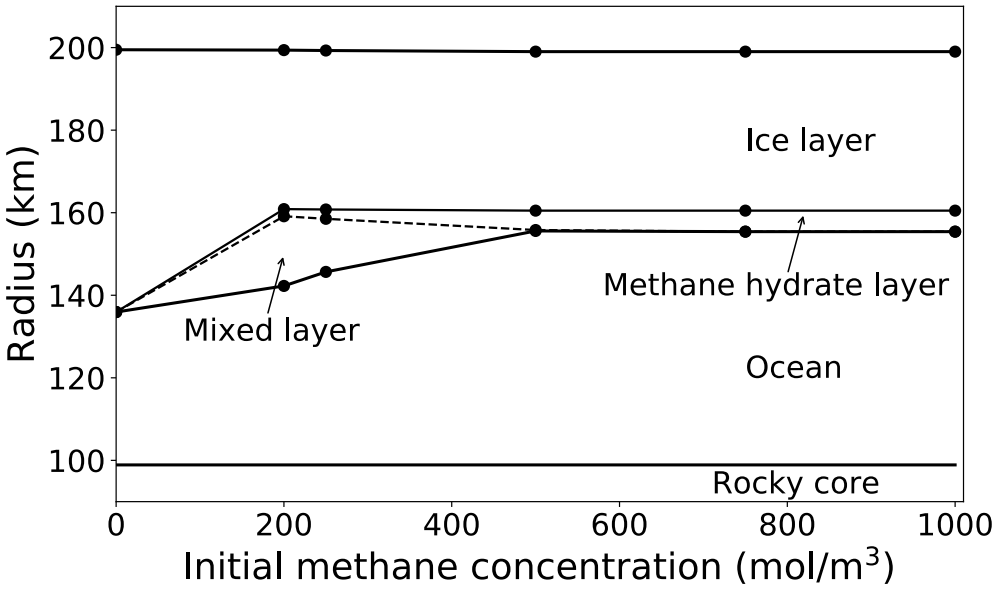

Figure 3.7: The final internal structure of Mimas when starting with different initial methane concentrations. In all cases, the initial temperature is 573 K and the tidal heating rate is 3 GW.

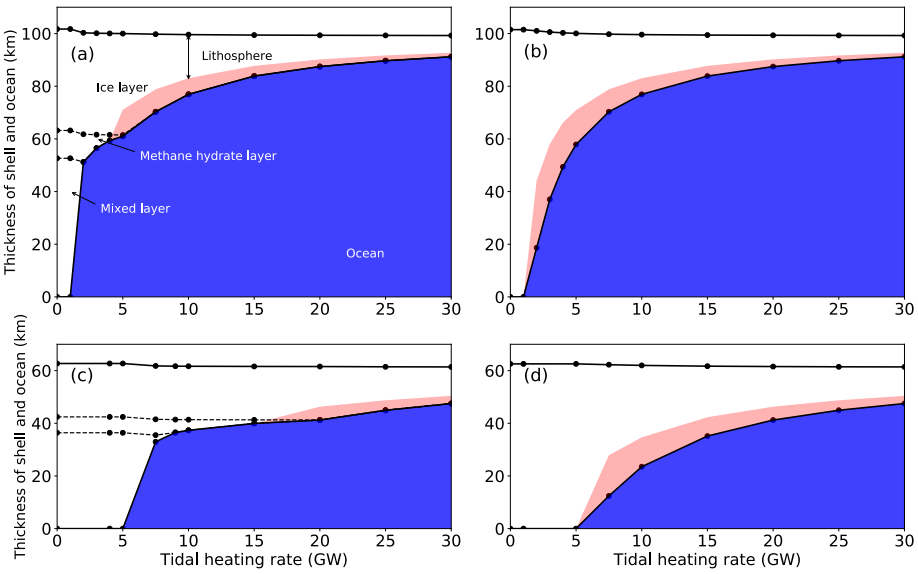

Figure 3.8: The relationship between the tidal heating rate and the final internal structure is shown. (a) and (b) are Mimas, both with an initial core temperature of 573 K. (c) and (d) are Enceladus, both of which have an initial core temperature of 1273 K. In (a) and (c), the initial methane concentration is 1000 mol m^{-3}, and in (d) and (e), the initial methane concentration is 0 mol m^{-3}. The pink-colored region is the convection area. The lithosphere is the thickness of the icy shell minus the convection area.

3.3.4 Differences in final shell thickness and lithosphere among different tidal heating rates

Figure 3.8 shows the difference in the final internal structure and thickness of the lithosphere when different tidal heating is applied. The lithosphere is defined as the nonconvective area within the icy shell, i.e., $F_{\mathrm{conv}}/F_{\mathrm{tot}} < 0.1\%$. As the figure shows, if the tidal heating for Enceladus and Mimas are the same, the heating per unit mass is greater for Mimas because it is smaller. Therefore, the final thickness of the subsurface ocean is thicker in Mimas. In Figure 3.8 (a) and (c), the final ocean thickness is close to a plateau in the region where the tidal heating for Enceladus is between 7.5 GW and 20 GW and the tidal heating for Mimas is between 2.0 GW and 5.0 GW. This means that the thickness change of methane hydrate layer is insensitive to the change in tidal heating rate. In addition, the presence of methane hydrate does not cause convection at all. In other words, the thickness of the icy shell is directly the thickness of the lithosphere. In the figure, methane hydrate layer does not appear when the tidal heating for Enceladus is more than 25 GW and the tidal heating for Mimas is more than 7.5 GW. This means that the icy shell is thin and the pressure in the icy shell is too low for methane hydrate to be formed.

3.3.5 Surface heat flux of Mimas

Figure 3.9 shows the final surface heat flux of Mimas. When methane hydrate layer is present, i.e., when the initial methane is 1000 $\mathrm{mol\,m^{-3}}$ and the icy shell is more than 40 km, the surface heat flux is well suppressed. In other words, it is possible to have both the presence of an ocean and an inactive surface in Mimas.

3.3.6 Summary of results

Figure 3.10 summarizes the results of Figure 3.8 and shows the conditions under which the ocean exists in both Enceladus and Mimas, and the lithosphere of Mimas is thicker than that of Enceladus. Although the thickness of the ocean is not completely known from the observation, it is believed that a thick ocean exists in both Enceladus and Mimas. In this study, I adopt about half of the H_2O layer

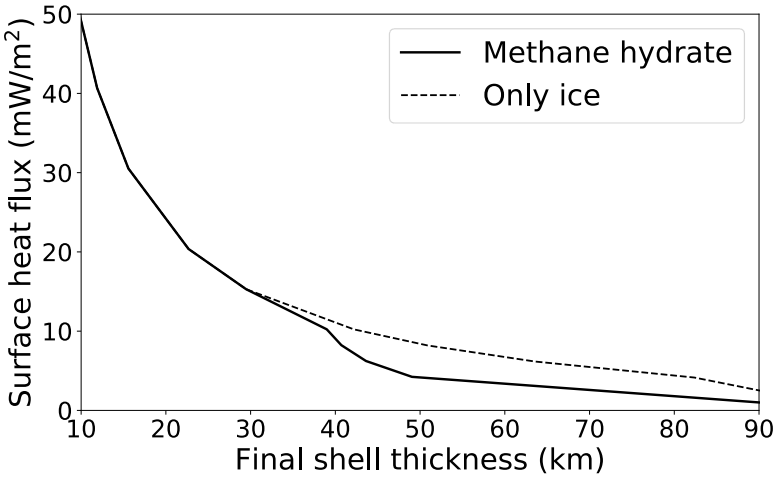

Figure 3.9: Current surface heat flux on Mimas.In all cases, the initial core temperature is 573 K. The dashed line shows the case where the initial methane concentration is 0 mol m^{-3}, i.e., only ice is produced. The solid line shows the case where the initial methane concentration is 1000 mol m^{-3}.

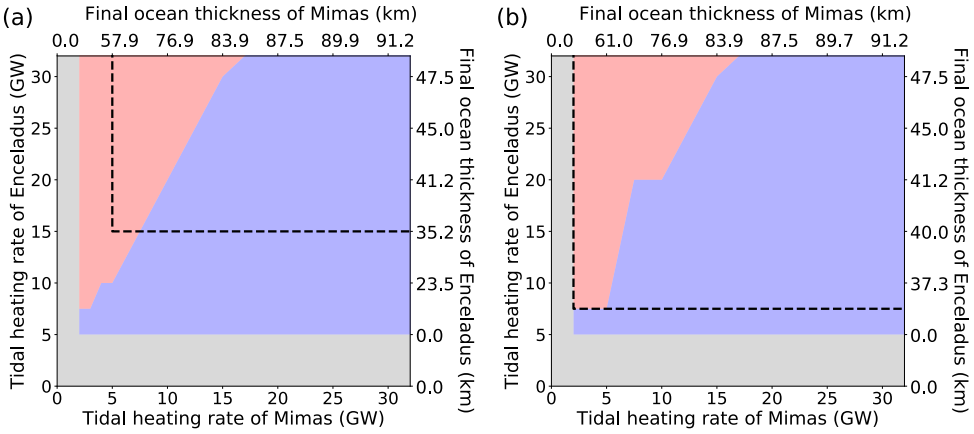

Figure 3.10: It shows the condition where there is a thick ocean in both Enceladus and Mimas and where the Mimas lithosphere is thicker than the Enceladus lithosphere.The horizontal axis is the tidal heating rate added to Mimas and the vertical axis is the tidal heating rate added to Enceladus. On the opposite side of each axis is the final subsurface ocean thickness corresponding to the tidal heating rate. The dashed line represents the condition where there is more than 25 km of ocean in Enceladus or more than 50 km of ocean in Mimas. The red-colored regions represent conditions where the Mimas lithosphere is thicker than the Enceladus lithosphere.

(including the icy shell and the subsurface ocean), i.e., 25 km in Enceladus and 50 km in Mimas, as a criterion for "thick ocean". The area surrounded by black dashed lines in the figure indicates the existence of thick oceans in both Enceladus and Mimas. In the case that methane hydrate layer exists, more than 7.0 GW of tidal heating for Enceladus and more than 2.0 GW of tidal heating for Mimas are required to realize the thick ocean. In the case that ice layer only exists, 15 GW of tidal heating for Enceladus and 5.0 GW of tidal heating for Mimas are required to realize the thick ocean. The red region in the figure shows the region where the Mimas lithosphere is thicker than the Enceladus lithosphere. Therefore, the plausible region that can explain the current Enceladus and Mimas, i.e., "the preferred region", is the region surrounded by dashed lines and colored red. It is found that the preferred region is larger when methane hydrate layer exists than when only ice layer exists.

3.4 Discussions

3.4.1 Dependence on tidal dissipation factor

As mentioned earlier, thermal evolution and orbital evolution are closely associated. This is because the tidal heating rate to a satellite is related to its internal structure and orbital elements. One of the factors that have a great influence on the orbital evolution of a satellite is the tidal dissipation factor $Q_{\rm p}$ of the planet. $Q_{\rm p}$ is a value that represents the degree of dissipation within a planet due to tidal forces acting on it. The current value of $Q_{\rm p}$ is estimated by astrometry to be $\sim$2000 [72]. If $Q_{\rm p}$ has been constant at 2000 during Saturn's evolution, then from the perspective of orbital evolution, Enceladus and Mimas may have formed recently [73]. Even if Enceladus and Mimas are relatively recently formed, they approach equilibrium within a few hundred Myr, as shown in Figure 3.3, and the current internal structure may form. Note, however, that this study does not take into account differentiation, failure, or crater relaxation. On the other hand, Fuller et al. (2016) suggest that $Q_{\rm p}$ has not been constant until now and may have been larger in the past [74]. Based on this theory, both Enceladus and Mimas form 4.6 Gyr ago. If the orbital evolution is calculated based on this

theory, Mimas may experience a 3:2 mean motion resonance with Enceladus 0.34 Gyr ago. The $Q_{\rm p}$ at this time is 4600, and the equilibrium tidal heating is 3.6 GW [61]. Also, as mentioned earlier, Enceladus is currently in a 2:1 mean motion resonance with Dione, with an equilibrium tidal heating of 10 GW. By applying these tidal heating rates to the result in figure, it is found that the condition of the preffered region is satisfied when both moons have methane hydrate layer.

3.4.2 Relevance to observation

The icy shell thickness of Enceladus is estimated from a number of studies. Estimated icy shell thicknesses range from about 14 km to 41 km [52, 53, 54, 7, 55, 75]. Thus, assuming an Enceladus radius of 252.0 km and a core radius of 190.7 km, the ocean must be at least 20 km thick. With the estimated equilibrium tidal heating of 10 GW, a 20 km ocean is realized regardless of the presence or absence of methane hydrate as shown in figure. If the thickness of the ocean can be constrained by future observations, it may be possible to further constrain the presence of methane hydrate. For Mimas, there is only one study that estimated the thickness of the icy shell from observations. According to Tajeddine et al. (2014), the thickness of the icy shell estimated from the libration is between 24 and 31 km [8]. This implies an ocean thickness of 68.3 km to 75.3 km, assuming Mimas radius of 198.2 km and the core radius of 98.9 km. The estimated equilibrium tidal heating of 3.6 GW cannot achieve this ocean thickness even if methane hydrate is present. Furthermore, it is found that methane hydrate cannot exist at this thickness of the icy shell. This may be because only pure methane hydrate was considered in this study. For example, CO_2 hydrate and Xe hydrate have higher dissociation points than methane hydrate [19], which is expected to make the depth at which gas hydrates can exist stably shallower. The effect of dissolved different gaseous species is described in detail in a later section.

The lack of geological activity at the surface of Mimas is a strong constraint on its thermal evolution. Rhoden et al. (2017) discussed the possibility that tidal stress could crack the surface of Mimas [56]. When the viscosity of the icy shell is 10^{12} Pas, the tidal stress is up to 1300 kPa, while when the viscosity of the ice

is 10^{13} Pas, the tidal stress is up to 80 kPa. As the viscosity increases, the tidal stress decreases. Considering the fact that the tensile failure strength of ice is a few MPa, although it depends on the grain size and porosity of the ice [76], the higher the viscosity of the icy shell, the less likely the icy shell fails. If methane hydrate layer exists, the temperature of the icy shells can be kept low and the viscosity can be kept high because they insulate the heat from the inside, and it is thought that the icy shell is less likely to crack due to tidal stress.

The fact that the Herschel crater does not relax on Mimas is also a big constraint on the internal thermal structure. Tian and Nimmo (2019) assume that the surface heat flux is less than 10 $\mathrm{mW\,m^{-2}}$ as a condition for the Herschel crater not to relax [61]. The present study uses the same assumption and considers Figures 3-5. If methane hydrate layer exists, the thickness of the icy shell must be approximately 40 km or more for the surface heat flux to be less than 10 $\mathrm{mW\,m^{-2}}$. This is equivalent to the thickness of the ocean being less than 59.3 km. In the case of the ice layer alone, the thickness of the icy shell must be approximately 50 km or more. In other words, the thickness of the ocean must be less than 49.3 km. Comparing these results with figure 3.10, it is found that the presence of methane hydrate layer enables both the low surface heat flux on Mimas and the thick ocean, i.e., the condition of the preferred region is satisfied.

Many of the craters on the Enceladus surface are relaxed in contrast to Mimas. This is thought to be due to the porous layer of ice formed by the deposit of plume-derived ice grains on the Enceladus surface. The porous layer has a lower thermal conductivity than the underlying ice layer, and thus acts as an insulating layer similar to methane hydrate layers. This insulating layer has the effect of increasing the thermal gradient near the surface, which is thought to be responsible for the relaxation of the surface craters [77]. Therefore, it is difficult to argue whether there is methane hydrate layer inside Enceladus from the appearance of surface craters.

3.4.3 Dissolved gaseous species

Gas hydrates are capable of containing not only methane but also other gaseous species. The gas composition in the Enceladus plume is found to form mixed hy-

drate under the temperature and pressure inside Enceladus [18]. Methane hydrate and mixed hydrate have different dissociation points and densities. The difference in dissociation points may affect the depth at which gas hydrates emerge in the icy shell. The higher the dissociation point, the shallower the depth at which the melting point of ice and the dissociation point of mixed hydrate reverse, and thus the shallower the depth at which mixed hydrate appears. The difference in density may affect whether gas hydrate can ascent in the ocean, i.e., whether gas hydrate layer can be formed in the icy shell. If mixed hydrates are formed with the Enceladus plume composition, either Structure I with a density of 1040 $\mathrm{kg\,m^{-3}}$ or Structure II with a density of 970 $\mathrm{kg\,m^{-3}}$ is formed [18]. In the case of Structure II, the hydrate can ascend in the ocean, but in the case of Structure I, the possibility of ascending depends on the density of the ocean. Ascended mixed hydrate forms layer beneath the ice layer, but sunk mixed hydrate eventually melts due to the heat from the rocky core. Among the dissolved gases, CO_2, which is heavier than methane, is considered to be important. Methane and carbon dioxide can coexist in the ocean. The ratio of carbon dioxide to methane is determined by temperature [78]. Depending on the temperature, hydrate layer may not form.

3.5 Summary

In this section, the developed model is used to explore the conditions where both Enceladus and Mimas have thicker oceans and the lithosphere of Mimas is thicker than that of Enceladus, i.e., the preferred region. In the presence of methane hydrate layer, it was found that Enceladus needs 7.5 GW to maintain more than 25 km of ocean, and Mimas needs more than 2.0 GW to maintain more than 50 km of ocean. These tidal heating values are lower than those for the ice layer only. When methane hydrate layer is present in both moons, the estimated equilibrium tidal heating is found to be in the preferred region. In addition, the presence of methane hydrate layer suppressed the surface heat flux of Mimas and prevented the relaxation of the Herschel crater. Considering the methane hydrate layer may explain the structure of Enceladus and Mimas.

Chapter 4

Methane hydrate as a reservoir of atmospheric methane on Titan

4.1 Introduction

Titan is the only satellite with a thick atmosphere, and it is a mystery why Titan is the only one with a thick atmosphere. Titan has a radius of 2575 km, which is the second largest satellite in the solar system after Ganymede. Figure 4.1 shows Titan's image. The physical and orbital properties of Titan are listed in Table 4.1.

Table 4.1: The thermal and physical properties of Mimas and Enceladus.

Parameter	Symbol	Units	Titan
Mean surface radius	R	km	2575
Bulk density	ρ	kg m^{-3}	1880
Surface temperature	$T_{\rm surf}$	K	93.7
Orbital eccentricity	e		0.0292

In addition, observations predict the existence of an internal ocean inside Titan. From observations, Titan's moment of inertia is found to be around 0.33 to 0.34, indicating that its interior is not completely differentiated [79]. The measurements of low frequency waves and atmospheric conductivity on Titan revealed a Schuman-like resonance trapped within Titan's atmospheric cavity [80]. This is interpreted as the presence of a subsurface conductive layer of about 45 km, i.e., the existence of an internal ocean. Bills and Nimmo (2008), based on long-length topography and a theoretical model, suggested the existence of

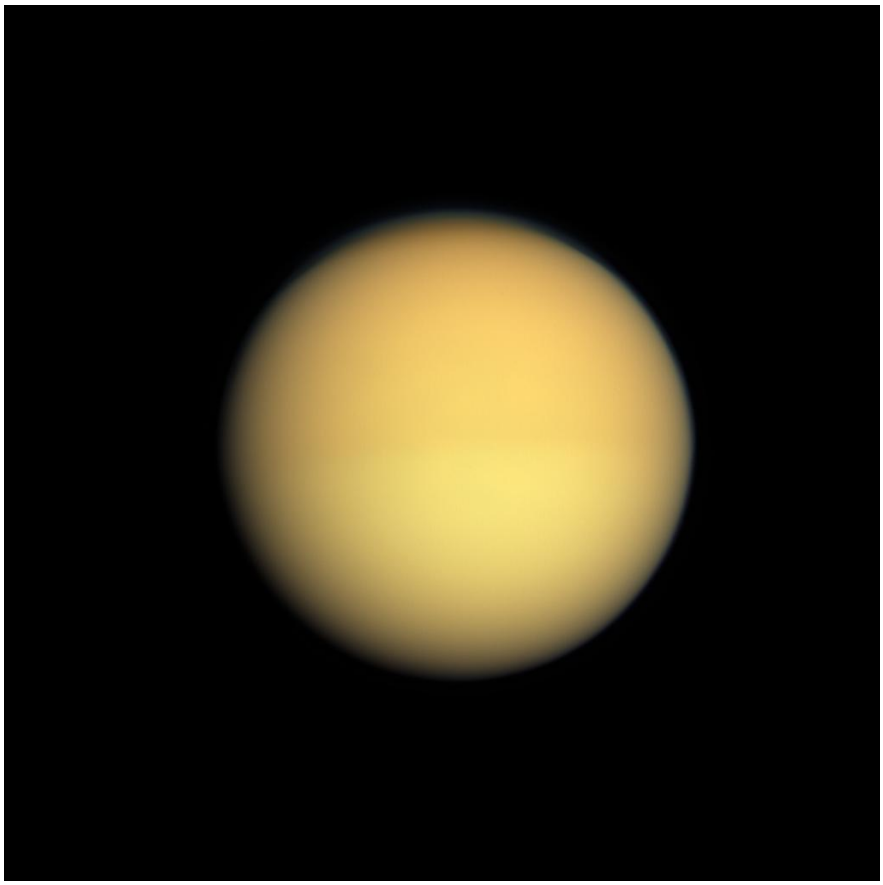

Figure 4.1: Titan's image. Credit:NASA/JPL/Space Science Institute

an subsurface ocean beneath a not-convective icy shell of about 100 km [81]. Hemingway et al. (2013) also investigated the long-length topography of the icy shell, and suggested that the icy shell is conductive, i.e., it has high viscosity [82].

Titan has an atmospheric pressure of about 0.15 MPa and is composed of large amounts of nitrogen, methane, and other elements [83]. One of the major problems on Titan is the lack of atmospheric methane. The amount of methane in the atmosphere is about 5% near the surface, depending on the altitude. It is known that this methane will be destroyed by photolysis in tens of million years, so it must be supplied to the atmosphere by some means [84]. The process of methane formation is debated from various perspectives. Since comets, which are candidates for Titan's raw materials, contain methane, it is possible that the methane remains intact. However, when Titan-sized satellites accrete they may have lost a lot of volatiles, depending on the accretion model. In this case, the methane could have been generated inside Titan. Assuming that a mixture of rock and ice accumulated, the decay of short-lived radioactive elements and accretion heating can melt the ice, and the reaction of the melt with the rock (e.g., serpentinization reaction and carbon dioxide reduction) can produce methane. It is also possible that there is an ongoing serpentinization reaction between the subsurface ocean and the rocky core after differentiation. The ongoing hydrothermal reaction of the rocky core is supported by the finding of large fraction of ^{40}Ar in Titan's atmosphere, which was formed by radiative decay in the rock [83].

In Tobie et al. (2006), methane hydrate layer on the surface is assumed to be the source of atmospheric methane, and thermal evolution calculations were performed assuming the formation of methane hydrate layer during the accretion.[23] As a consequence, they found that within 1 Gyr, convection in the icy shell can cause cryovolcanism, which can supply methane to the atmosphere. On the other hand, when methane hydrate layer exists on the surface, it is known that the viscosity in the icy shell decreases because the heat is trapped in the underlying ice layer [62]. Therefore, the assumption of the existence of methane hydrate layer on the surface contradicts the inference from observations that the inside of the icy shell is high viscous. It is also unclear whether hydrate formation can take place fast enough in a low-temperature, low-pressure environment such as interstellar space. In the case of hydrate formation in interstellar space, noble

gases such as Xe and Kr must have been taken in at the cage of the gas hydrate, which is inconsistent with the low noble gas content in Titan's atmosphere [83].

Therefore, in this study, I consider the possibility of methane hydrate formation in the subsurface ocean of Titan instead of the initial accumulation of methane hydrate. The purpose of this study is to investigate whether the existence of methane hydrate layer in the interior of Titan can explain the current viscosity in the icy shell and the amount of atmospheric methane using the one-dimensional thermal evolution model developed in section 2.

4.2 Methods

In this study, I use the thermal evolution model developed in section 2. The differences from section 2 and the initial setup are described below.

4.2.1 Interior structure

The density of rock is assumed to be 2500 $\mathrm{kg\,m^{-3}}$, the density of the ocean is assumed to be 1000 $\mathrm{kg\,m^{-3}}$, and the density of ice and methane hydrate is assumed to be 920 $\mathrm{kg\,m^{-3}}$. The density of HP ice is listed in Table 2.2. The radius of the rocky core is determined to be 2135.9 km using the formula. Because of the large size of Titan, most of its interior is a stable region of methane hydrate. Therefore, the thickness of the ice formed in the initial stage of accretion may determine the depth at which methane hydrate appears. Therefore, in this study, the initial icy shell thickness is set as a free parameter ranging from 25 km to 200 km. This simulates at what stage during the initial accretion the primordial ocean became methane supersaturated.

4.2.2 Initial methane concentration

The initial methane concentration in the ocean is set to be 1% in the entire H_2O layer (icy shells, ocean, and HP ice layers). In addition, in order to consider the case of methane hydrate formation during long-term evolution, the emergence

time of methane hydrate layer is set as a free parameter. When the beginning of the calculation is set to 0 yr, the emergence time of the methane hydrate layer is varied from 0 yr to 1 Gyr after the formation time. This parameter means at what time the ocean was supersaturated with methane by the ongoing methane production. As the treatment in the calculation, methane is injected into the ocean when the thermal evolution time gets over the set methane hydrate emergence time. In the case where only ice layers are considered, the initial methane concentration is set to zero.

4.2.3 Methane leakage into the atmosphere

It is assumed that the methane leakage into the atmosphere is caused by the instantaneous transport of methane to the surface when methane hydrate dissociates. In large icy moons such as Titan, when the icy shell gets thicker, the surface of the icy shell is subjected to high tensile stress. Or, the large amount of methane gas from the dissociation of methane hydrates causes excessive pressure at the bottom of the icy shell. Therefore, it is thought that there is a pathway in the icy shell through which methane gas can escape during methane hydrate dissociation. In Europa, the stress exceeding the tensile strength of ice is generated when the icy shell grows about 20 km [85]. Even if the ice does not fail, the large amount of methane gas produced would increase the buoyancy of the surrounding area and allow the methane gas to reach the surface [86]. Therefore, the assumption of this study is not so bad.

Methane hydrate contains $C_{\mathrm{CH4,MH}} = 7419\ \mathrm{mol\,m^{-3}}$ methane as described in section 2. Therefore, when methane hydrate dissociates by ΔV_{hyd}, $C_{\mathrm{CH4,MH}}\Delta V_{\mathrm{hyd}}$ mol of methane is generated. Since the molar mass of methane is $1.6 \times 10^{-2}\,\mathrm{kg\,mol^{-1}}$, the amount of methane supplied to the surface by the dissociation of methane hydrate is $C_{\mathrm{CH4,MH}}\Delta V_{\mathrm{hyd}} \times 1.6 \times 10^{-2}$ kg. Since this is added to the surface pressure, the change in surface atmospheric pressure is as follows:

$$\Delta P = \frac{C_{\mathrm{CH4,MH}}\Delta V_{\mathrm{hyd}} \times 1.6 \times 10^{-2} \times g_{\mathrm{surf}}}{S_{\mathrm{top}}} \tag{4.1}$$

where g_{surf} is the gravitational acceleration at moon's surface, and S_{top} is the

moon's surface area. It is known that the amount of methane lost at the surface per unit time due to photolysis, dissipation, and condensation is $C_{\rm loss} = 1.3 \times 10^{14}\,{\rm m^{-2}\,s^{-1}}$ [87]. Note, however, that this is the current value. Assuming that the atmospheric methane continues to decrease at the current value, the change in atmospheric pressure is as follows:

$$\Delta P = \frac{\left(C_{\rm CH4,MH}\Delta V_{\rm hyd} - C_{\rm loss}S_{\rm top}\Delta t/\left(6.02\times10^{23}\right)\right)\times 1.6\times10^{-2}\times g_{\rm surf}}{S_{\rm top}} \quad (4.2)$$

The above equation is used to determine the change in methane atmospheric pressure to the present.

4.2.4 Initial condition

Ice thickness is assumed to be a free parameter as described earlier. Initial methane hydrate layer thickness and HP ice layer thickness are set to 0 km. It is assumed that it takes about 500 Myr from accumulation to the formation of differentiated structures, and the beginning of calculations is 500 Myr after CAI formation [88]. The initial temperature of the top of the icy shell is fixed at the surface temperature 93.7 K. The temperature at the bottom of the icy shell and in the subsurface ocean is set to the melting point at the bottom of the icy shell. The temperature inside the icy shell is a linear function of the temperature at the bottom of the icy shell and the surface temperature. The rocky core and ocean temperatures are the same as the melting point at the bottom of the icy shell.

4.3 Results

4.3.1 Time evolution of the rocky core temperature

If the rocky core exceeds 900 K, the rocky core will dehydrate. If the rocky core was dehydrated, it cannot reproduce the moment of inertia consistent with observations.

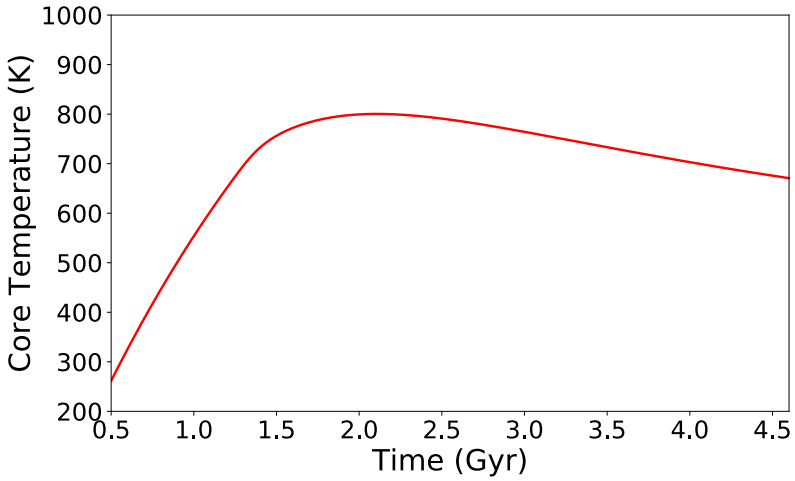

Figure 4.2: Time evolution of central temperature of rocky core in Titan. The initial ice shell thickness is 100 km, and 1% methane is dissolved in the entire H_2O layer.

Figure 4.2 shows the evolution of the temperature of the rocky core center in the presence of methane hydrate layer and an initial ice shell thickness of 100 km. The temperature of the rocky core does not reach 900 K at the highest, so it can escape differentiation. In all calculations, the temperature of the rocky core does not exceed 900 K.

4.3.2 Time evolution of internal structure

Figure 4.3 and figure 4.5 show the evolution of the internal structure when the initial icy shell thickness is set to 100 km. Figure 4.3 shows the case without methane hydrate, and Figure 4.5 shows the case with the presence of methane hydrate. The color contour represents the temperature. Comparing the two results, it was found that a thick subsurface ocean can be obtained when methane hydrate is present. When methane hydrate is present, HP ice layer does not appear. This is because the dissociation point of methane hydrate is higher than the melting point of ice, and thus the temperature of the subsurface ocean is kept high. In addition, when methane hydrate is present, the temperature in the icy shell is kept lower than that in the case of only ice. This indicates the insulating

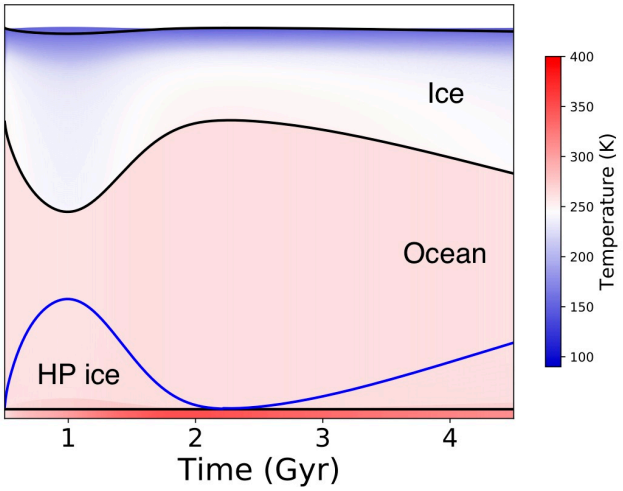

Figure 4.3: Time evolution of Titan's internal structure.The initial icy shell thickness is 100 km, and the initial ocean does not contain methane. The color contour represents the temperature.

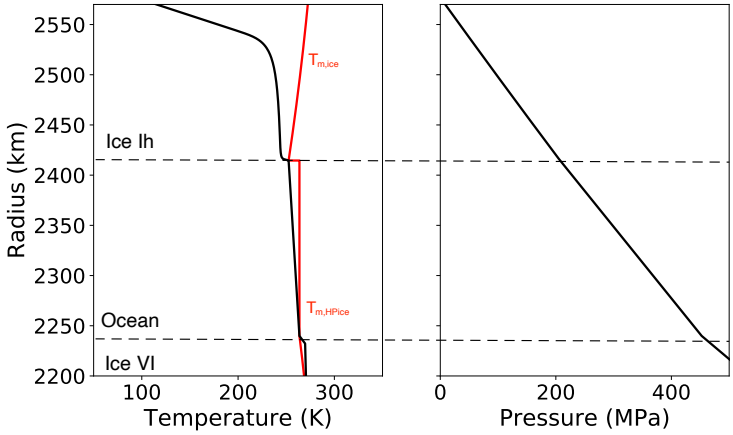

Figure 4.4: The temperature and pressure profiles of the final H_2O layer in the case that the initial ocean does not contain methane is shown. Red line represents the melting point of ice. The red line inside the ocean represents the melting point of HP ice under the pressure at the top of the rocky core.

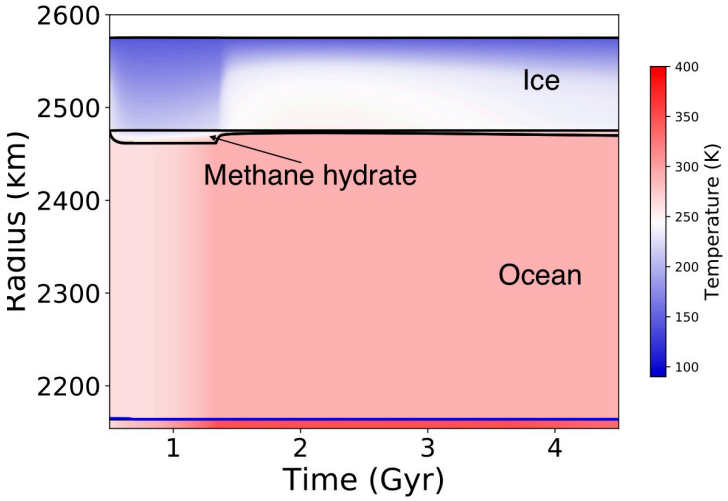

Figure 4.5: Time evolution of Titan's internal structure.The initial icy shell thickness is 100 km, and the initial ocean contains 1% methane in the entire H_2O layer. The color contour represents the temperature.

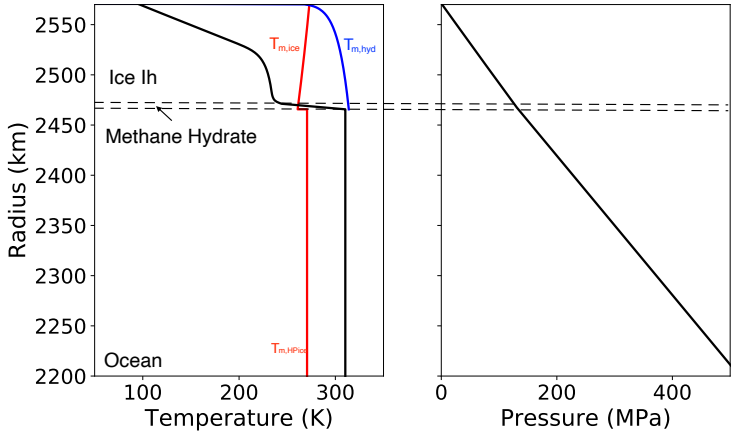

Figure 4.6: The temperature and pressure profiles of the final H_2O layer in the case that the initial ocean 1% methane in the entire H_2O layer. Red line represents the melting point of ice. The red line inside the ocean represents the melting point of HP ice under the pressure at the top of the rocky core. Blue line represents the dissociation point of methane hydrate.

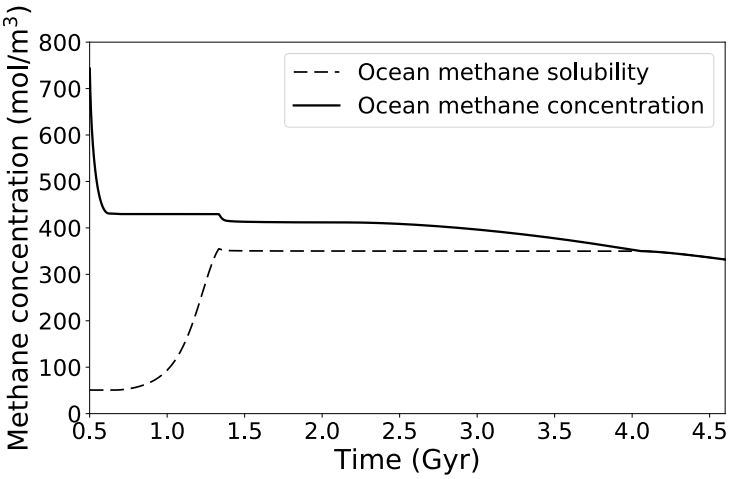

Figure 4.7: The temperature and pressure profiles of the final H_2O layer in the case that the initial ocean 1% methane in the entire H_2O layer. Red line represents the melting point of ice. The red line inside the ocean represents the melting point of HP ice under the pressure at the top of the rocky core. Blue line represents the dissociation point of methane hydrate.

property of methane hydrate. The lower temperature in the icy shell means that the viscosity of the icy shells is higher, and this is consistent with previous study that indicates the icy shells are conductive [82]. Figure 4.4 and figure 4.6 show the temperature and pressure profiles of the final H_2O layers in the figure 4.3 and figure4.5. As shown in figure 4.6, the subsurface ocean is kept hot by fairly thin methane hydrate layer. Consequently, the interior ocean is too warm for HP ice to exist. Figure 4.7 shows the time evolution of the ocean methane concentration. The methane concentration in the ocean decreases with the formation of methane hydrate. When the growth of methane hydrate stops, the methane concentration becomes constant. As the methane hydrate dissociates, the methane gas in the methane hydrate is supplied to the atmosphere. The methane concentration in the ocean decreases as methane hydrate dissociates because the volume of the ocean increases due to the dissociation of the methane hydrate layer.

Figure 4.8 and figure 4.9 show the final structure of the H_2O layer against the initial thickness of the icy shell. In the case of ice alone, the initial structure does not significantly affect the final structure, but in the case of the presence of methane hydrate, the initial icy shell thickness significantly affects the final

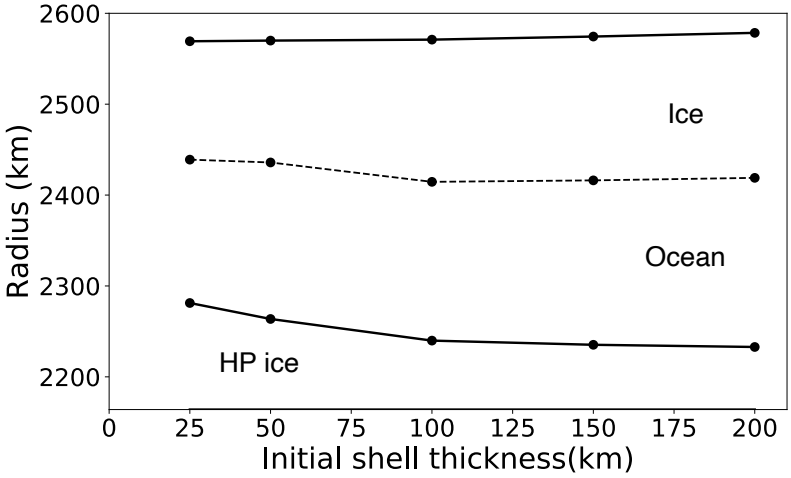

Figure 4.8: The relationship between the initial icy shell thickness and the final internal structure is shown. In all cases, the initial ocean does not contain methane.

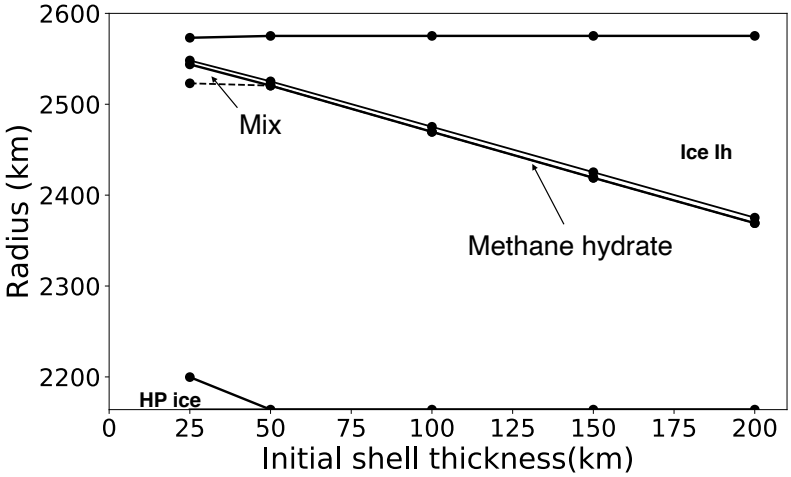

Figure 4.9: The relationship between the initial icy shell thickness and the final internal structure is shown. In all cases, the initial ocean contains 1% methane dissolved in the entire H_2O layer.

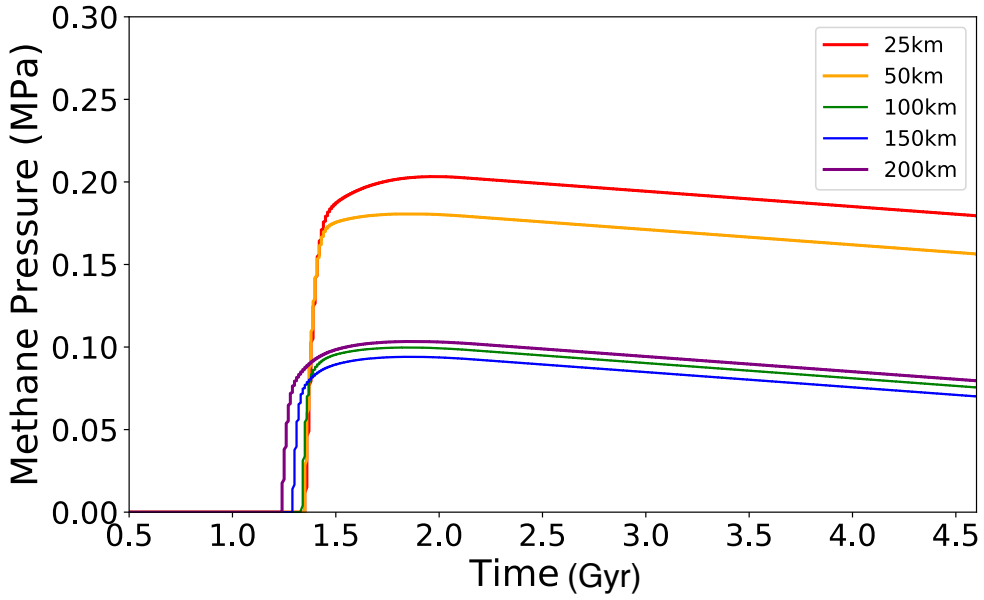

Figure 4.10: The time evolution of methane atmospheric pressure at different initial icy shell thicknesses.In all cases, the initial ocean contains 1% methane dissolved in the entire H_2O layer.

structure. When methane hydrate is present, the final icy shell thickness is almost equal to the initial icy shell thickness. This is because the heat generated by the rocky core cannot melt the methane hydrate layer whole.

4.3.3 Time evolution of atmospheric pressure

Figure 4.10 shows the evolution of the atmospheric thickness. In all cases, the methane atmosphere remained until now, but the amount of methane released to the atmosphere depends on the initial icy shell thickness. Figure 4.10 shows the current methane atmospheric pressure against the initial icy shell thickness. The thicker the initial icy shell, the less methane is released into the atmosphere. This is thought to be due to the difference in methane solubility of the ocean at different depths. When the icy shell is thick, the pressure at the bottom of the icy shell increases, and the dissociation point of methane hydrate in the lower part of the icy shell becomes higher. Then, the ocean temperature rises and the

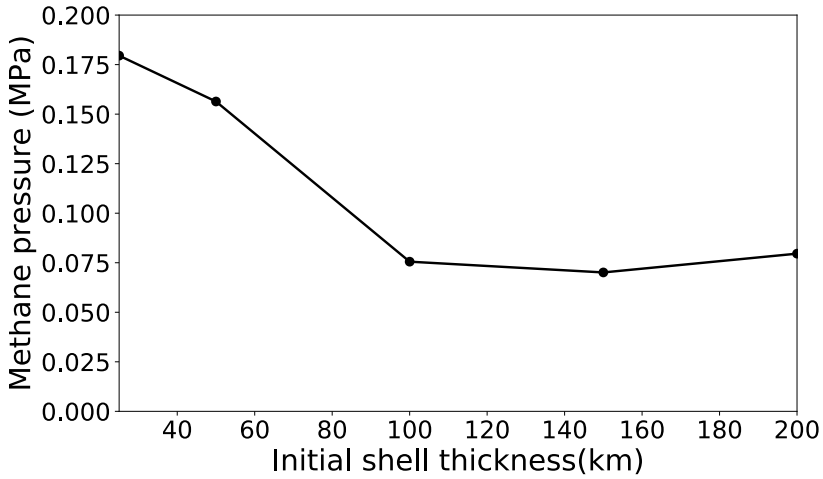

Figure 4.11: The relationship between the final methane atmospheric pressure and the initial ice shell thickness is shown. In all cases, the initial ocean contains 1% methane dissolved in the entire H_2O layer.

amount of methane that can be dissolved into ocean increases. As a consequence, less methane hydrate is formed than when the icy shell is thin, and less methane hydrate is dissociated.

4.3.4 Effect of methane hydrate emergence time

Figure 4.12 shows the final internal structure of the H_2O layer in relation to the emergence time of methane hydrate. The final internal structure is almost the same when methane hydrate starts to be formed after 500 Myr from calculation start time. If methane hydrate starts to form before 400 Myr after formation, the larger the methane hydrate emergence time is, the thicker the final icy shell becomes.

Figure 4.13, figure 4.14 and figure 4.15 show the evolution of the internal structure at different methane hydrate emergence times. The final icy shell thickness is largely determined by the icy shell thickness at the time of the emergence of methane hydrate. When the methane hydrate emergence time is 400 Myr, the methane hydrate layer grows from 400 Myr after formation. After that, the ocean temperature rises to the dissociation point of methane hydrate due to the heat of

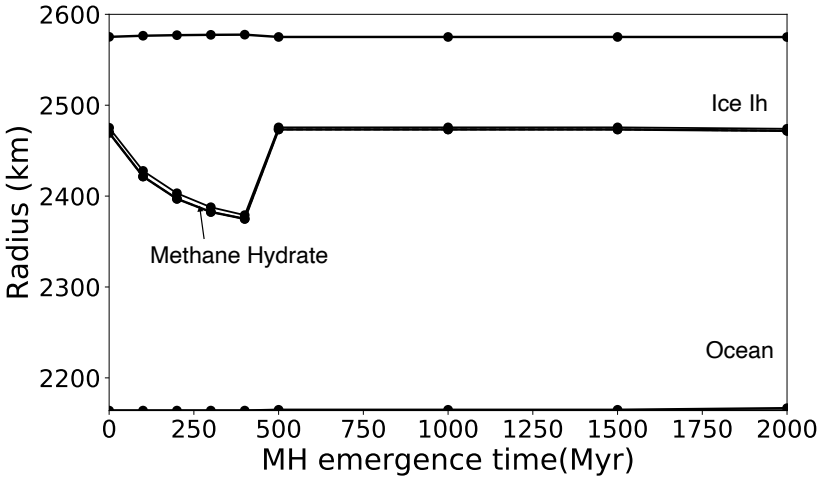

Figure 4.12: The relationship between the final internal structure of Titan and the methane hydrate emergence time is shown. In all cases, the initial ocean contains 1% methane dissolved in the entire H_2O layer.

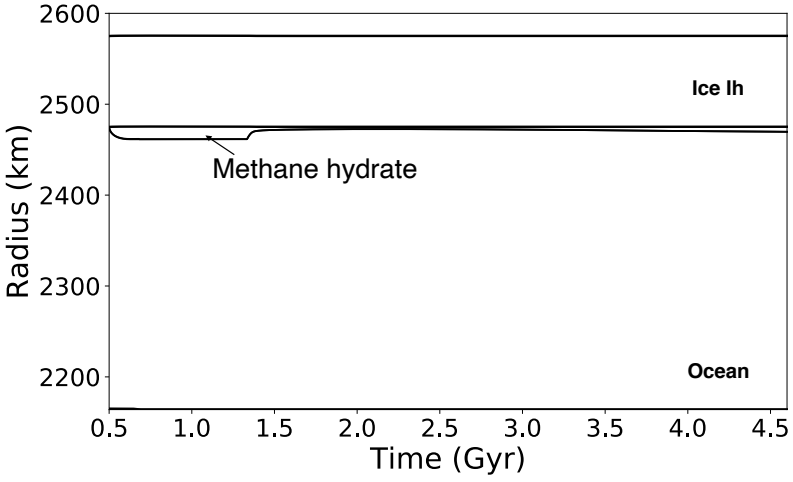

Figure 4.13: Time evolution of the internal structure of Titan when the Methane hydrate emergence time is 0 Myr is shown. The initial icy shell thickness is 100 km and the initial methane is 1% of the total H_2O layer.

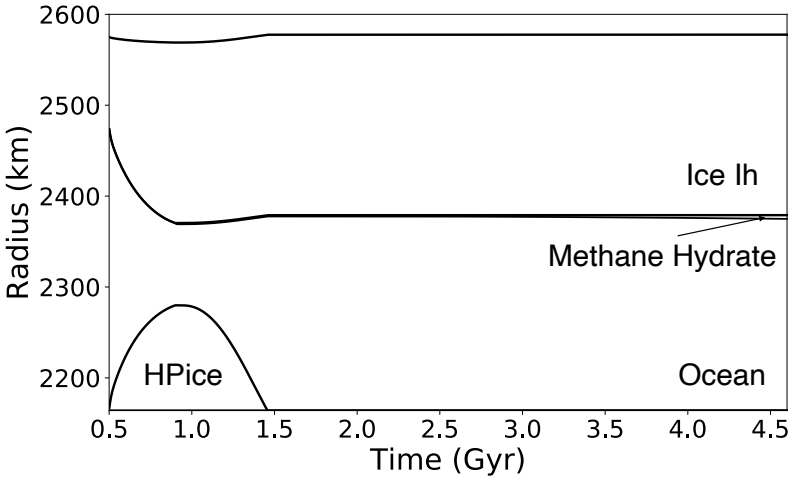

Figure 4.14: Time evolution of the internal structure of Titan when the Methane hydrate emergence time is 400 Myr is shown. The initial icy shell thickness is 100 km and the initial methane is 1% of the total H_2O layer.

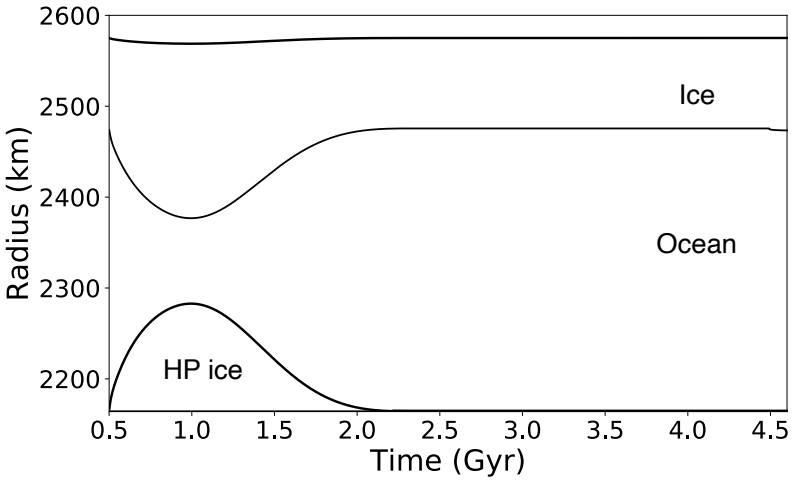

Figure 4.15: Time evolution of the internal structure of Titan when the Methane hydrate emergence time is 500 Myr is shown. The initial icy shell thickness is 100 km and the initial methane is 1% of the total H_2O layer.

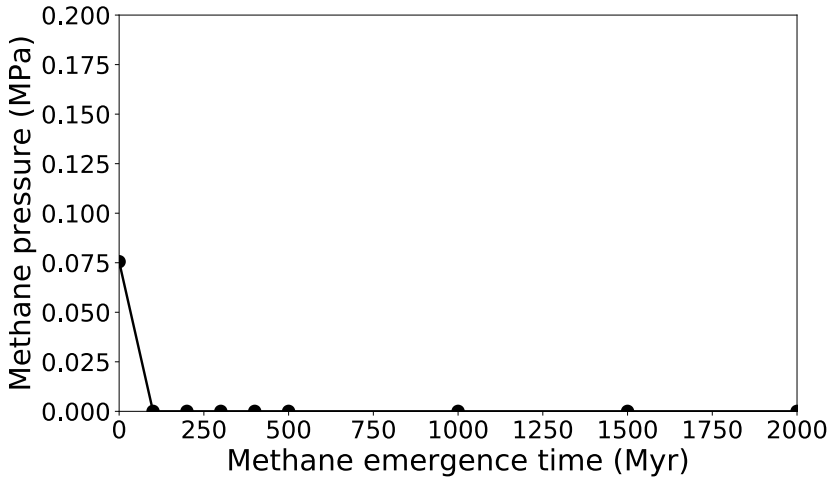

Figure 4.16: The relationship between methane hydrate emergence time and final methane atmospheric pressure is shown. In all cases, the initial icy shell thickness is 100 km and the initial ocean contains 1% methane dissolved in the entire H_2O layer.

radioactive decay from the rocky core. After the ocean temperature rises to the methane hydrate dissociation point, the methane hydrate dissociates, although the methane hydrate layer remains because they could not be fully dissociated by the heat of radioactive decay. As a result, the final shell thickness remains thick.

Figure 4.16 shows the current methane atmospheric pressure against the methane hydrate emergence time. It is found that methane is not released to the atmosphere unless methane hydrate exists from the beginning. This is because the methane hydrate layer did not have a chance to dissociate or to be formed if methane hydrate is formed after icy shell gets to thick once. In order to supply methane to the atmosphere through the dissociation of methane hydrate, it is necessary for methane hydrate to be formed and then dissociate. As shown in figure 4.14, the formed methane hydrate layer in the case that the methane hydrate emergence time is 400 Myr is thinner than that in the case that the emergence time is 0 Myr. As a result, less methane hydrate was dissociated and less methane that was supplied to the atmosphere. Also, as shown in figure 4.15, methane hydrate is not formed during the period of 1 Gyr after 500 Myr from

the formation of Titan, because of high heat flux from the rocky core. Although methane hydrate can be formed after that time, it is not possible for the hydrate to be melt. Therefore, in order to supply methane to the atmosphere through the dissociation of methane hydrate, it is necessary for methane hydrate to be formed in the early stages of Titan's evolution.

4.4 Discussions

4.4.1 Possibility of methane atmospheric leakage

In this study, it is assumed that the initial ocean is supersaturated with methane. At this time, the methane could not be fully dissolved into the ocean. The residual methane that cannot be dissolved in the ocean is thought to exist as microbubbles. The methane microbubbles may be covered with a thin film of methane hydrate [89]. The thin methane hydrate shell of the microbubbles act like a pressure-resistant container and hold methane gas inside. As the methane hydrate grows in the lower part of the icy shell, the methane concentration in the ocean decreases. Then, some of the microbubbles covered with methane hydrate shell collapse, which supplies methane to the ocean. Therefore, the initial methane in the ocean can be retained in without erupting to the surface.

Since methane hydrate holds a large amount of methane gas, when the methane hydrate layer dissociates, a large amount of methane gas is generated locally. The large amount of methane is considered to be transported to the surface by fracturing of the icy shell and/or migration with solid-phase convection. The methane gas generated by the dissociation of methane hydrate creates excess pressure in the subsurface ocean. The excess pressure generated in the ocean creates fractures in the lower part of the icy shell [90]. The subsequent fracture propagation depends on the magnitude of the excess pressure, buoyancy, and the length of the fracture [91]. If the excess pressure satisfies the following inequality, the crack propagates in the icy shell. The condition is given by

$$\Delta P_{\mathrm{ex}} > \frac{K_{\mathrm{Ic}}}{\sqrt{\pi l}} + \frac{2g}{\sqrt{\pi l}} \frac{l}{\pi} \left(\rho_{\mathrm{fluid}} - \rho_{\mathrm{shell}} \right) \tag{4.3}$$

where ΔP_{ex} is the excess pressure, K_{Ic} is the critical stress intensity and l is the crack length. K_{Ic} of ice Ih is 0.10-0.12 $\mathrm{MPa\,m^{1/2}}$ [86]. Consider the case where methane hydrate dissociates by ΔV_{hyd} . If there is no volume change due to the methane hydrate dissociation, the bulk density of the fluid remains the same before and after the dissociation. Therefore, the fluid does not generate buoyancy as a bulk, i.e., the second term on the left-hand side of equation 4.3 is zero. This assumption underestimates the crack propagation because in reality, the gas phase and the liquid phase should be separated and buoyancy should be generated. When methane hydrate dissociates, the volume change ΔV_1 derived from the density difference between methane hydrate, water, and methane gas and the volume change ΔV_2 caused by the compression of methane gas are generated [92]. Since I assume the case where no volume change occurs due to the dissociation of methane hydrate, the sum of ΔV_1 and ΔV_2 is zero. ΔV_1 can be expressed as follows:

$$\begin{aligned}\Delta V_1 &= \Delta V_{\mathrm{gas}} + \Delta V_{\mathrm{liq}} + \Delta V_{\mathrm{hyd}} \\ &= \left(-r_g \left(\frac{\rho_{\mathrm{hyd}}}{\rho_{\mathrm{gas}}}\right) - (1 - r_g)\left(\frac{\rho_{\mathrm{hyd}}}{\rho_{\mathrm{liq}}}\right) + 1\right)\Delta V_{\mathrm{hyd}} \\ &= -R_v \Delta V_{\mathrm{hyd}}\end{aligned} \tag{4.4}$$

where ΔV_{gas} is the volume change of the methane gas, ΔV_{liq} is the volume change of the water, ΔV_{hyd} is the volume change of the methane hydrate and r_g is the mass fraction of gas in methane hydrate. r_g is 0.127 assuming that the compositional formula of methane hydrate is $\mathrm{CH_4 \cdot 6\,H_2O}$. ρ_{gas} is the methane gas density and the density is 0.717 $\mathrm{kg\,m^{-3}}$ under the standard conditions for temperature and pressure [93]. Assuming that only the methane gas compresses, ΔV_2 is expressed as follows:

$$\begin{aligned}\Delta V_2 &= -\kappa \Delta P_{\mathrm{ex}} \Delta V_{\mathrm{gas}} \\ &= \kappa \Delta P_{\mathrm{ex}} r_g \left(\frac{\rho_{\mathrm{hyd}}}{\rho_{\mathrm{gas}}}\right)\Delta V_{\mathrm{hyd}}\end{aligned} \tag{4.5}$$

where κ is the compressivity. Therefore, since ΔV_1 is equal to $-\Delta V_2$ the excess

pressure can be expressed as follows:

$$\Delta P_{\mathrm{ex}} = \frac{R_v}{\kappa r_g \left(\frac{\rho_{\mathrm{hyd}}}{\rho_{\mathrm{gas}}}\right)}. \tag{4.6}$$

Assuming the gas is an ideal gas, the compressibility can be expressed as $\frac{1}{\gamma P}$ where γ is the heat capacity ratio and P is the pressure. For an ideal gas, γ is 1.33. Considering a depth of 100 km in Titan, the pressure is about 150 MPa as shown in figure 4.6 and κ is 5.0×10^{-6}. Substituting these values into the equation 4.6 gives the excess pressure of about 200 MPa. This excess pressure is much higher than the tensile strength of the ice (a few MPa), so it is possible to create cracks in the lower part of the icy shell [76]. Assuming the crack length is $\sim$ 100 km, It also causes crack propagation because the equation 4.3 is satisfied. The crack propagation is expected to take place quickly, so the methane is well supplied to atmosphere. Even if volume change occurs due to methane hydrate dissociation, the buoyancy will increase because the volume fraction of gas will increase. Therefore, even if the volume change is allowed, the leakage of methane gas is considered to occur. It is also possible that methane gas was transported to the surface by convection. When methane hydrate dissociates, bubbles are supplied into the icy shell. In the case of the Earth's magma, it is known that the effective viscosity decreases when bubbles are present in the magma [94]. Similarly, if the viscosity of the icy shell is reduced by the presence of bubbles, convection in the icy shell will be promoted. It is conceivable that the buoyancy of the bubbles and the convection of the ice shells may supply methane to the atmosphere quickly during the period of methane hydrate dissociation. In both cases, the large amount of gas produced by the dissociation of methane hydrate is considered to enable the rapid supply of methane to the atmosphere. In this study, it is assumed that all the methane gas released by methane hydrate dissociation is supplied to the atmosphere. However, in reality, there is a possibility that the methane will return to the methane hydrate as it moves through the icy shell, and/or there is a possibility that the methane will dissolve back into the ocean due to the excess pressure. Therefore, the methane atmospheric pressure shown in this study is considered to be the maximum value.

4.4.2 Reproducibility of the current atmosphere

Titan's current atmospheric pressure is about 0.15 MPa. As shown in figure 4.9, methane can be released from methane hydrate as much as atmospheric pressure. However, the current atmosphere contains not only methane but also nitrogen, and the partial pressure of methane is about 5% of the total pressure. Therefore, the dissociation of methane hydrate causes the problem that too much methane remains in the atmosphere. There are several possible reasons for this problem. First, the methane atmospheric pressure determined in this study is considered to be a maximum value as mentioned in the previous subsection. In this study, it is assumed that all the methane is immediately released to the atmosphere when the methane hydrate dissociates. In fact, some of the released methane may stay in the ocean or form hydrate again in the icy shell. Second, the formed gas hydrate in Titan may not be pure methane hydrate, but mixed hydrate. In the Titan environment, not only methane hydrate but also other gas hydrates can be formed. Not only methane, but also Ar, Kr, Xe, and N_2 can be major components of gas hydrates in Titan[95]. It is possible that the amount of methane gas contained in gas hydrate decreased as a result of the incorporation of these other gas molecules. Finally, the effect of the timing of methane hydrate formation on the methane atmospheric pressure revealed in this study can be considered as the reason for the low methane atmospheric pressure. If the methane hydrate formed by ongoing methane production after accretion, that is, if the methane hydrate formed too late, it would not be able to supply methane gas to the atmosphere. In addition, if the methane hydrate was formed when the icy shell was thin immediately after the accretion, the methane atmosphere would be too much. Therefore, it may be necessary that the methane hydrate formation started after the thickness of the icy shell thickened to about 100 km after the accretion. As shown in figure 4.8, when methane hydrate exists from the initial stage, the thickness of the icy shell remains almost unchanged from the initial stage. Therefore, if the icy shell thickness and the presence of methane hydrate are confirmed by future exploration, it may provide a significant constraint on the history of Titan's evolution.

4.4.3 Perspectives for future exploration

The Titan exploration mission, DragonFly, is planned by NASA. Dragonfly is equipped with a sensor called DragMet (Dragonfly Geophysics and Meteorology Package) to obtain information on the surface and interior of Titan [96]. DragMet will investigate the interior structure with seismic surveys. Also, the electrical properties near the surface will be investigated. The Young's modulus of ice and methane hydrate is similar, but the Poisson's ratio of methane hydrate is larger than that of ice [19]. Therefore, the velocity ratios of P-waves and S-waves are different. In addition, the dielectric constant is smaller in methane hydrate [19]. Therefore, there is a possibility that methane hydrate layer in the lower part of the icy shell assumed in this study can be detected. So far, no reliable evidence of methane hydrate has been found outside the Earth. I hope that Dragonfly will be the first to observe methane hydrate outside the Earth.

4.5 Summary

In this section, the effects of methane hydrate on the evolution of the internal structure and the methane atmosphere on Titan are investigated using the developed numerical model. The presence of methane hydrate can simultaneously indicate the existence of conductive icy shell and a subsurface ocean. In this case, I obtained the result that the HP ice layer conventionally considered to exist in the interior does not exist. Due to the stability of methane hydrate throughout the interior of Titan, it was found that the thickness of the initial icy shell has a significant influence on the present thickness of the subsurface ocean when methane hydrate exists. It was also found that the formation and dissociation of methane hydrate can supply a large amount of methane gas to Titan's atmosphere. In order to supply methane to the atmosphere from methane hydrate, the formation of methane hydrate must occur at least within 500 Myr from the formation of Titan, because methane is not supplied to the atmosphere when the formation of methane hydrate is late. The amount of methane supplied to the atmosphere depends on the initial icy shell thickness. If methane hydrate exists, the initial icy shell thickness is almost equal to the present icy shell thickness.

Therefore, if future exploration confirms icy shell thickness and the existence of methane hydrate, it will place significant constraints on the history of Titan's evolution.

Chapter 5

Possible existence of methane hydrate in generic icy moons

5.1 Introduction

There are many icy bodies in the solar system, and their appearance varies widely. Figure 1.2 shows the bulk density and radius of icy bodies. The appearance and geological characteristics of icy bodies are roughly determined by their bulk density and radius. Another major factor is how the early moons accureted. The difference between the moons of the Jupiter and Saturnian systems may represent the difference in the accretion process in the circumplanetary disk [97]. If considering a single planetary system, bulk density and radius are thought to be the major factors that determine the moon's present state. The bulk density represents the amount of rock, i.e., the amount of heat derived from the decay of radioactive elements in the rocky core. The radius represents the pressure inside the moon, i.e., the phase of ice that appears. In the previous sections, it is found that the presence or absence of methane hydrate has a significant impact on the thermal evolution of icy moons. In order for methane hydrates to exist, the subsurface ocean must not only be saturated with methane but also have high pressure. Therefore, methane hydrate formation is likely to be easier in larger bodies, but less likely in smaller ones. While, if there is a large amount of rock, there is a possibility that methane hydrate will dissociate or that methane hydrate will not be formed due to the large amount of heat from the radioactive decay from the rocky core. Therefore, the possibility of the existence of methane hydrate may be greatly related to the size of the icy body and the amount of

rock (i.e., bulk density). What sizes and bulk densities of icy bodies can have methane hydrate? In addition, does the presence of methane hydrate increase the possibility of the existence of a subsurface ocean in icy moons? Thus, in this study, I investigate the thermal evolution of generic icy moons with hypothetical bulk density and radius using the developed thermal evolution model. The goal of this section is to find the icy moon size and bulk density conditions that would allow methane hydrate to exist and to find the conditions where subsurface oceans can exist in icy moons when methane hydrate exists.

5.2 Methods

In this study, I use the thermal evolution model developed in section 2. The differences from section 2 and the initial setup are described below.

5.2.1 Interior structures

In every icy moon, the density of rock is 2500 $\mathrm{kg\,m^{-3}}$, the density of ocean is 1000 $\mathrm{kg\,m^{-3}}$, and the density of ice Ih and methane hydrate is 920 $\mathrm{kg\,m^{-3}}$ The thickness of the initial icy shell is set to 50 km. If the moon's size is small and its rocky core is large, a 50 km H_2O layer cannot be prepared. For such moons, I set the initial icy shell thickness to 10 km. The thickness of the initial methane hydrate layer and that of the initial HP ice layer are 0 km. The size of the rocky core is obtained using equation (3.4).

5.2.2 Parameter setting

Generic icy moons are assumed to exist in the Saturn system. This assumption affects the surface temperature and the methane loss rate. The size and bulk density of the bodies are considered to be from about Mimas to Titan. The radius ranges from 250 km to 3000 km. The bulk density ranges from 1250 $\mathrm{kg\,m^{-3}}$ to 2250 $\mathrm{kg\,m^{-3}}$. Figure 5.1 shows the parameter sets of bulk density and radius used in the calculation. In this study, I assume rocky cores with a density of 2500 $\mathrm{kg\,m^{-3}}$, so moons with bulk density greater than 2500 $\mathrm{kg\,m^{-3}}$ cannot be

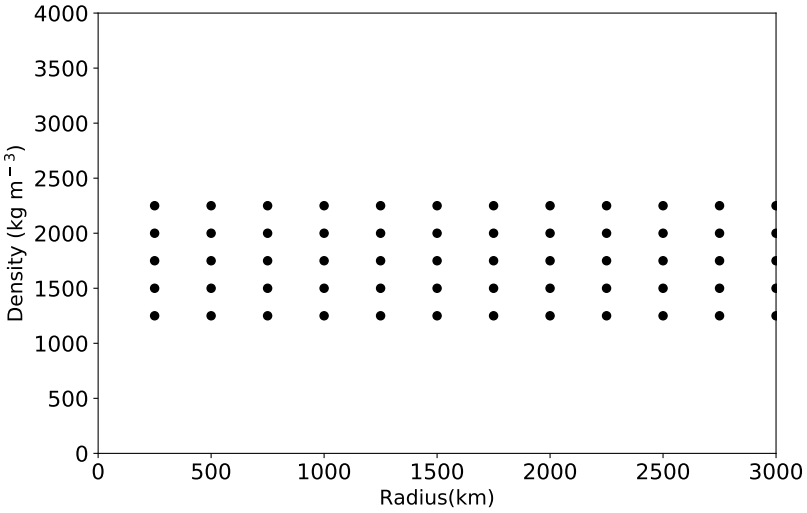

Figure 5.1: The parameter sets of bulk density and radius used in the calculation are shown.

calculated. Also, since the density of ice is assumed to be 920 kg m^{-3}, moons with bulk density less than 920 kg m^{-3} cannot be calculated.

5.2.3 Initial conditions

The initial methane concentration in ocean is set to be 1% in the entire H_2O layer (icy shell, ocean, and methane hydrate layer, and HP ice layer) or 1.0×10^9 mol m^{-3}. The latter condition means that there is always methane supersaturation in the ocean, i.e., there is always enough methane in the subsurface ocean for methane hydrate to be formed due to ongoing methane production. In the case of no methane hydrate formation, the initial methane concentration is set to 0 mol m^{-3}. The surface temperature was set to 80.0 K for all the moons. The calculation starts at the 100 Myr after CAI, which is assumed to already have a differentiated structure at this time. The initial temperature of the top of the icy shell is fixed at the surface temperature. The temperature at the bottom of the icy shell and in the subsurface ocean is set to the melting point at the bottom of the icy shell. The temperature inside the icy shell is a linear function of the temperature at the bottom of the icy shell and the surface temperature. The rocky

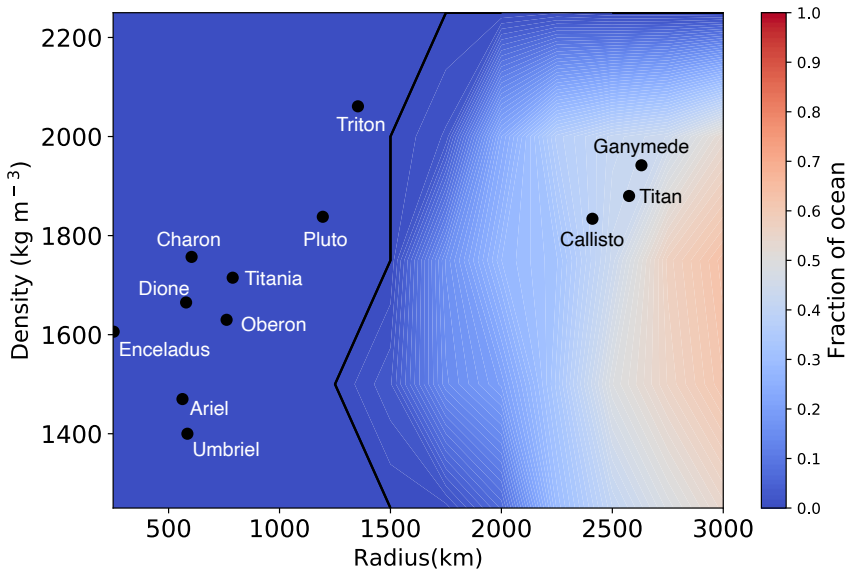

Figure 5.2: The color contour shows the ratio of the final subsurface ocean to the total H_2O layer. The initial ocean contains no methane. The solid black line means that the final ocean is 0 km.

core and ocean temperatures are the same as the melting point at the bottom of the icy shell. The rate of methane destroyed by photolysis on the moon's surface is assumed to be equal to the present value on Titan. For simplicity, ongoing methane production and tidal heating are not considered.

5.3 Results

5.3.1 Final ocean thickness

Figure 5.2, figure 5.3, and figure 5.4 show the final ocean thickness as a percentage of the total H_2O layer. Figure 5.2 shows ice only, figure 5.3 shows 1% initial methane, and figure 5.4 shows the case where initial methane is plentiful. The color contours show the ratio of the subsurface ocean volume to the total H_2O layer volume. It is found that the higher the initial methane content, the more

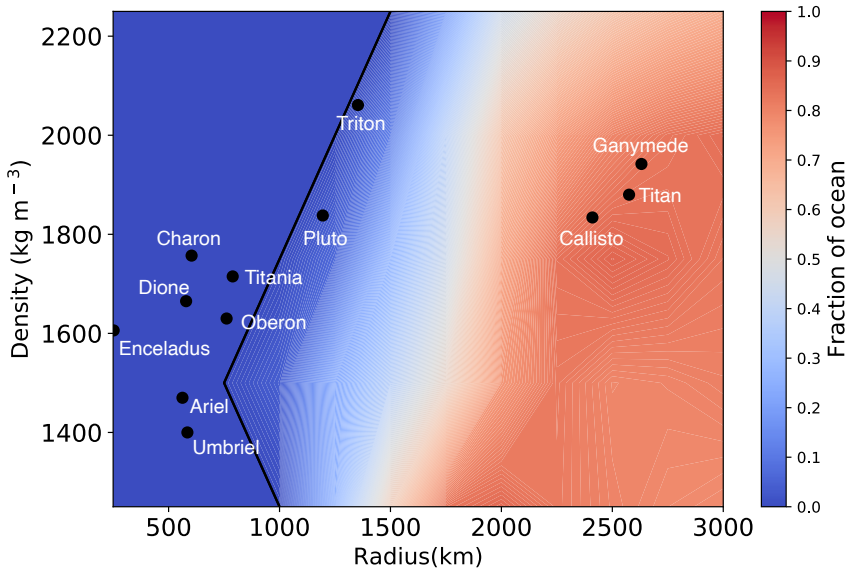

Figure 5.3: The color contour shows the ratio of the final subsurface ocean to the total H_2O layer. The initial ocean contains 1% methane in the entire H_2O layer. The solid black line means that the final ocean is 0 km.

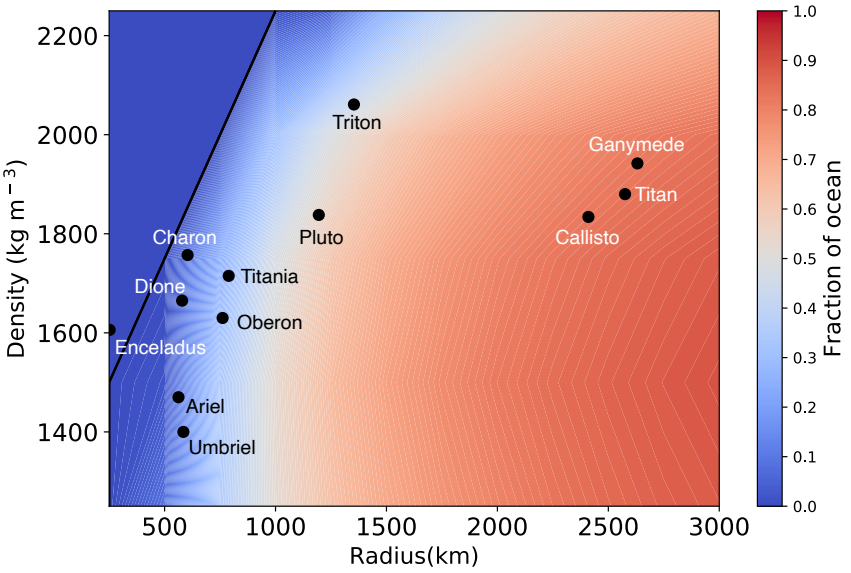

Figure 5.4: The color contour shows the ratio of the final subsurface ocean to the total H_2O layer. The initial ocean contains enough methane to create methane hydrate layer of sufficient thickness. In other words, the ocean is always supersaturated with methane. The solid black line means that the final ocean is 0 km.

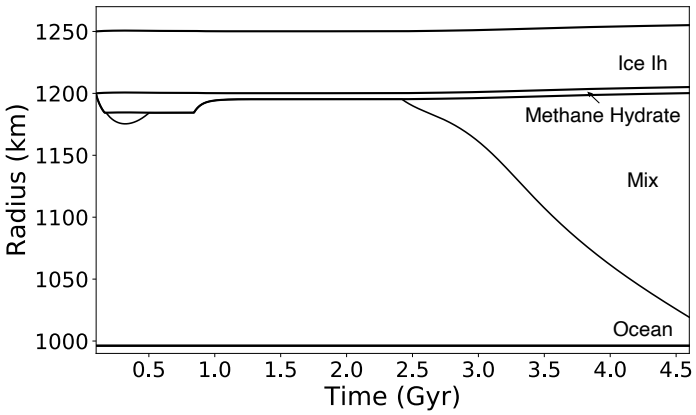

Figure 5.5: The time evolution of the internal structure for the radius of 1250 km, the bulk density of 1750 kg m^{-3}, and the initial methane concentration of 1% in the H_2O layer is shown.

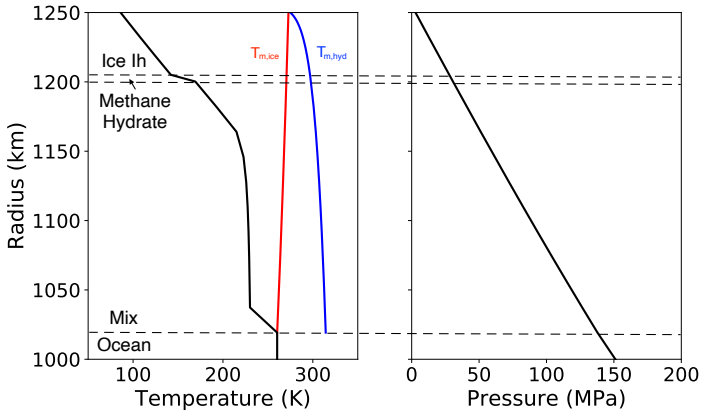

Figure 5.6: The final temperature and pressure profiles in the H_2O layer in figure 5.5 is shown. Red line represents ice melting point. Blue line represents the methane hydrate dissociation point.

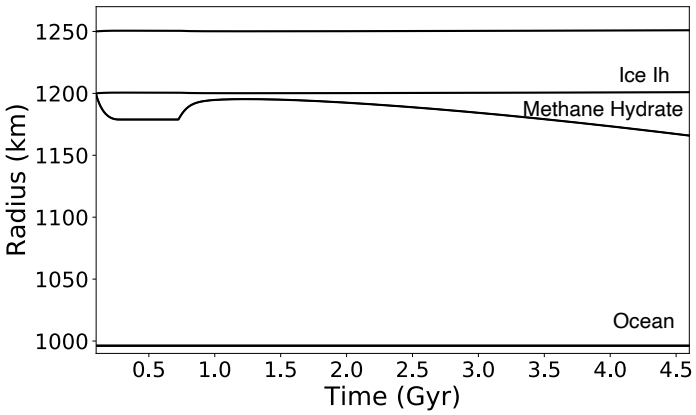

Figure 5.7: The time evolution of the internal structure for the radius of 1250 km, the bulk density of 1750 $\mathrm{kg\,m^{-3}}$, and the plenty methane concentration in the H_2O layer is shown.

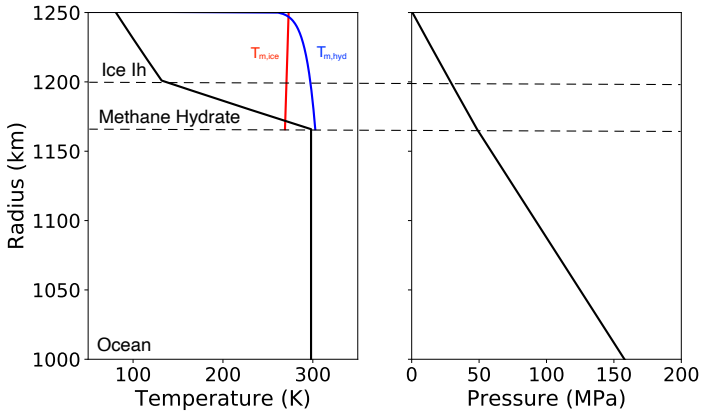

Figure 5.8: The final temperature and pressure profiles in the H_2O layer in figure 5.7 is shown. Red line represents ice melting point. Blue line represents the methane hydrate dissociation point.

moons have the subsurface oceans. The difference of results between the case with 1% methane and the case with plenty of methane is the presence or absence of a mix layer in the moon. Figure 5.5 shows the time evolution of the internal structure for the radius of 1250 km, the bulk density of 1750 $\mathrm{kg\,m^{-3}}$, and the initial methane concentration of 1% in the H_2O layer. Figure 5.6 shows the final temperature and pressure profiles in the H_2O layer at that time. Figure 5.7 and figure 5.8 show the results in the case that initial methane concentration is plenty. When there is enough methane, the mix layer does not appear because the methane hydrate formation does not use up the methane in the ocean. When the initial methane is 1%, the moon with the largest volume ratio in the ocean has a radius of 2500 km and a bulk density of 1750 $\mathrm{kg\,m^{-3}}$. If the bulk density is too large, it is difficult to maintain much methane hydrate in the moon due to the large amount of heat from radioactive decay. Therefore, there is little insulation effect by methane hydrate layer. On the other hand, if there are too few heat sources, it is not possible to maintain the ocean. This balance determines what moon have the thickest ocean. Therefore, the moon with the thickest ocean is different from the one with plenty of methane.

It is the medium-sized moons with a radius of 750 to 1,500 km that are affected by the presence or absence of methane hydrate to have a subsurface ocean. Large moons can have a subsurface ocean regardless of the presence or absence of methane hydrate, while small moons do not have a subsurface ocean regardless of the presence or absence of methane hydrate.

5.3.2 Final methane hydrate layer thickness

Figure 5.9 shows the volume fraction of methane hydrate layer in the entire final H_2O layer when the initial methane is 1%. Methane hydrate can be found in icy moons of almost any size and density. When the radius is less than 1500km, the fraction of methane hydrate layer is large. This means that even if methane hydrate layer is formed, the layer does not receive enough heat to melt. For a radius of 250 t0 500 km and a bulk density of 2250 $\mathrm{kg\,m^{-3}}$, there are no methane hydrate layers. This is because the icy layer is too thin, that is, the pressure in the icy layer is too low to form methane hydrate. If the radius is large (more

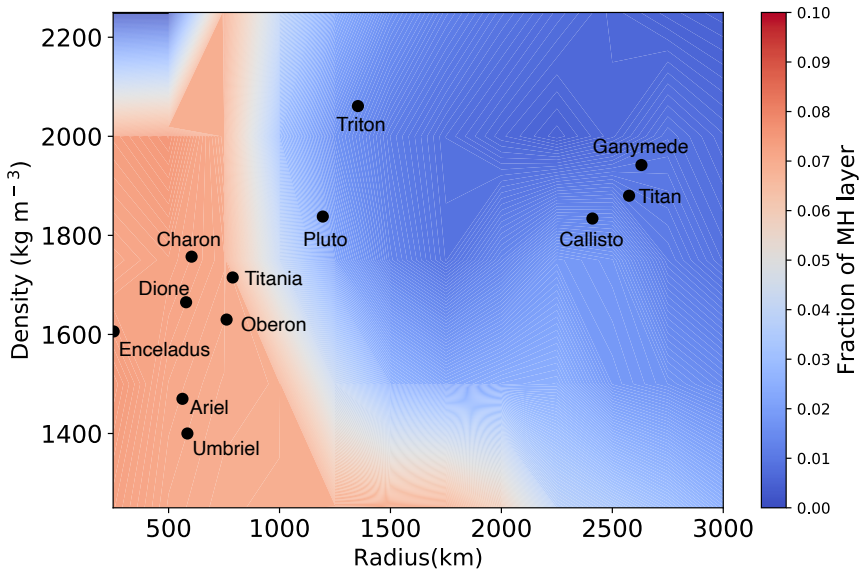

Figure 5.9: The color contours show the ratio of the final methane hydrate layer to the total H_2O layers. The maximum value of the color contour is 0.1. The initial ocean contains 1% methane in the entire H_2O layer.

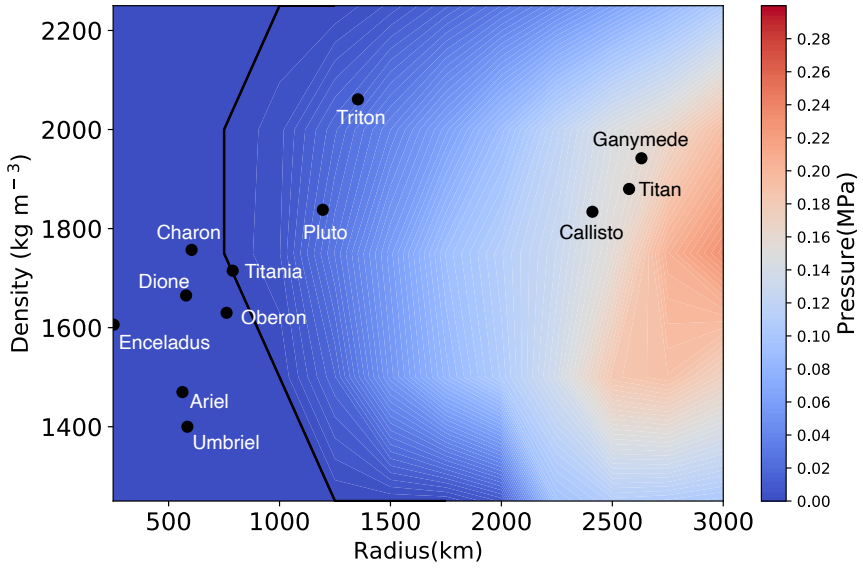

Figure 5.10: The color contours show the final methane atmospheric pressure. The initial ocean contains 1% methane in the entire H_2O layer.

than 2000 km) and the bulk density is large (more than 1750 kg m^{-3}), the heat from the rocky core is too large and it is difficult to maintain the much methane hydrate layer. However, the fact that the thick ocean remains as shown in figure 5.3 shows that the subsurface ocean is maintained by the thin methane hydrate layer.

5.3.3 Atmospheric methane pressure

Figure 5.10 and figure 5.11 show the final methane pressure. Figure 5.10 shows the case where the initial methane is 1%, and figure 5.11 shows the case where the initial methane is plentiful. If 1% of the initial methane is present in the entire H_2O layer, methane atmosphere remains in an icy moon of about 1000 km in size. If initial methane in the ocean is plentiful, methane atmosphere remains for most sizes and bulk densities of icy moons The maximum methane atmospheric pressure is ∼0.2 MPa when the initial methane is 1% and ∼0.3 MPa when the

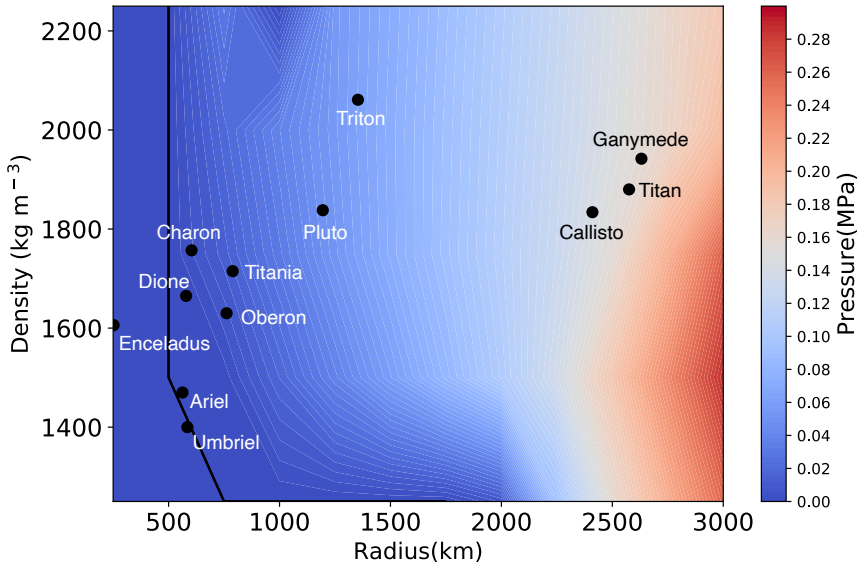

Figure 5.11: The color contours show the final methane atmospheric pressure. The initial ocean contains enough methane to create methane hydrate layer of sufficient thickness. In other words, the ocean is always supersaturated with methane.

initial methane is plentiful. It was found that a medium-sized moon of about 750 to 1500 km can have a methane atmosphere, depending on the amount of initial methane content. For moons with a radius of 2500 km to 3000 km, it is possible to have a thick methane atmosphere similar to Titan.

5.4 Discussions

5.4.1 Icy moons where methane hydrate can exist

As shown in the figure 5.9, methane hydrate layer is confirmed in all the calculated icy moons in the presence of methane in the ocean, except for the icy moons with a radius of less than 500 km and high bulk density. The presence of 1% methane in the H_2O layer, consistent with the composition of the comet[14], suggests that methane hydrate may be universally present in icy moons. As shown in the figure 5.9, most of the icy moons in the solar system have internal structures that allow methane hydrate to exist stably. Note that the rocky core density assumed in this study is different from the actual rocky core density of the icy moon.

On the other hand, as shown in figure 5.10, the existence of methane hydrate layer does not necessarily mean the existence of a methane atmosphere. If the initial methane is 1%, a radius of about 1000 km is required to retain the methane atmosphere to the present. Pluto is close to the above conditions, and in fact a thin methane atmosphere has been found on Pluto. Note, however, that in this study, the methane loss rate is assumed to be the same as that of Titan today.

5.4.2 Icy moons whose thermal evolution is affected by the presence of methane hydrates

Based on the results of this study, medium-sized icy moons with a radius of 750 km to 1,500 km are the most affected by the presence of methane hydrate. If methane hydrate is present in these icy moons, the subsurface ocean and methane atmosphere can be maintained until now. If there is a lot of initial methane, or ongoing methane production, even smaller icy moons could have a subsurface

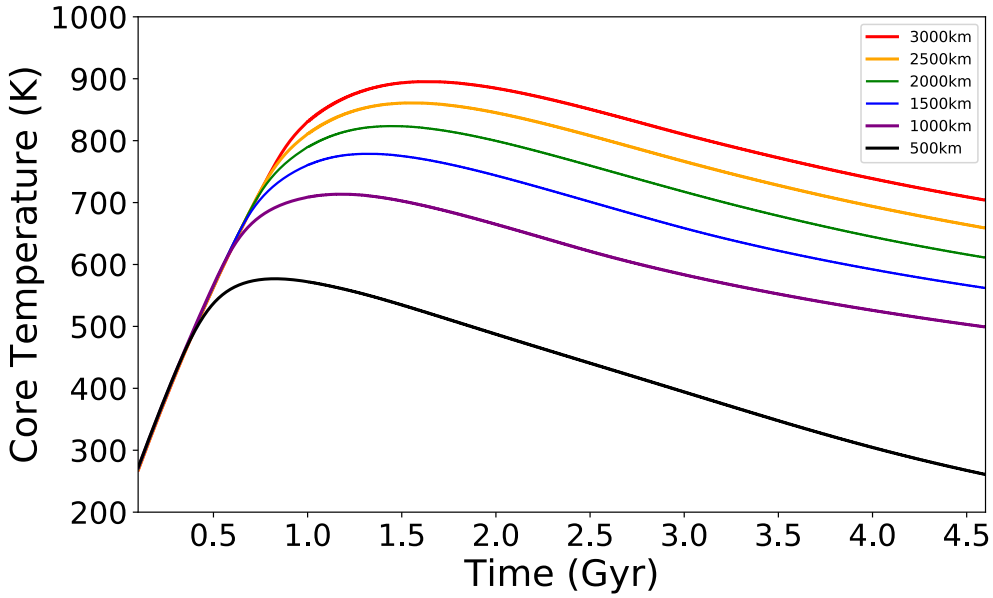

Figure 5.12: The time evolution of the temperature at the center of the rock core is shown. The bulk density is 1750 kg m^{-3}.

ocean and methane atmosphere. Pluto and Neptune's satellite Triton are the closest icy moons that can be assumed to exist in the solar system. It may be possible that the methane present on the surface of Pluto and Triton once experienced methane hydrates.

Also, if the moon size is large, it is possible to have a thick atmosphere like Titan. However, if the size of the satellite is too large, the rocky core may become too warm and differentiate, and the internal structure may not be like Titan. Figure 5.12 shows the time evolution of the core temperature. When the radius is 3000 km, the maximum temperature reaches 900 K, which is the dehydration temperature of serpentine. In other words, an icy moon with a radius of about 3,000 km can have a thick atmosphere like Titan, but it cannot have a partially differentiated structure like Titan.

5.5 Summary

Thermal evolution calculations were carried out for generic icy moons of various sizes and bulk densities using the model developed in this study. It was found that methane hydrate can be universally present if about 1% methane is present. The presence of methane hydrate layer increases the possibility of the existence of an icy moon's subsurface ocean. For moons with a radius of about 750-1500 km, the existence of methane hydrate layer has a significant impact on whether the moon has a subsurface ocean and atmospheric methane. The amount of methane in the early stages of the formation of the icy moon greatly affects the current state of the icy moon, including the atmosphere and the presence or absence of subsurface oceans, because the amount of methane hydrate varies. If the internal structure and the presence of methane hydrate of icy moons can be clarified through future exploration, we may be able to get closer to the history of icy moons.

Chapter 6

Summary

In order to investigate the role of methane hydrate on the thermal evolution of icy moons, I developed a one-dimensional thermal evolution model that takes into account methane in ocean, which has not been considered so far. In Chapter 2, the necessary equations were introduced for the newly introduced methane hydrate layer, mixed layer, and high-pressure ice layer. The validity of the developed model was confirmed by comparison with previous studies. In Chapter 3, the conditions for the existence of the subsurface ocean in Enceladus and Mimas were investigated using the model developed in this study. When methane hydrate is considered, the present thick ocean can be explained by the same amount of tidal heating rate as that predicted by the orbital evolution calculation and astrometry. In addition, when methane hydrate is present in the Mimas, it was found that both a thick ocean and the inactive surface can be achieved. These results indicate that methane hydrate has a role as an insulator inside icy moons. In Chapter 4, the role of methane hydrate to the Titan atmosphere was investigated using the model developed in this study. Methane contained in the subsurface ocean of the Titan forms methane hydrate once and then releases methane to the atmosphere through dissociation. The amount of methane released by the dissociation of methane hydrate was enough to maintain the methane atmosphere of Titan until now, even taking into account the effect of photolysis. It was also found that the amount of methane remaining in the atmosphere changed depending on the timing of methane hydrate formation. These results indicate that methane hydrate plays a role as a reservoir of methane in icy moons. In Chapter 5, the icy moons with methane hydrate and the icy moons with subsurface oceans that change depending on the presence of methane hydrate are

investigated by performing thermal evolution calculations for icy moons of various radii and bulk densities. Even with 1% methane, which is consistent with the composition of comets, the existence of methane hydrate was confirmed in a number of icy moons. I also showed that the presence of methane hydrate could make the subsurface ocean in icy moons more universal.

These studies showed that methane hydrate exists in a number of icy moons with realistic amounts of methane, and that the subsurface oceans may exist universally. Methane hydrate plays a major role in the thermal evolution of icy moons by maintaining the subsurface ocean and atmosphere. Methane hydrate may be a key compound in the thermal evolution of icy moons.

Acknowledgements

I would like to express my great appreciation to everyone who contributed to the completion of this thesis. I would like to appreciate Prof. Sho Sasaki for his generous and sincere instructions that allowed me to do my research freely. His precise and constructive comments in the seminars helped me to grow as a researcher. I was also very encouraged by the messages in our casual conversation and the way of thinking as a researcher. I would like to appreciate Dr. Kazuto Saiki for providing me with many stimulating topics and opportunities. I was greatly inspired by his vitality and broad perspective on research. Because of him, I was able to challenge many things, not just research. What I learned from his attitude is my treasure. I am very grateful to Dr. Osamu Otaka for teaching me points of view that I did not know. I learned a lot from his point of view on materials. He has also been very helpful to me outside of my research. The interaction with "Oyaji" that I have never experienced before has greatly expanded my horizons. I would like to express my gratitude to Dr. Jun Kimura for his careful and attentive instruction. Without his help, I would not have been able to complete the simulation of this study. The discussions with him helped me to understand not only the icy moons but also the fun of simulations and the evolution of solar system solid bodies. I greatly appreciate Dr. Atsushi Tani to his active discussions and many constructive directions. All the experiments that I conducted with him, which I could not mention in this thesis, are my assets. Without him, I would not have been able to do research in this field and go on to a PhD course. I would like to express my gratitude to him for the many valuable opportunities such as to participate in conferences, to enter doctoral courses, and to study ice. I would like to express my gratitude to Professor Sho Sasaki, Professor Tadashi Kondo, Professor Kentaro Terada, Dr. Kazuto Saiki, and Dr. Atsushi Tani for their many constructive comments on this thesis. All the comments have improved this thesis. I would not have been able to continue my research without all the members who have been in our laboratory. The

discussions and trivial conversations I had with them helped me a lot. I would like to thank them for their involvement with me . I wish to express my gratitude to my friend Ryota Ochiai for his many encouragements. Without him, I would not have been able to continue my research until now. Finally, I would like to express my gratitude to my family for allowing me to continue my research so freely. Thanks to all the people who have been involved with me, I have been able to lead a happy school life.

Bibliography

[1] F. Nimmo and R. T. Pappalardo, "Ocean worlds in the outer solar system: OCEAN WORLDS," *Journal of Geophysical Research: Planets*, vol. 121, no. 8, pp. 1378–1399, Aug. 2016.

[2] J. H. Waite Jr, W. S. Lewis, B. A. Magee, J. I. Lunine, W. B. McKinnon, C. R. Glein, O. Mousis, D. T. Young, T. Brockwell, J. Westlake, M.-J. Nguyen, B. D. Teolis, H. B. Niemann, R. L. McNutt Jr, M. Perry, and W.-H. Ip, "Liquid water on Enceladus from observations of ammonia and 40Ar in the plume," *Nature*, vol. 460, no. 7254, pp. 487–490, Jul. 2009.

[3] L. Roth, J. Saur, K. D. Retherford, D. F. Strobel, P. D. Feldman, M. A. McGrath, and F. Nimmo, "Transient Water Vapor at Europa's South Pole," *Science*, vol. 343, no. 6167, pp. 171–174, Jan. 2014.

[4] H. Hussmann, F. Sohl, and T. Spohn, "Subsurface oceans and deep interiors of medium-sized outer planet satellites and large trans-neptunian objects," *Icarus*, vol. 185, no. 1, pp. 258–273, Nov. 2006.

[5] C. Zimmer, "Subsurface Oceans on Europa and Callisto: Constraints from Galileo Magnetometer Observations," *Icarus*, vol. 147, no. 2, pp. 329–347, Oct. 2000.

[6] M. G. Kivelson, "The Permanent and Inductive Magnetic Moments of Ganymede," p. 16.

[7] T. V. Hoolst, R.-M. Baland, and A. Trinh, "The diurnal libration and interior structure of Enceladus," *Icarus*, vol. 277, pp. 311–318, Oct. 2016.

[8] R. Tajeddine, N. Rambaux, V. Lainey, S. Charnoz, A. Richard, A. Rivoldini, and B. Noyelles, "Constraints on Mimas' interior from Cassini ISS libration measurements," *Science*, vol. 346, no. 6207, pp. 322–324, Oct. 2014.

[9] J. Kimura and S. Kamata, "Stability of the subsurface ocean of pluto," *Planetary and Space Science*, vol. 181, p. 104828, Feb. 2020.

[10] M. Neveu and A. R. Rhoden, "Evolution of Saturn's mid-sized moons," *Nature Astronomy*, Apr. 2019.

[11] U. Malamud and D. Prialnik, "Modeling serpentinization: Applied to the early evolution of Enceladus and Mimas," *Icarus*, vol. 225, no. 1, pp. 763–774, Jul. 2013.

[12] S. Kamata, "One-Dimensional Convective Thermal Evolution Calculation Using a Modified Mixing Length Theory: Application to Saturnian Icy Satellites: 1-D THERMAL CONVECTION CALCULATION," *Journal of Geophysical Research: Planets*, vol. 123, no. 1, pp. 93–112, Jan. 2018.

[13] M. Choukroun and O. Grasset, "Thermodynamic data and modeling of the water and ammonia-water phase diagrams up to 2.2 GPa for planetary geophysics," *The Journal of Chemical Physics*, vol. 133, no. 14, p. 144502, Oct. 2010.

[14] M. J. Mumma and S. B. Charnley, "The Chemical Composition of Comets—Emerging Taxonomies and Natal Heritage," *Annual Review of Astronomy and Astrophysics*, vol. 49, no. 1, pp. 471–524, Sep. 2011.

[15] N. P. Hammond, E. Parmenteir, and A. C. Barr, "Compaction and melt transport in ammonia-rich ice shells: Implications for the evolution of triton," *Journal of Geophysical Research: Planets*, vol. 123, no. 12, pp. 3105–3118, 2018.

[16] M. Arakawa and N. Maeno, "Effective viscosity of partially melted ice in the ammonia-water system," *Geophysical Research Letters*, vol. 21, no. 14, pp. 1515–1518, Jul. 1994.

[17] S. Kamata, F. Nimmo, Y. Sekine, K. Kuramoto, N. Noguchi, J. Kimura, and A. Tani, "Pluto's ocean is capped and insulated by gas hydrates," *Nature Geoscience*, vol. 12, no. 6, pp. 407–410, Jun. 2019.

[18] A. Bouquet, O. Mousis, J. H. Waite, and S. Picaud, "Possible evidence for a methane source in Enceladus' ocean," *Geophysical Research Letters*, vol. 42, no. 5, pp. 1334–1339, Mar. 2015.

[19] E. D. Sloan Jr and C. A. Koh, *Clathrate hydrates of natural gases*. CRC press, 2007.

[20] W. F. Waite, J. C. Santamarina, D. D. Cortes, B. Dugan, D. N. Espinoza, J. Germaine, J. Jang, J. W. Jung, T. J. Kneafsey, H. Shin, K. Soga, W. J. Winters, and T.-S. Yun, "Physical properties of hydrate-bearing sediments," *Reviews of Geophysics*, vol. 47, no. 4, p. RG4003, Dec. 2009.

[21] W. B. Durham, S. H. Kirby, L. A. Stern, and W. Zhang, "The strength and rheology of methane clathrate hydrate: THE RHEOLOGY OF METHANE CLATHRATE HYDRATE," *Journal of Geophysical Research: Solid Earth*, vol. 108, no. B4, Apr. 2003.

[22] K. Kalousová and C. Sotin, "Dynamics of Titan's high-pressure ice layer," *Earth and Planetary Science Letters*, vol. 545, p. 116416, Sep. 2020.

[23] G. Tobie, J. I. Lunine, and C. Sotin, "Episodic outgassing as the origin of atmospheric methane on Titan," *Nature*, vol. 440, no. 7080, pp. 61–64, Mar. 2006.

[24] K. Lodders, "Solar system abundances and condensation temperatures of the elements," *The Astrophysical Journal*, vol. 591, no. 2, p. 1220, 2003.

[25] T. Spohn and G. Schubert, "Oceans in the icy Galilean satellites of Jupiter?" *Icarus*, vol. 161, no. 2, pp. 456–467, Feb. 2003.

[26] S. Sasaki and K. Nakazawa, "Metal-silicate fractionation in the growing Earth: Energy source for the terrestrial magma ocean," *Journal of Geophysical Research*, vol. 91, no. B9, p. 9231, 1986.

[27] J. Kimura, T. Nakagawa, and K. Kurita, "Size and compositional constraints of Ganymede's metallic core for driving an active dynamo," *Icarus*, vol. 202, no. 1, pp. 216–224, Jul. 2009.

[28] J. Leliwa-Kopystyński, M. Maruyama, and T. Nakajima, "The Water–Ammonia Phase Diagram up to 300 MPa: Application to Icy Satellites," *Icarus*, vol. 159, no. 2, pp. 518–528, Oct. 2002.

[29] D. L. Goldsby and D. L. Kohlstedt, "Superplastic deformation of ice: Experimental observations," *Journal of Geophysical Research: Solid Earth*, vol. 106, no. B6, pp. 11 017–11 030, Jun. 2001.

[30] A. C. Barr and W. B. McKinnon, "Convection in ice i shells and mantles with self-consistent grain size," *Journal of Geophysical Research: Planets*, vol. 112, no. E2, 2007.

[31] W. B. Durham, O. Prieto-Ballesteros, D. Goldsby, and J. Kargel, "Rheological and thermal properties of icy materials," *Space science reviews*, vol. 153, no. 1, pp. 273–298, 2010.

[32] M. Běhounková, G. Tobie, G. Choblet, and O. Čadek, "Impact of tidal heating on the onset of convection in Enceladus's ice shell," *Icarus*, vol. 226, no. 1, pp. 898–904, Sep. 2013.

[33] N. Hilairet, B. Reynard, Y. Wang, I. Daniel, S. Merkel, N. Nishiyama, and S. Petitgirard, "High-Pressure Creep of Serpentine, Interseismic Deformation, and Initiation of Subduction," *Science*, vol. 318, no. 5858, pp. 1910–1913, Dec. 2007.

[34] L. Bezacier, B. Journaux, J.-P. Perrillat, H. Cardon, M. Hanfland, and I. Daniel, "Equations of state of ice vi and ice vii at high pressure and high temperature," *The Journal of chemical physics*, vol. 141, no. 10, p. 104505, 2014.

[35] R. J. Macke, G. J. Consolmagno, and D. T. Britt, "Density, porosity, and magnetic susceptibility of carbonaceous chondrites," *Meteoritics & Planetary Science*, vol. 46, no. 12, pp. 1842–1862, 2011.

[36] V. Tchijov, "Heat capacity of high-pressure ice polymorphs," *Journal of Physics and Chemistry of Solids*, vol. 65, no. 5, pp. 851–854, 2004.

[37] P. V. Hobbs, *Ice physics*. Oxford university press, 2010.

[38] R. Ross, P. Andersson, and G. Bäckström, "Effects of h and d order on the thermal conductivity of ice phases," *The Journal of Chemical Physics*, vol. 68, no. 9, pp. 3967–3972, 1978.

[39] W. Durham and L. Stern, "Rheological properties of water ice—applications to satellites of the outer planets," *Annual Review of Earth and Planetary Sciences*, vol. 29, no. 1, pp. 295–330, 2001.

[40] K. Hester, Z. Huo, A. Ballard, C. Koh, K. Miller, and E. Sloan, "Thermal expansivity for si and sii clathrate hydrates," *The Journal of Physical Chemistry B*, vol. 111, no. 30, pp. 8830–8835, 2007.

[41] G. K. Anderson, "Enthalpy of dissociation and hydration number of methane hydrate from the clapeyron equation," *The Journal of Chemical Thermodynamics*, vol. 36, no. 12, pp. 1119–1127, 2004.

[42] Z. Duan and S. Mao, "A thermodynamic model for calculating methane solubility, density and gas phase composition of methane-bearing aqueous fluids from 273 to 523K and from 1 to 2000bar," *Geochimica et Cosmochimica Acta*, vol. 70, no. 13, pp. 3369–3386, Jul. 2006.

[43] M. Choukroun, O. Grasset, G. Tobie, and C. Sotin, "Stability of methane clathrate hydrates under pressure: Influence on outgassing processes of methane on Titan," *Icarus*, vol. 205, no. 2, pp. 581–593, Feb. 2010.

[44] T. Uchida, T. Hirano, T. Ebinuma, H. Narita, K. Gohara, S. Mae, and R. Matsumoto, "Raman spectroscopic determination of hydration number of methane hydrates," *AIChE Journal*, vol. 45, no. 12, pp. 2641–2645, Dec. 1999.

[45] A. N. Dunaeva, D. V. Antsyshkin, and O. L. Kuskov, "Phase diagram of H2O: Thermodynamic functions of the phase transitions of high-pressure ices," *Solar System Research*, vol. 44, no. 3, pp. 202–222, Jun. 2010.

[46] K. Kalousová and C. Sotin, "Melting in High-Pressure Ice Layers of Large Ocean Worlds—Implications for Volatiles Transport," *Geophysical Research Letters*, vol. 45, no. 16, pp. 8096–8103, 2018.

[47] M. Neveu and A. Rhoden, "The origin and evolution of a differentiated Mimas," *Icarus*, vol. 296, pp. 183–196, Nov. 2017.

[48] J. H. Waite, C. R. Glein, R. S. Perryman, B. D. Teolis, B. A. Magee, G. Miller, J. Grimes, M. E. Perry, K. E. Miller, A. Bouquet, J. I. Lunine, T. Brockwell, and S. J. Bolton, "Cassini finds molecular hydrogen in the Enceladus plume: Evidence for hydrothermal processes," *Science*, vol. 356, no. 6334, pp. 155–159, Apr. 2017.

[49] H.-W. Hsu, F. Postberg, Y. Sekine, T. Shibuya, S. Kempf, M. Horányi, A. Juhász, N. Altobelli, K. Suzuki, Y. Masaki, T. Kuwatani, S. Tachibana, S.-i. Sirono, G. Moragas-Klostermeyer, and R. Srama, "Ongoing hydrothermal activities within Enceladus," *Nature*, vol. 519, no. 7542, pp. 207–210, Mar. 2015.

[50] C. J. A. Howett, J. R. Spencer, J. Pearl, and M. Segura, "High heat flow from Enceladus' south polar region measured using 10–600 cm $^{-1}$ Cassini/CIRS data," *Journal of Geophysical Research*, vol. 116, no. E3, p. E03003, Mar. 2011.

[51] M. R. Kirchoff and P. Schenk, "Crater modification and geologic activity in Enceladus' heavily cratered plains: Evidence from the impact crater distribution," *Icarus*, vol. 202, no. 2, pp. 656–668, Aug. 2009.

[52] L. Iess, D. J. Stevenson, M. Parisi, D. Hemingway, R. A. Jacobson, J. I. Lunine, F. Nimmo, J. W. Armstrong, S. W. Asmar, M. Ducci, and P. Tortora, "The Gravity Field and Interior Structure of Enceladus," *Science*, vol. 344, no. 6179, pp. 78–80, Apr. 2014.

[53] P. Thomas, R. Tajeddine, M. Tiscareno, J. Burns, J. Joseph, T. Loredo, P. Helfenstein, and C. Porco, "Enceladus's measured physical libration requires a global subsurface ocean," *Icarus*, vol. 264, pp. 37–47, Jan. 2016.

[54] O. Čadek, G. Tobie, T. Van Hoolst, M. Massé, G. Choblet, A. Lefèvre, G. Mitri, R.-M. Baland, M. Běhounková, O. Bourgeois, and A. Trinh, "Enceladus's internal ocean and ice shell constrained from Cassini gravity, shape, and libration data: ENCELADUS'S INTERIOR FROM CASSINI DATA," *Geophysical Research Letters*, vol. 43, no. 11, pp. 5653–5660, Jun. 2016.

[55] M. Beuthe, "Enceladus's crust as a non-uniform thin shell: I tidal deformations," *Icarus*, vol. 302, pp. 145–174, Mar. 2018.

[56] A. R. Rhoden, W. Henning, T. A. Hurford, D. A. Patthoff, and R. Tajeddine, "The implications of tides on the Mimas ocean hypothesis: DOES MIMAS HAVE AN INTERNAL OCEAN?" *Journal of Geophysical Research: Planets*, vol. 122, no. 2, pp. 400–410, Feb. 2017.

[57] B. Noyelles, "Interpreting the librations of a synchronous satellite – How their phase assesses Mimas' global ocean," *Icarus*, vol. 282, pp. 276–289, Jan. 2017.

[58] M. Segatz, T. Spohn, M. Ross, and G. Schubert, "Tidal dissipation, surface heat flow, and figure of viscoelastic models of Io," *Icarus*, vol. 75, no. 2, pp. 187–206, Aug. 1988.

[59] J. Meyer and J. Wisdom, "Tidal heating in Enceladus," *Icarus*, vol. 188, no. 2, pp. 535–539, Jun. 2007.

[60] F. Nimmo, A. C. Barr, M. Beˇhounkova, and W. B. McKinnon, "The thermal and orbital evolution of Enceladus: Observational constraints and models," p. 19.

[61] Z. Tian and F. Nimmo, "Implications of Second Order Resonance for the Thermal and Orbital Evolution of Mimas," *Monthly Notices of the Royal Astronomical Society*, p. stz3427, Dec. 2019.

[62] K. Kalousová and C. Sotin, "The Insulating Effect of Methane Clathrate Crust on Titan's Thermal Evolution," *Geophysical Research Letters*, vol. 47, no. 13, Jul. 2020.

[63] G. Schubert, J. D. Anderson, B. J. Travis, and J. Palguta, "Enceladus: Present internal structure and differentiation by early and long-term radiogenic heating," *Icarus*, vol. 188, no. 2, pp. 345–355, Jun. 2007.

[64] S. Kamata, I. Matsuyama, and F. Nimmo, "Tidal resonance in icy satellites with subsurface oceans: TIDAL RESONANCE IN ICY SATELLITES," *Journal of Geophysical Research: Planets*, vol. 120, no. 9, pp. 1528–1542, Sep. 2015.

[65] J. H. Roberts and F. Nimmo, "Tidal heating and the long-term stability of a subsurface ocean on Enceladus," *Icarus*, vol. 194, no. 2, pp. 675–689, Apr. 2008.

[66] G. Choblet, G. Tobie, C. Sotin, M. Běhounková, O. Čadek, F. Postberg, and O. Souček, "Powering prolonged hydrothermal activity inside Enceladus," *Nature Astronomy*, vol. 1, no. 12, pp. 841–847, Dec. 2017.

[67] O. Souček, M. Běhounková, O. Čadek, J. Hron, G. Tobie, and G. Choblet, "Tidal dissipation in Enceladus' uneven, fractured ice shell," *Icarus*, vol. 328, pp. 218–231, Aug. 2019.

[68] G. Tobie, "Tidally heated convection: Constraints on Europa's ice shell thickness," *Journal of Geophysical Research*, vol. 108, no. E11, p. 5124, 2003.

[69] T. H. Vu, E. Gloesener, M. Choukroun, A. Ibourichene, and R. Hodyss, "Experimental Study on the Effect of Ammonia on the Phase Behavior of Tetrahydrofuran Clathrates," *The Journal of Physical Chemistry B*, vol. 118, no. 47, pp. 13 371–13 377, Nov. 2014.

[70] T. M. McCollom, "Abiotic methane formation during experimental serpentinization of olivine," *Proceedings of the National Academy of Sciences*, vol. 113, no. 49, pp. 13 965–13 970, Dec. 2016.

[71] R.-S. Taubner, P. Pappenreiter, J. Zwicker, D. Smrzka, C. Pruckner, P. Kolar, S. Bernacchi, A. H. Seifert, A. Krajete, W. Bach, J. Peckmann, C. Paulik, M. G. Firneis, C. Schleper, and S. K.-M. R. Rittmann, "Biological methane production under putative Enceladus-like conditions," *Nature Communications*, vol. 9, no. 1, p. 748, Dec. 2018.

[72] V. Lainey, Ö. Karatekin, J. Desmars, S. Charnoz, J.-E. Arlot, N. Emelyanov, C. Le Poncin-Lafitte, S. Mathis, F. Remus, G. Tobie, and J.-P. Zahn, "STRONG TIDAL DISSIPATION IN SATURN AND CONSTRAINTS ON ENCELADUS' THERMAL STATE FROM ASTROMETRY," *The Astrophysical Journal*, vol. 752, no. 1, p. 14, Jun. 2012.

[73] S. Charnoz, A. Crida, J. C. Castillo-Rogez, V. Lainey, L. Dones, Karatekin, G. Tobie, S. Mathis, C. Le Poncin-Lafitte, and J. Salmon, "Accretion of

Saturn's mid-sized moons during the viscous spreading of young massive rings: Solving the paradox of silicate-poor rings versus silicate-rich moons," *Icarus*, vol. 216, no. 2, pp. 535–550, Dec. 2011.

[74] J. Fuller, J. Luan, and E. Quataert, "Resonance locking as the source of rapid tidal migration in the Jupiter and Saturn moon systems," *Monthly Notices of the Royal Astronomical Society*, vol. 458, no. 4, pp. 3867–3879, Jun. 2016.

[75] D. J. Hemingway and T. Mittal, "Enceladus's ice shell structure as a window on internal heat production," *Icarus*, vol. 332, pp. 111–131, Nov. 2019.

[76] E. M. Schulson, "The fracture of water ice Ih: A short overview," *Meteoritics & Planetary Science*, vol. 41, no. 10, pp. 1497–1508, Oct. 2006.

[77] M. T. Bland, K. N. Singer, W. B. McKinnon, and P. M. Schenk, "Enceladus' extreme heat flux as revealed by its relaxed craters: CRATER RELAXATION ON ENCELADUS," *Geophysical Research Letters*, vol. 39, no. 17, pp. n/a–n/a, Sep. 2012.

[78] T. M. McCollom and J. S. Seewald, "Abiotic Synthesis of Organic Compounds in Deep-Sea Hydrothermal Environments," *Chemical Reviews*, vol. 107, no. 2, pp. 382–401, Feb. 2007.

[79] L. Iess, N. J. Rappaport, R. A. Jacobson, P. Racioppa, D. J. Stevenson, P. Tortora, J. W. Armstrong, and S. W. Asmar, "Gravity Field, Shape, and Moment of Inertia of Titan," *Science*, vol. 327, no. 5971, pp. 1367–1369, Mar. 2010.

[80] C. Béghin, C. Sotin, and M. Hamelin, "Titan's native ocean revealed beneath some 45km of ice by a Schumann-like resonance," *Comptes Rendus Geoscience*, vol. 342, no. 6, pp. 425–433, Jun. 2010.

[81] B. Bills and F. Nimmo, "Forced obliquity and moments of inertia of Titan," *Icarus*, vol. 196, no. 1, pp. 293–297, Jul. 2008.

[82] D. Hemingway, F. Nimmo, H. Zebker, and L. Iess, "A rigid and weathered ice shell on Titan," *Nature*, vol. 500, no. 7464, pp. 550–552, Aug. 2013.

[83] H. B. Niemann, S. K. Atreya, S. J. Bauer, G. R. Carignan, J. E. Demick, R. L. Frost, D. Gautier, J. A. Haberman, D. N. Harpold, D. M. Hunten, G. Israel, J. I. Lunine, W. T. Kasprzak, T. C. Owen, M. Paulkovich, F. Raulin, E. Raaen, and S. H. Way, "The abundances of constituents of Titan's atmosphere from the GCMS instrument on the Huygens probe," vol. 438, p. 6, 2005.

[84] Y. L. Yung, M. Allen, and J. P. Pinto, "Photochemistry of the atmosphere of Titan - Comparison between model and observations," *The Astrophysical Journal Supplement Series*, vol. 55, p. 465, Jul. 1984.

[85] F. Nimmo, "Stresses generated in cooling viscoelastic ice shells: Application to Europa," *Journal of Geophysical Research*, vol. 109, no. E12, p. E12001, 2004.

[86] M. Neveu and S. J. Desch, "Geochemistry, thermal evolution, and cryovolcanism on Ceres with a muddy ice mantle: EVOLUTION OF CERES," *Geophysical Research Letters*, vol. 42, no. 23, pp. 10,197–10,206, Dec. 2015.

[87] E. H. Wilson and S. K. Atreya, "Titan's Carbon Budget and the Case of the Missing Ethane †," *The Journal of Physical Chemistry A*, vol. 113, no. 42, pp. 11 221–11 226, Oct. 2009.

[88] G. Tobie, J. Lunine, J. Monteux, O. Mousis, and F. Nimmo, "The origin and evolution of Titan," in *Titan: Interior, Surface, Atmosphere, and Space Environment*, Feb. 2014, pp. 29–62.

[89] M. Takahashi, T. Kawamura, Y. Yamamoto, H. Ohnari, S. Himuro, and H. Shakutsui, "Effect of shrinking microbubble on gas hydrate formation," *The Journal of Physical Chemistry B*, vol. 107, no. 10, pp. 2171–2173, 2003.

[90] M. Manga and C.-Y. Wang, "Pressurized oceans and the eruption of liquid water on europa and enceladus," *Geophysical Research Letters*, vol. 34, no. 7, 2007.

[91] G. D. Crawford and D. J. Stevenson, "Gas-driven water volcanism and the resurfacing of europa," *Icarus*, vol. 73, no. 1, pp. 66–79, 1988.

[92] W. Xu and L. N. Germanovich, "Excess pore pressure resulting from methane hydrate dissociation in marine sediments: A theoretical approach," *Journal of Geophysical Research: Solid Earth*, vol. 111, no. B1, 2006.

[93] N. A. O. of Japan, *Rika Nenpyo (Chronological Scientific Tables 2013)*. Maruzen Publishing Co., Ltd., 2012.

[94] E. Llewellin, H. Mader, and S. Wilson, "The rheology of a bubbly liquid," *Proceedings of the Royal Society of London. Series A: Mathematical, Physical and Engineering Sciences*, vol. 458, no. 2020, pp. 987–1016, 2002.

[95] C. R. Glein, "Noble gases, nitrogen, and methane from the deep interior to the atmosphere of Titan," *Icarus*, vol. 250, pp. 570–586, Apr. 2015.

[96] R. D. Lorenz, E. P. Turtle, J. W. Barnes, M. G. Trainer, D. S. Adams, K. E. Hibbard, C. Z. Sheldon, K. Zacny, P. N. Peplowski, D. J. Lawrence *et al.*, "Dragonfly: A rotorcraft lander concept for scientific exploration at titan," *Johns Hopkins APL Technical Digest*, vol. 34, no. 3, p. 14, 2018.

[97] T. Sasaki, G. R. Stewart, and S. Ida, "ORIGIN OF THE DIFFERENT ARCHITECTURES OF THE JOVIAN AND SATURNIAN SATELLITE SYSTEMS," *The Astrophysical Journal*, vol. 714, no. 2, pp. 1052–1064, May 2010.

List of Publications and Presentations

Publications
Submitted Paper

1. Ryusuke Nishitani, Jun Kimura, Atsushi Tani, Sho Sasaki
"Methane hydrates achieve both thick oceans and thick lithospheres in Enceladus and Mimas" Submitted to *Earth, Planets and Space*

Presentation in international conference

1. Ryusuke Nishitani, Atsushi Tani, Sho Sasaki
"Partition of Ammonium Ion Between Water and Clathrate in Formation of Tetrahydrofuran Hydrate" International Symposium on Present and Future of Material Sciences, 7, Osaka, Japan, Nov. 2015

2. Ryusuke Nishitani, Atsushi Tani, Sho Sasaki
"Partition of Ammonium Ion Between Water and Clathrate Hydrate in a Subsurface Ocean of Icy Bodies", 47th Lunar and Planetary Science Conference, 1984, The Woodlands, Texas, USA, Mar. 2016

3. Ryusuke Nishitani, Atsushi Tani, Sho Sasaki
"The effect of clathrate formation on concentrations of ammonia and ammonium ion in a subsurface ocean of Enceladus", JpGU-AGU Joint Meeting 2017, PS01-P10, Makuhari, Chiba, Japan, May 2017

4. Ryusuke Nishitani, Atsushi Tani, Sho Sasaki, Jun Kimura
"Inclusion of ammonium ion into clathrate hydrate in subsurface ocean of icy moons", 14th Internatinal Conference on the Physics and Chemistry of Ice, 101, Zurich, Switzerland Jan. 2018

Presentation in domestic conference

Oral

1. 西谷隆介, 谷篤史, 佐々木晶
“THF 氷天体内部海におけるクラスレートハイドレート形成によるアンモニウムへの影響濃度”, 日本惑星科学会 2015 年秋季講演会, 東京, 2015 年 10 月

2. 西谷隆介, 谷篤史, 佐々木晶
“THF ハイドレート形成に伴うアンモニウムイオンの取り込み”, 雪氷研究大会 (2016・名古屋), 愛知, 2016 年 9 月

3. 西谷隆介, 谷篤史, 佐々木晶
“氷衛星の内部海におけるクラスレートハイドレート形成によるアンモニウムイオン濃度への影響”, 日本惑星科学会 2016 年秋季講演会, 岡山, 2016 年 9 月

4. 西谷隆介, 谷篤史, 佐々木晶
“THF ハイドレートに対するアンモニウムイオンの分配係数”, 第 26 回日本エネルギー学会大会, 愛知, 2017 年 8 月

5. 西谷隆介, 谷篤史, 佐々木晶, 木村淳
“土星衛星エンセラダスのプリューム組成に対する氷・クラ スレートハイドレート形成の影響”, 日本惑星科学会 2017 年秋季講演会, 大阪, 2017 年 9 月

6. 西谷隆介, 木村淳, 谷篤史, 佐々木晶
”土星衛星エンセラダス熱進化におけるクラスレートハイド レートの役割”, 日本惑星科学会 2018 年秋季講演会, 大阪, 2018 年 9 月

7. 西谷隆介, 木村淳, 谷篤史, 佐々木晶
”土星衛星 Enceladus と Mimas におけるメタンハイドレートの形成と熱進化”, 日本惑星科学会 2019 年秋季講演会, 京都, 2019 年 10 月

Poster

1. 西谷隆介, 木村淳, 谷篤史, 佐々木晶
“氷天体熱進化に対するクラスレートハイドレートの影響”, 第 6 回衛星系研究会, 東京, 2018 年 8 月

2. 西谷隆介, 谷篤史, 佐々木晶, 木村淳
Inclusion of brine into icy shell of Enceladus”, JpGU Meeting 2019, 千葉, 2019 年 5 月